NTNU

Norwegian University of
Science and Technology

Using SeaFAST to Analyze the Rate of Change of Iron Release and Removal During the Decomposition of Planktonic Materials

Stephen Kohler

Environmental Toxicology and Chemistry
Submission date: May 2017
Supervisor: Murat Van Ardelan, IKJ

Norwegian University of Science and Technology
Department of Chemistry

Abstract

The cycling of iron in the ocean plays an important role within both the biological carbon pump and the nitrogen cycle. As much of primary production in the euphotic zone depends upon the internal recycling of iron, the effect of biotic and abiotic processes on the remineralization, or solubilization, of this essential trace metal from decomposing organic matter must be explored.

Part of the Ocean CERTAIN project, this thesis aimed to assess the release and change in concentration of iron in the decomposition of varying natural communities from the oligotrophic Cretan Sea. A mesocosm experiment consisting of natural seawater communities was amended with increased zooplankton concentrations and an increasing carbon gradient. Upon completion of the mesocosm experiment, seawater was transferred to dark bottles for community decomposition where time-based sampling for total dissolvable iron, dissolved iron, and macronutrients was taken. Analysis of iron samples was done with SeaFAST, a commercially available preconcentration system available through ESI. Instrument parameters were assessed for recovery and accuracy while quantification was done via ICP-MS.

Recovery of iron within the SeaFAST system varied between 84-101%, most likely affected by a combination of background iron levels, SeaFAST elution volume accuracy, and post-preconcentration storage, emphasizing the proper cleaning and evaluation of SeaFAST parameters prior to any sample analysis.

Iron concentrations over time in dark bottles showed an initial increase, consistent with remineralization. Tanks with different grazing treatments did not show statistical significance in initial rates of change, and the highest carbon gradient group initial rate of change was statistically different from only one other group. A subsequent decrease in rates of change of dFe and decrease in TFe concentrations for all tanks suggested high adsorption was occurring within the bottles and that the release rate of iron within dark bottle decomposition experiments may follow a non-linear rate of change.

A non-linear release rate implicates the importance of both abiotic and biotic mechanisms for iron recycling, and that models of iron remineralization will likely need to incorporate both processes to accurately predict dissolved iron concentrations within varying aquatic communities.

Acknowledgment

I would like to thank my supervisor Murat Ardelan for his help, guidance, and enthusiasm for the master thesis project and for letting me participate within the Ocean CERTAIN project.

I would like to thank Nicolas Sanchez for his advice and support when dealing with the SeaFAST system in both setup and troubleshooting.

I would like to thank Syverin Lierhagen for his analysis, help, advice, and patience for all the ICP-MS samples, both testing and otherwise.

I would like to thank the Ocean Certain Team for the opportunity to participate in a large project and for the scientific knowledge and collaboration during my time in Heraklion.

I would like to thank HCMR and the staff technicians for assisting in the nutrient sample analysis.

I would like to thank Mathew Avarachen and Kjersti Andresen for the analysis of the TOC and POC samples and for assistance at TBS.

I would like to thank Stephanie Liefmann for her help and guidance in the trace metal washing bottle procedures.

And lastly, I would like to thank my friends, family, and Ole Hansen for making my time in Norway so memorable and for their support during this master thesis project.

Table of Contents

List of Figures

List of Tables

Abbreviations

POC – particulate organic carbon

HNLC – high nutrient low chlorophyll

POM – particulate organic matter

DOM – dissolved organic matter

HCMR – Hellenic Centre for Marine Research

ICP-MS – Inductively Coupled Plasma Mass Spectrometry

ESI – Elemental Scientific Incorporated

IDA – iminodiacetate

ED3A - ethylenediaminetriacetate

NTNU – Norwegian University of Science and Technology

PFA - PerFluoroAlkoxy

PTFE - polytetrafluoroethylene

PE – polyethylene

DI – de-ionized

LG – low grazing

HG – high grazing

DOC – dissolved organic carbon

TOC – total organic carbon

PON – particulate organic nitrogen

TBS – Trondheim Biological Station

dFe – dissolved iron

TFe – total dissolvable iron

ANOVA – analysis of variance

NRCC – National Research Council Canada

REE – rare earth element

1 Introduction

1.1 Biogeochemical Cycle and Role of Iron in the Ocean

The biological pump begins in the euphotic layer of the ocean and serves to transport organically fixed carbon to the deep ocean and ultimately, the sediments. Phytoplankton and autotrophic microorganisms take up and transform CO_2 and other macronutrients such as inorganic nitrogen in the forms of NH_4 or NO_3 and inorganic phosphate to produce biomass at proportions termed the Redfield ratio (Moore et al., 2013). This ratio of 106C:16N:1P has been widely used as marker of phytoplankton biomass, however significant departures from this ratio have been observed, suggesting nitrogen limitation or phosphate limitation.

As biomass, carbon can operationally be separated as particulate organic carbon >0.2µm or dissolved organic carbon <0.2µm. Picophytoplankton and heterotrophic bacteria are included in particulate carbon phase and the smallest size class between 0.2µm - 2µm, while viruses are considered in the dissolved phase. The 2-20µm size class consist of small diatoms and flagellates; the 20-200µm size class includes larger diatoms and heterotrophic protists (microzooplankton); and copepods and other mesozooplankton are included in the 0.2-2mm size.

Within the biological pump these forms of biomass can follow several different paths such as ingestion and defecation by zooplankton, destruction via viral lysis, or become sinking detritus upon their death. As this sinking POC degrades thermodynamically or via bacterial decomposition to DOC, the resulting pathways of fixed carbon and the other macronutrients enter the microbial loop (Azam et al., 1983). The microbial loop includes heterotrophic bacteria which consume DOC and remineralize the macronutrients via respiration, returning nutrients back to the water column so they can be reused within the euphotic layer or returned to the euphotic layer via upwelling. A small proportion of the POC, termed refractory POC, is resistant to bacterial decomposition and can sink out of the water column to the ocean sediments and be sequestered. The sequestration of fixed refractory CO_2 to seafloor sediments via the biological carbon pump represents an important feedback mechanism in regulating increasing atmospheric CO_2 levels.

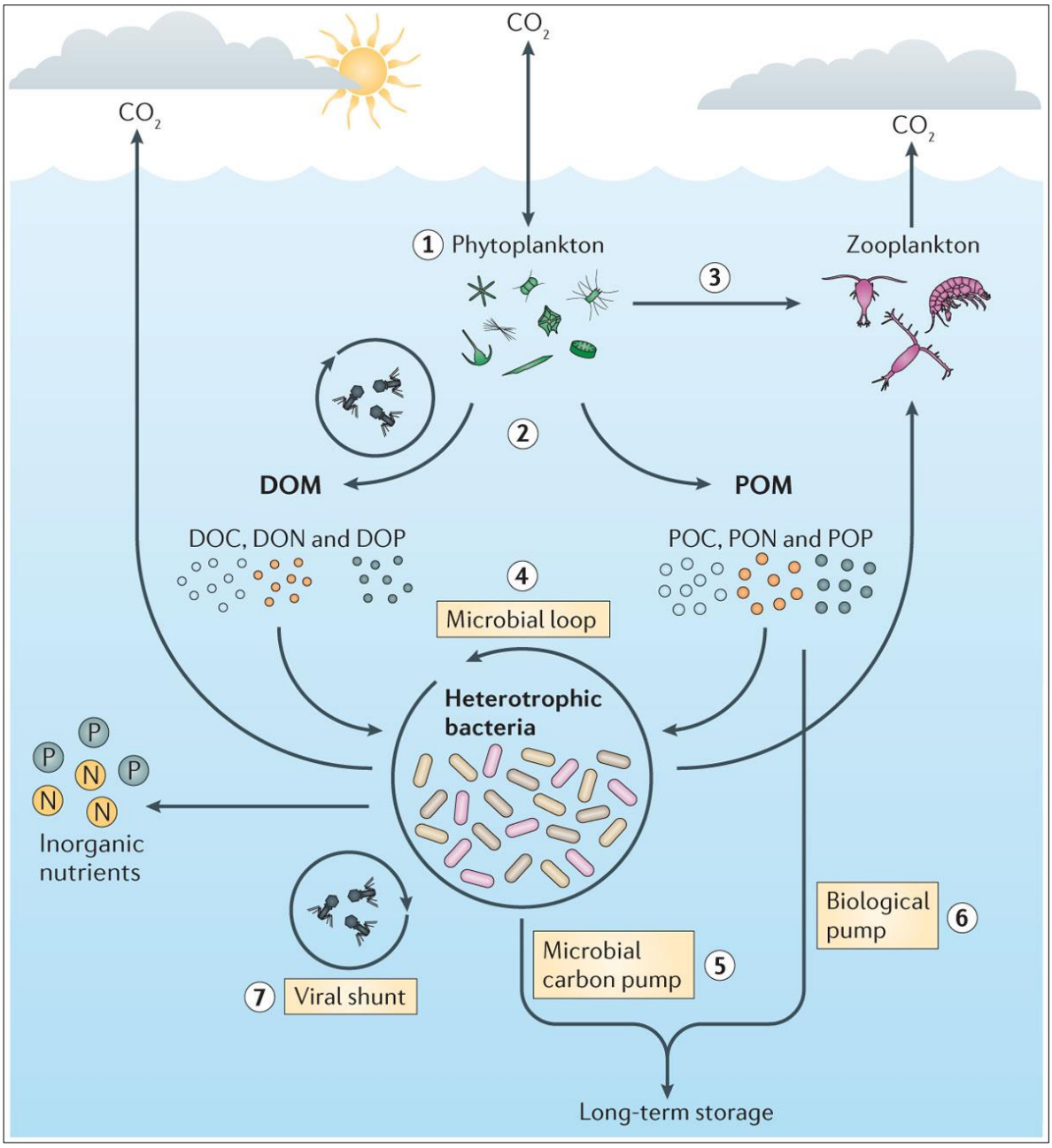

Figure 1: Visual representation of the biological pump including the microbial loop. Reproduced from (Buchan et al., 2014).

As CO_2 is not a limiting nutrient for autotrophic organisms in the ocean due to equilibrium with the atmosphere, macronutrients nitrate and phosphate typically restrict primary production (Moore et al., 2013). Thus, the seawater N:P ratio is an indicator of which macronutrient is limiting, with a high N:P indicating phosphate limitation and a low N:P indicating nitrate limitation, both in relation to the Redfield ratio. However, high nutrient low chlorophyll zones (HNLC), with low primary production despite high levels of macronutrients, led John Martin to conclude that iron could also be a major limiting micronutrient in what he termed “The Iron Hypothesis” (Martin, 1990).

The importance of iron to primary production and phytoplankton has led to vast research on the biogeochemical cycling of iron and that it is intricately linked to the biological pump via several pathways (W. Sunda, 2012). Iron and other trace metals have been shown to be both indirectly and directly important in the carbon and nitrogen cycles, acting as structural components of enzymes and proteins, or as cofactors and electron acceptors in photosynthetic or respiratory mechanisms (Whitfield, 2001). As iron is a key component of the electron transport chain and ammonium oxidizing enzymes, bacterial demand, uptake, and release of iron in the microbial loop is known as the microbial ferrous wheel (D. L. Kirchman, 1996). The measurement of bacterial abundance (BA) and bacterial production (BP) may give an indication as to the extent of the bacterial mobilization of iron (P. Boyd et al., 2010). The resulting communities of both bacteria and phytoplankton such as diatoms can compete for dissolved iron if concentrations are limiting (Boyd et al., 2012). Uptake and release leads to internal cycling of iron with low concentrations of dissolved iron in the euphotic layer where primary production takes place. There is a gradual increase with depth as iron is remineralized, or solubilized, following a similar pattern as macronutrients nitrogen and phosphorus (Johnson et al., 1997). The cycling of iron within the euphotic zone remains an important factor for biological pump efficiency, with some regions having a low *fe* ratio, indicating primary production relies heavily on internally recycled iron rather than external sources (Boyd et al., 2017). From the deeper ocean, iron can be externally resupplied to the surface layer via upwelling, sediment resuspension, and hydrothermal vents (P. W. Boyd et al., 2010). Other important external sources of iron to the ocean are due to input from rivers, glacial melt, and atmospheric dust. Dust input from aeolian transport accounts for large sources of dissolved iron to areas adjacent desert regions, such as the Atlantic ocean near the coast of Africa and the Mediterranean Sea (Jickells et al., 2005). Despite its initial source, iron in seawater is rapidly affected by biological uptake and adsorption processes, with the latter leading to a high tendency of dissolved iron to aggregate and precipitate leading to the removal of iron from the water column to sediments (P. W. Boyd et al., 2010).

1.2 Iron Speciation in Seawater

Free metal ions in water tend to undergo either redox or coordinative reactions to improve their stability (Stumm et al., 1996). Typically, free metal ions form a coordinative compound, also known as a complex, with other ions or molecules which are called ligands. Because of the electron configuration of trace metals, and iron in particular, these ions can form multidentate complexes called chelates, where the ligand molecule has more than one atom bonded to the central metal ion. Due to metal concentration, pH, temperature, ligand concentrations, redox state, and biology, iron and other trace metals can exist as several reversible forms in solution, termed speciation (Stumm et al., 1996).

In seawater at approximately pH 8, iron typically exists in redox states Fe(III) or Fe(II) and prefers ligand atoms of oxygen or nitrogen, respectively, and undergoes both biotic and abiotic mediated redox reactions throughout the water column (Melton et al., 2014). Thermodynamically however, Fe(II) rapidly undergoes oxidation to form Fe(III) in the presence of oxygen. At the surface of the ocean, this Fe(III) can either be photochemically reduced back to Fe(II) or rapidly hydrolyzed by water molecules and exist as thermodynamically stable inorganic iron hydroxides and oxyhydroxides, particularly as highly insoluble $Fe(OH)_3^0$. This inorganic iron tends to precipitate, as it's solubility in 0.7nM NaCl solution was theoretically as low as 0.01nM (Liu et al., 2002). Other hydrolyzed species of Fe(III) such as $FeOH^{2+}$ and $Fe(OH)_4^-$ also exist. However, open ocean concentrations of dissolved iron at approximately 0.2nM are much higher than expected and are due to the presence of and complexation with natural organic ligands (Rue et al., 1995; van den Berg, 1995).

Research into the elevated concentrations has shown that 99% of dissolved iron is complexed with organic ligands in seawater (Gledhill et al., 2012) and these ligands are thought to be divided into a least two different complexing strength ligand classes, L1 and L2 (P. W. Boyd et al., 2010). L1 ligands include strong complexing agents called siderophores that are primarily produced by marine bacteria in iron-deficient conditions while L2 ligands are weaker complexing agents and suggested to be bacterial degradation products or compounds created via photolysis of siderophores (P. W. Boyd et al., 2010). Additional ligand classes, such as L3 or L4, with weaker conditional stability constants have also been recently shown to exist (Buck et al., 2015). These ligands not only facilitate the solubility of iron in seawater but they are thought to act as transporters for iron uptake by phytoplankton and bacteria. The uptake rate of iron at the cell surface is a function of the kinetics involved between the metal ion and the

concentration of ligands on the cell surface (F. M. M. Morel, 2008). Both redox forms of iron are thought to be usable by the cell as bioavailable, soluble Fe(II) or via reduction reactions at the surface for insoluble Fe(III).

Due to the quantity of redox and complexation reactions within the water column, iron analysis was traditionally focused on identifying size fractions. Operationally, dissolved iron is defined as iron species that can pass through a 0.2µm filter, while the larger remainder (>0.2µm) is termed particulate iron (Stumm et al., 1996). Particulate iron can encompass lithogenic particles like minerals and small colloids, biogenic iron that is adsorbed to or within living or dead microorganisms, and fecal pellets produced from grazing zooplankton. Within the dissolved phase (<0.2µm), research indicated that a substantial portion of iron in the water column is further subdivided between truly soluble and colloidal forms, with most iron being in the colloidal form and consisting of iron bound to weak ligands, proteins, enzymes, and colloidal inorganic iron. (Wu et al., 2001). The colloidal fraction is defined between 0.02µm - 4µm. Thus, the truly soluble form (<0.02µm) contains free metal ions as well as small siderophore compounds. For a visual aid, Figure 2 illustrates that iron is therefore distributed between various size fractions, two redox states, and partitioned between organic and inorganic ligands.

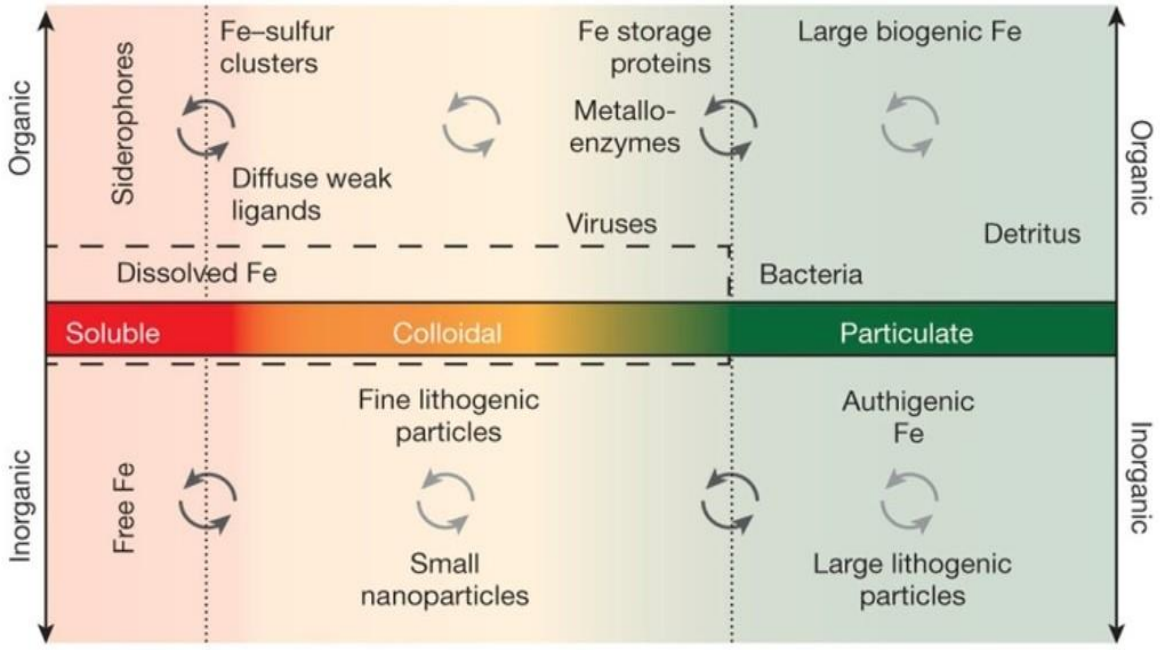

Figure 2: Summary of iron in seawater, complexed with organic and inorganic ligands in various size fractions. Reproduced from Tagliabue et al. 2017

1.3 Thermodynamics of Iron in Seawater

Inorganic and Organic Complexation

The distribution of iron, its partitioning between organic and inorganic forms and between the size fractions, and its non-equilibrium behavior is dependent on its thermodynamics (Waite, 2001). To find the inorganic equilibrium speciation of Fe(III) in seawater, the equation must first be corrected for ionic strength. Ionic strength is measure of the concentration of ions in a solution and a medium like seawater, with many conservative ions like Na^+ and Cl^-, will affect the formation, solubility, and disassociation of iron species and has an ionic strength higher than that of pure water (Stumm et al., 1996). The ionic strength of seawater, typically around $I = 0.7 mol L^{-1}$ (Waite, 2001), can then be used in a modified form of the Debye-Hückel equation called the Davies equation, which is commonly employed for speciation in seawater. With adjustment for ionic strength, the true formation constant K for hydrolysis species can be estimated based on an observed experimental conditional constant, ${}^cK$, presented in equation 1. The formation constants indicated that $Fe(OH)_3$ is the dominant species at pH 8 of seawater (Millero et al., 1995).

Equation 1

$$ {}^cK = \frac{\left[FeOH^{2+}\right]}{\left[Fe^{3+}\right][OH^-]} $$

Due to the high concentration of iron complexed with natural organic ligands in seawater, the thermodynamic equilibrium of iron with these ligands must also be considered. In an observed ionic strength medium, such as $I = 0.7 nM\ L^{-1}$ for seawater, the conditional stability constant between Fe^{3+} and ligand (L^{2-}) with unbound charge of -2 is calculated according to equation 2.

Equation 2

$$ {}^cK_{FeL^+} = \frac{[FeL^+]}{\left[Fe^{3+}\right][L^{2-}]} $$

Observations and direct measurements of Fe^{3+} and L^{2-} are usually difficult to ascertain in seawater; therefore, it is easier to use Fe(III)' to represent Fe^{3+} as all inorganic hydrolyzed iron species and $Fe(III)L^+$ as iron species bound to natural organic ligands. With the same approach for ligands, conditional stability constant K can be derived for equation 3 for the reaction between uncomplexed inorganic iron species and uncomplexed ligand species.

Equation 3

$$K^{cond}_{Fe(III)'/L'} = \frac{[Fe(III)L^+]}{[Fe(III)'][L']}$$

The K^{cond} is related to both the formation of organic chelates and the thermal disassociation of organic chelates and can be expressed as the change in concentration of the organic iron chelate over time, with a negative change indicating disassociation and a positive change indicating formation (Stumm et al., 1996). From this reasoning, a positive change in concentration of iron chelate over time can be written as a function of rate constant k_f multiplied by the concentrations of organically uncomplexed iron and uncomplexed organic ligands. Additionally, a negative change in concentration of iron chelate, or disassociation, can be written as a function of rate constant k_d.

Equation 4 & 5

$$\frac{d[Fe(III)L^+]}{dt} = k_f[Fe(III)'][L'] \text{ and } -\frac{d[Fe(III)L^+]}{dt} = k_d[Fe(III)L^+]$$

In seawater, particularly in the surface layer, photodisassociation of ligands and Fe(III) complexes (Melton et al., 2014) along with microbial transformation dictate that equations 4 and 5 need to include additional variables to truly estimate rates of formation and disassociation (Stumm et al., 1996). In darkness however, photodisassociation of iron-complexes do not occur.

Adsorption

Another equally yet highly important process influencing the speciation of iron in seawater is adsorption. In seawater at pH 8, surfaces of particles tend to have a small negative charge and can therefore attract positively charged cations. As these cations become coordinatively bound at the surface by various ligand groups such as hydroxides or oxides, the particle may sink out of the water column to the sediments in a process termed scavenging (Libes, 2009). Initial adsorption is characterized by cation exchange or a surface atom behaving as a Lewis base (Stumm et al., 1996). Iron can exchange with either another metal or a proton and also form a coordinative reaction with two surface atoms. S<< represents a surface in equation 6.

Equation 6

$$Fe_{aq}^{3+} + \{Cu^{+}\text{«}S\} \leftrightarrow Cu_{aq}^{2+} + \left\{Fe^{2+}\text{«}S\right\} \text{ or } \{S\text{«}O^{-}\} + Fe^{3+} \leftrightarrow \left\{S\text{«}OFe^{2+}\right\}$$

Rates of adsorption are determined by the rate of transport of the adsorbate to the surface and then by intrinsic adsorption, or transfer from solution to solid (Stumm et al., 1996). Like organic complexation, these reactions can also incorporate rate constants, like k_{ads} for adsorption and k_b for desorption. As adsorption influences the distribution between aqueous and particulate phases due to changes in electrostatic interactions, soluble iron can quickly aggregate to form colloids and then precipitate to particulate iron and sink out of the water column, reducing its overall bioavailability. As iron has a low residence time in seawater, this indicates that iron is quickly scavenged from seawater onto sinking particles, particularly on large biogenic and lithogenic material.

1.4 Decomposition and Subsequent Remineralization of Iron

The death of marine microorganisms and subsequent sinking of organic matter, termed marine snow, begin the stages of decomposition. Organic matter in its reduced form is thermodynamically unstable and undergoes redox transformations in oxygenated seawater and its degradation is facilitated by marine heterotrophic bacteria. At their small sizes between 0.2µm to 1µm, bacteria feed on dissolved organic matter through passive diffusion through their rigid cell walls (Libes, 2009). To assist the breakdown of particulate organic matter, bacteria use compound specific exoenzymes such as proteases to reduce large molecular weight compounds to an appropriate size for diffusion and cellular respiration. Aerobic cellular respiration in bacteria consists of glycolysis or the breakdown of glucose to generate energy in the form of ATP, followed by the Krebs cycle and oxidative phosphorylation. Catabolism, or the degradation of organic matter for energy and nutrients, is a reverse reaction for photosynthesis, converting organic biomass into remineralized nutrients, represented by the following formula.

$$(CH_2O)_{106}(NH_3)_{16}H_3PO_4 + 138\ O_2 \rightarrow 106\ CO_2 + 122\ H_2O + 16\ HNO_3 + H_3PO_4$$

Besides dead microorganisms, marine snow can also consist of fecal pellets generated by zooplankton, structural materials such as calcium carbonate shells, and mucous membranes. Due to the incorporation of iron by biological organisms, much of the decomposing POM and DOM is rich in proteins and enzymes that contain iron that can be remineralized. Once the iron is solubilized with depth, its speciation is affected by both biotic and abiotic processes (Boyd et al., 2017).

Biotically, the release and retention of dissolved iron is supported through release of organic ligands including siderophores, viral lysis of bacterial cell membranes (Poorvin et al., 2004), and grazing by zooplankton (Sato et al., 2007). Decomposition experiments have demonstrated the concurrent release of four different complexing strength ligands along with dissolved iron (Bundy et al., 2016). These ligands increase dissolved iron concentration in the ocean, although the magnitude of iron release rates depends upon both the predator and prey and community trophic structure (Hutchins et al., 1994). The presence of additional copepods has shown that higher grazing rates of diatoms (Sarthou et al., 2008) and changes in community structuring (Sato et al., 2007) can influence and increase the iron remineralization rate. Additionally, the percentage of iron regenerated to the dissolved phase after 24 hours was higher for heterotrophic bacteria as prey compared to cyanobacteria, a picoautotroph (Strzepek

et al., 2005). In the absence of micrograzers, bacterial mobilization of iron from phytoplankton to the bacterial fraction accounted for more than 40% of remineralized iron (P. Boyd et al., 2010), illustrating bacterial uptake will also affect iron remineralization. The presence of viruses can also increase bacterial respiration rates, suggesting increased remineralization of nutrients (Bonilla-Findji et al., 2008).

Further complicating the release of iron from these organisms is iron's high tendency of adsorption. Iron can be intracellular or adsorbed extracellularly, with research indicating that 36-86% of iron washed from biogenic particle surfaces is adsorbed extracellularly (Tovar-Sanchez et al., 2003), indicating that sinking particle surfaces serve as a ballast to remove iron from the water column. The released iron from remineralization or dissolution of externally supplied iron may desorb or resorb with these sinking biogenic or lithogenic particles. The aggregation of colloids, precipitation of iron hydroxides, and iron's adsorption decouple the remineralization rate from other metals and macronutrients (Boyd et al., 2017). Additional sources of decoupling iron from macronutrients is bacteria's preferential remineralization of both nitrogen and phosphorus, leading to faster remineralization rates for these macronutrients (Twining et al., 2014).

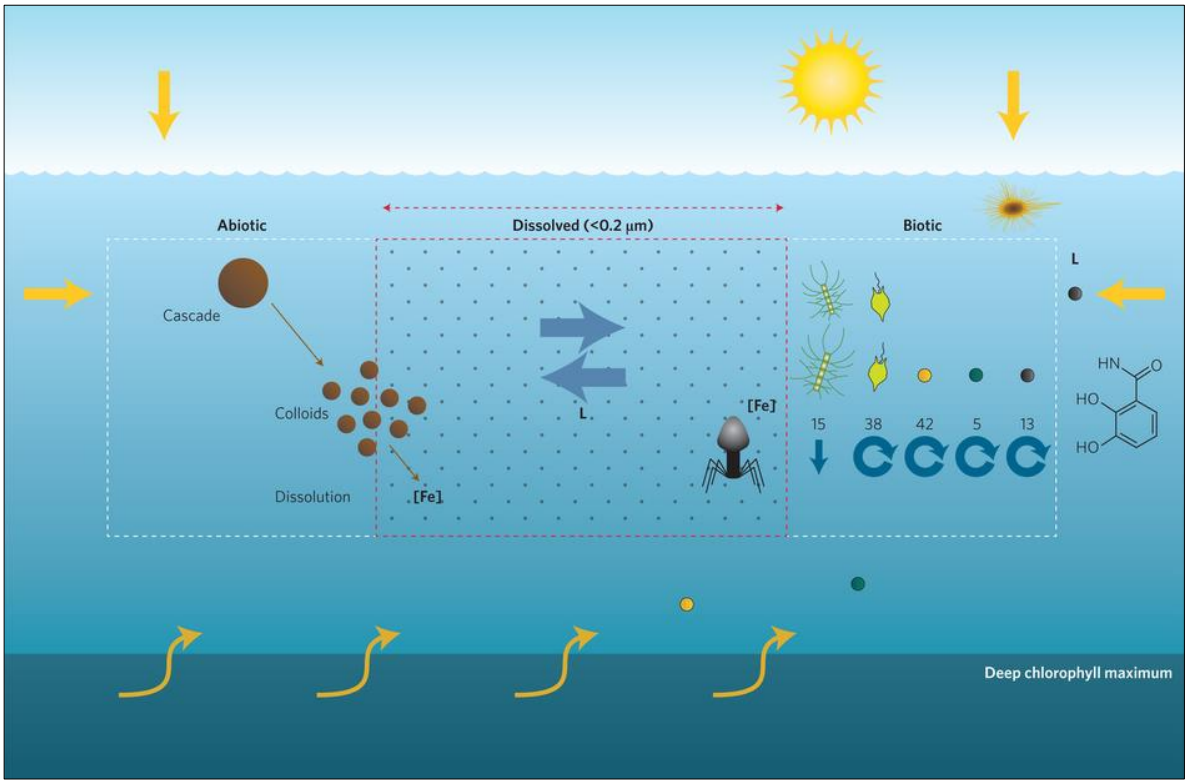

Figure 3: The variety of processes affecting iron remineralization. Includes external inputs from horizontal advection, atmospheric input, and sediments. Biotic recycling via microorganisms and viruses, abiotic dissolution and aggregation processes, each affect the partitioning of dissolved iron (<0.2µm). Reproduced from (Boyd et al., 2017).

1.5 Study Area

The Mediterranean Sea is a largely land-locked marginal sea bordered by the continents of Europe to the north, Africa to the south, and Asia to the east. The narrow Gibraltar strait connects the Mediterranean with the Atlantic Ocean. As only 10% of the sea is resupplied with water from rivers and rainfall, the remaining 90% is supplied by Atlantic water through Gibraltar (Blondel et al., 2010). The Eastern Mediterranean has a high salinity of around 37.15 primarily due to historical geological changes and a large evaporation loss of about 4500km^3 per year. The sea also has an unusually warm deep water temperature of approximately 13ºC when compared to the open ocean (Blondel et al., 2010). High saline Mediterranean deep water flows out through the Gibraltar strait into the Atlantic. For this thesis, fieldwork was performed at the Hellenic Centre for Marine Research (HCMR) outside of Heraklion, Crete, Greece.

Figure 4: Map of the Cretan Sea. Reproduced from WorldAtlas.com

Nutritionally, the Mediterranean is an oligotrophic region characterized by an increasing macronutrient deficiency from west to east (Pujo-Pay et al., 2011). The Eastern Mediterranean has low concentrations of chlorophyll *a* and low phytoplankton densities indicating low primary productivity. Particularly, the high N:P ratio coupled with low nitrogen

fixation (M. Krom et al., 2010) suggests that phosphorus is the key limiting nutrient (M. D. Krom et al., 1991). Studies have found that phosphorus could also be limiting the bacterial community (Thingstad et al., 2005) leading to competition with phytoplankton. Bacteria tend to outcompete diatoms for phosphorus, particularly at low concentrations (Amin et al., 2012) leading to POM with depth being dominated by the picoparticulate fraction (Danovaro et al., 2000); however, due to variations in hydrography (Tselepides et al., 2000) and atmospheric dust inputs of nutrients, the Eastern Mediterranean is also capable of supporting occasional primary productivity. Being a mostly enclosed marginal sea with varying nutrient concentrations, Mediterranean biology has developed a unique composition and high diversity of prokaryotes and picoplankton (Luna, 2015; Zaballos et al., 2006).

With regards to trace metals, the Mediterranean is influenced by both anthropogenic and natural atmospheric deposition (Migon, 2005) and concentrations are markedly higher when compared to the open ocean. The amount of iron supplied by dust, varying between 1.33-2.74nmol L^{-1} (Theodosi et al., 2010) suggest that the observed seasonal variations of 1.44nM-1.92nM in dissolved Fe concentrations in the Cretan Sea (Statham et al., 2005) may be exclusively supplied by atmospheric input and that iron is not a co-limiting nutrient in the Eastern Mediterranean. However, the amount of iron that remains in the euphotic layer depends on the amount of biological activity (Wagener et al., 2010) or iron-complexing ligands (Wuttig et al., 2013). Studies have indicated that dissolved iron concentrations influenced by high atmospheric deposition are influenced by water column stratification (Bonnet et al., 2005), number of dust events (Wuttig et al., 2013), and particle scavenging (Wagener et al., 2010). Due to this combination of processes, dissolved iron concentrations in the Eastern Mediterranean are suggested to be a delicate balance between ligand complexation and scavenging (Bressac et al., 2013), with lithogenic flux important due to dust input (Tagliabue et al., 2017).

1.6 SeaFAST

Because of low dissolved iron concentrations in the surface ocean, laboratories typically preconcentrated seawater samples before quantification (Worsfold et al., 2014). SeaFAST is a commercially available automated preconcentration system for undiluted seawater (Elemental Scientific Incorporated) that can be paired with an ICP-MS in online mode or without ICP-MS for offline mode. The autosampler unit is housed in a clean enclosure equipped with a low particulate air filter. Solutions are connected to a S400V syringe module with PFA tubing. For preconcentration, the autosampler probe aspirates and fills acidified seawater sample (approximately pH 2) into a 10mL PFA sample loop via vacuum. Before pushing the seawater sample onto the column, a 6.0 ± 0.2 ammonium acetate buffer is passed through a trace metal cleanup column, separate from the preconcentration column, to remove excess metals from the buffer solution and then combined with 18MΩ water (MilliQ). The combined buffer-water solution pushes the seawater sample onto and through the preconcentration column where an immobilized iminodiacetic acid and ethylenediaminetriacetic acid resin shown to have excellent selectivity for trace metal ions (Sohrin et al., 2008) chelates trace metal ions within a PFA column (Part #CF-N-200). The volume of seawater sample to be preconcentrated can be specified in the initial method parameters in intervals of 10, starting at 10mL.

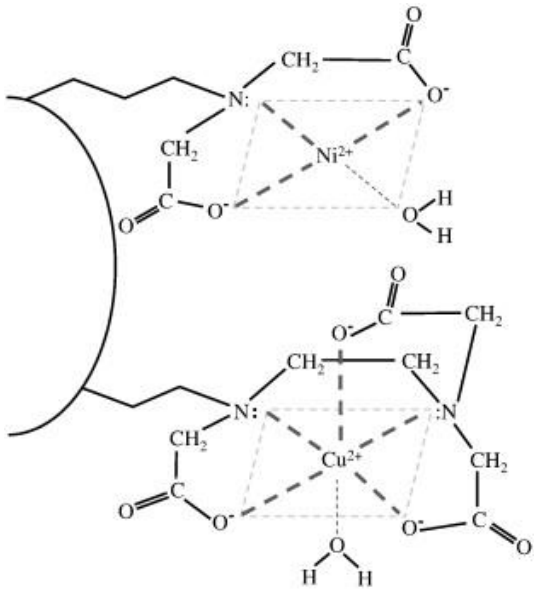

Figure 5: IDA and ED3A functional groups chelating metal ions. Modified from (Biller et al., 2012).

The column is maintained at pH 6 by a continuous flow of ammonium acetate buffer and the buffer-water solution pumped through the column to remove alkali and alkaline earth elements as well as other matrix ions. After vacuum shut off, solution flow is reversed and a

1.5M Ultrapure HNO_3 solution is passed through the column to elute metal ions into solution to be dispensed into a PTFE collection tube in offline mode via 1.0 bar pressurized Ar gas.

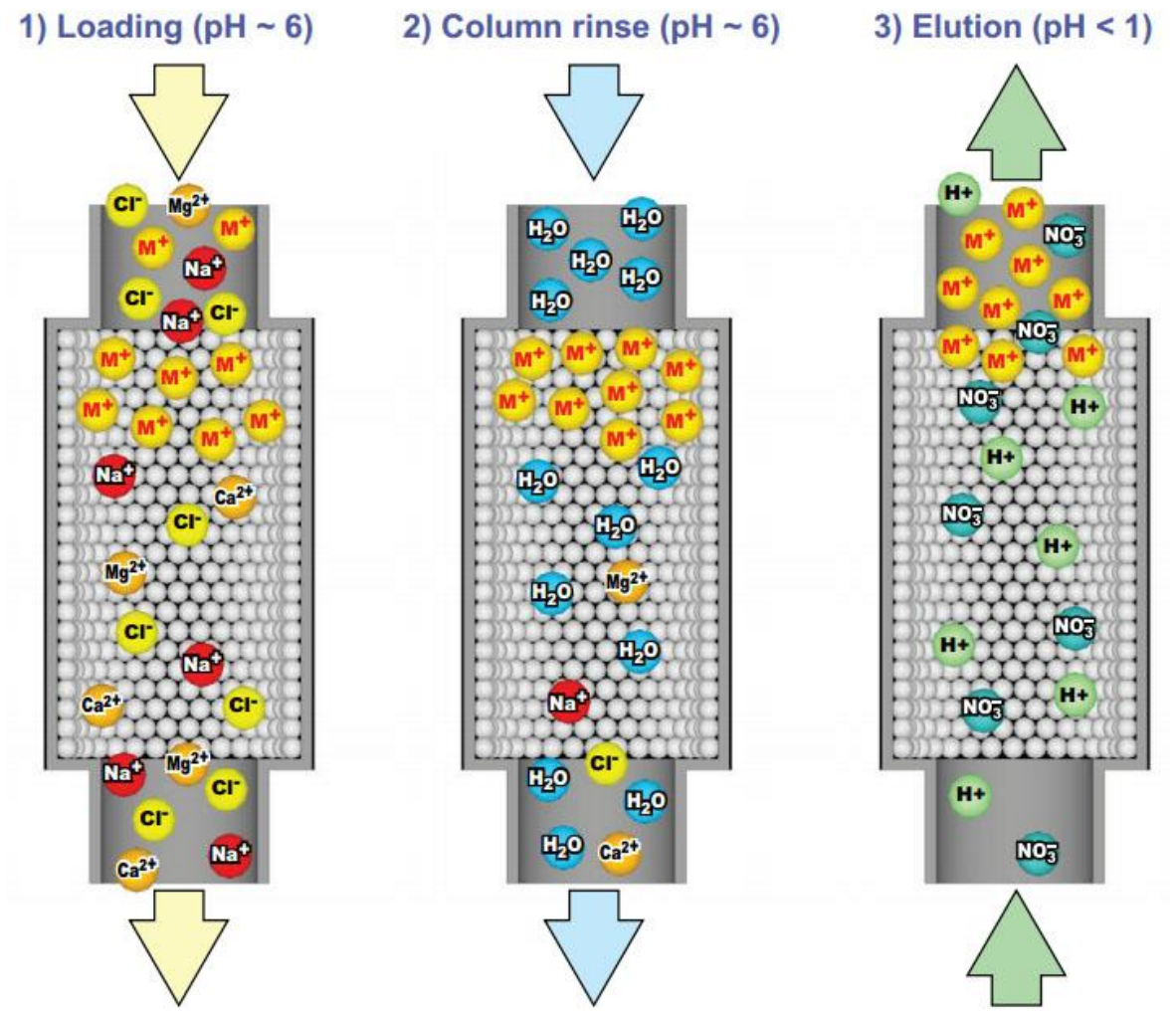

Figure 6: Column loading, rinsing, and elution. Reproduced from Elemental Scientific

After elution, sample probe is rinsed within a 0.1M HNO_3 solution and both preconcentration and trace metal cleanup columns are cleaned with elution solvent (1.5M Ultrapure HNO_3) and subsequently conditioned with buffer-water mixture in preparation for the next sample. After sequence run, samples can then be diluted with MilliQ water for ICP-MS run conditions and delivered for analysis.

According to ESI, metals can be analyzed via preconcentration mode or direct mode on its SeaFAST systems. Studies of the SeaFAST system and its precursor in preconcentration mode indicated a high recovery for micronutrient trace metals Fe, Zn, Ni, Cu, Mn, and labile Co (Lagerström et al., 2013), transition metals Ti, Zr, Nb, W, V, Mo (Poehle et al., 2015), and rare earth elements (Hathorne et al., 2012) in both online (Lagerström et al., 2013) and offline

modes (Behrens et al., 2016). In Figure 7, the following elements marked in green can be determined in preconcentration mode.

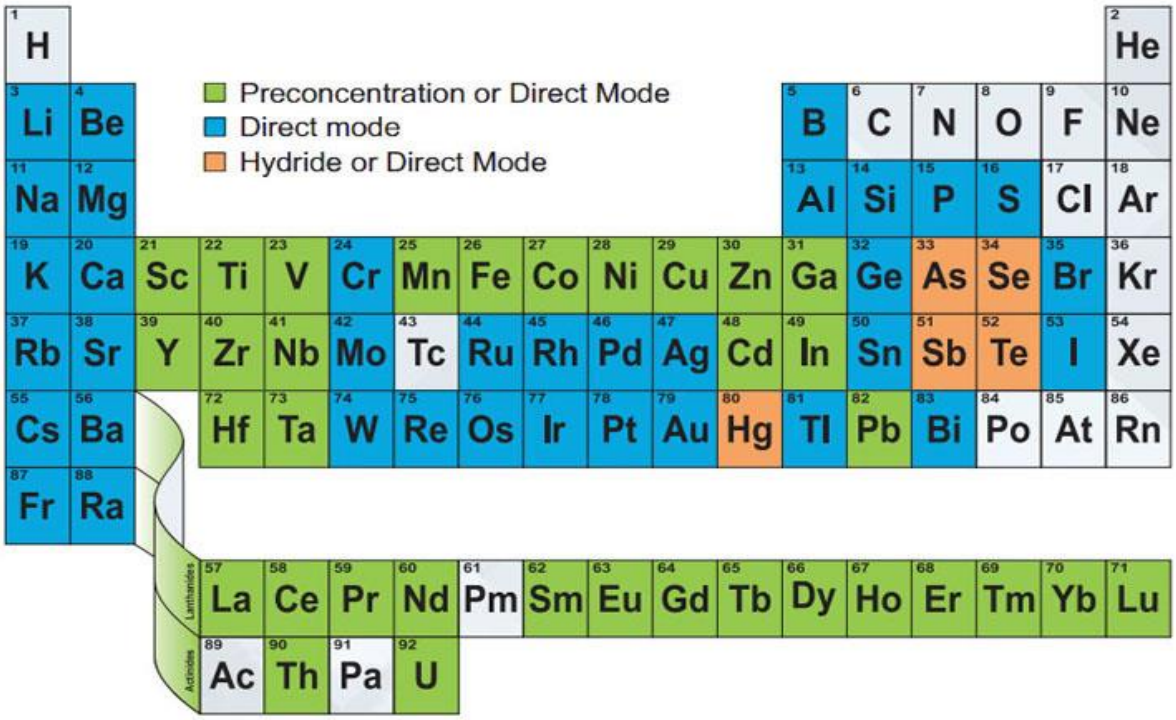

Figure 7: Periodic table of elements suitable for either direct or preconcentration mode. Reproduced from Elemental Scientific

Besides the column cleanup and conditioning in the *Sample Run* preconcentration method, a *Prime* method prepares the instrument for sample acquisition by first cleaning columns with elution solvent and eluting to waste via the probe at the rinse station. Then, the system conditions the columns and the sample loop with the buffer-water solution four times. For the *Prime* method, each of these actions are performed twice before termination of the method. The *Prime* method is recommended to be performed at least once by the manufacturer prior to all sample analysis. For system cleaning, all solution lines are to be placed in elution solvent reservoir and run on *Prime.* Afterwards, all lines are placed in MilliQ reservoir and two *Prime* methods are run. Columns are then removed and refrigerated to avoid bacterial growth (Watson, personal comm.).

1.7 ICP-MS

HR ICP-MS, or High Resolution Inductively Coupled Plasma – Mass Spectrometry has been widely preferred in the determination of iron in seawater due to its sensitivity and ability to resolve iron from other interferences (Worsfold et al., 2014). The sample is introduced into the plasma by aspiration and the plasma converts all atoms into ions and the solvent is removed. Ions are focused into the mass spectrometer via two interface cones called the sampler and the skimmer, and via electrostatic lenses (Wolf, 2005). The MS separates ions from their mass to charge ratio (m/z) with a quadrupole filter, where electric current is rapidly alternated between the four rods to select specific ions at a time. A rapid switch between rods allows the MS to separate many ions, allowing multielemental analysis. The high resolution MS uses both magnetic and electric sectors to reduce overlapping mass interferences, such as $Ar^{40}O^{16}$, from Fe^{56} (Wolf, 2005). Quantification determination of iron and other elements is typically done with isotope dilution where a known isotope blend is spiked to the sample and compared to an isotopically spiked calibration curve. The isotope dilution method in ICP-MS can be used in conjunction with a preconcentration method via chelation column such as SeaFAST, called online mode.

2 Objective and Hypothesis

The objective of our work is to evaluate the rate of change of iron concentrations over time in seawater during dark bottle decomposition of varying natural communities from the Cretan Sea. These natural communities will be subjected to two independent variables during a mesocosm experiment prior to dark bottle decomposition: a carbon gradient and grazing pressure. The increasing carbon gradient should stimulate bacterial communities and may affect the release of iron through increased iron mobilization, while an increase in zooplankton grazers may also influence the release of iron through increased predation and increased availability of natural organic ligands to complex iron.

Analytically, iron quantification will be done using SeaFAST in offline mode coupled with ICP-MS. As the NTNU SeaFAST instrument has not been evaluated yet, another objective of this thesis is to evaluate the use of this instrument through initial testing, quality control checks, and recovery of a known standard.

By varying the natural communities, the resulting biotic and abiotic factors will influence the rate of change of iron over time leading to variable and possibly non-linear rates of change. Increased grazing should facilitate an increase in dissolved iron concentrations while higher carbon gradients should increase bacterial activity.

3 Materials and methods

3.1 Pre-Experiment

For the decomposition experiment, 1L dark PE Nalgene™ bottles and 10L dark PE Nalgene™ bottles were used to ensure dark conditions and cleaned according to a modified trace metal clean procedure for timing purposes (Achterberg et al., 2001; Cutter et al., 2010). At Trondheim Biological Station (TBS), all bottles were washed with 3% alkaline detergent (Neodisher), filled with tap water and left to sit for three days. Then, bottles were emptied and rinsed three times with water and filled with 96% ethanol (VWR) for four days. Then, all bottles were emptied and rinsed four times with DI water and filled with 3M HCl for at least one week. Next, bottles were emptied and rinsed five times with DI water and filled with approximately 0.16M UltraPure HNO_3 for one week. Bottles were emptied, double bagged in plastic and transported to NTNU Gløshaugen Class 1000 clean lab for rinsing. All bottles were rinsed five times with 18 MΩ (MilliQ) water, emptied, and double-bagged until the beginning of the experiment.

At HCMR in Crete, trace metal subsampling collection tubes, PE bottles of either 50mL or 125mL, were filled with approximately 1M HCl, wrapped in plastic and placed in a sealed, opaque plastic box and left outside in the sun for several days. Sample tubes were then emptied and rinsed 2x with MilliQ water and finally 3x with seawater from the sample area. The final rinsing step took place in an entrance area of HCMR.

3.2 Mesocosm Experiment

Mesocosm collection ($1m^3$) tanks, incubation ($1.5m^3$) tanks, and collection and transfer hoses were cleaned and acid-washed with approximately 0.5M HCl, rinsed with water, and then acid-washed again. For final rinse, all equipment was rinsed with seawater to achieve an inner pH close to 8.1 for natural seawater incubation. Seawater characteristics from the collection site included salinity at ~39.18 and temperature at ~19°C. Collection tanks were taken by boat and filled with seawater off the coast of Heraklion at 35°24.957N, 25°14.441E, from approximately 10m depth and transferred to floating anchored incubation tanks in an outside pool via gravity flow through transfer hoses. A total of ten large tanks were in the outdoor pool, with five on each side. As part of the Ocean Certain project, tanks were separated based on their grazing (additional zooplankton) treatments and carbon gradients. Low grazing (LG) and high grazing (HG) were distinguished between odd and even numbers, respectively, and LG treatment water was filtered with a 200µm mesh into incubation tanks. HG treatments were distinguished by adding approximately 5 copepods L^{-1} that were collected from the same sampling site. Carbon gradient treatments were distinguished in number pairs, with zero glucose (0C) corresponding to the lowest number pair, tank 1 and 2, and 3C corresponding to the highest pair, tanks 9 and 10. All tanks were fitted with an input tube to allow addition of daily nutrients. Background concentrations of N_{Tot} ($NH_4 + NO_3 + NO_2$) from the collection site were measured at approximately 0.17µM. From May 11th, 2016 to May 22nd, 2016, nutrients glucose, nitrate, ammonium, phosphate and silicate were added once each day via the input tube at approximately 08:00 to stimulate phytoplankton production. Glucose concentration of 0C indicated no added glucose, 1C indicated Redfield ratio additions relative to ambient nitrogen concentration, and 3C indicated three times Redfield ratio of glucose relative to ambient nitrogen concentration. Tanks were mixed with a plastic paddle after nutrient addition. Measurements for bacterial production, TOC, POC, chlorophyll *a*, and nutrient concentrations were taken over the course of the experiment by the Ocean Certain team.

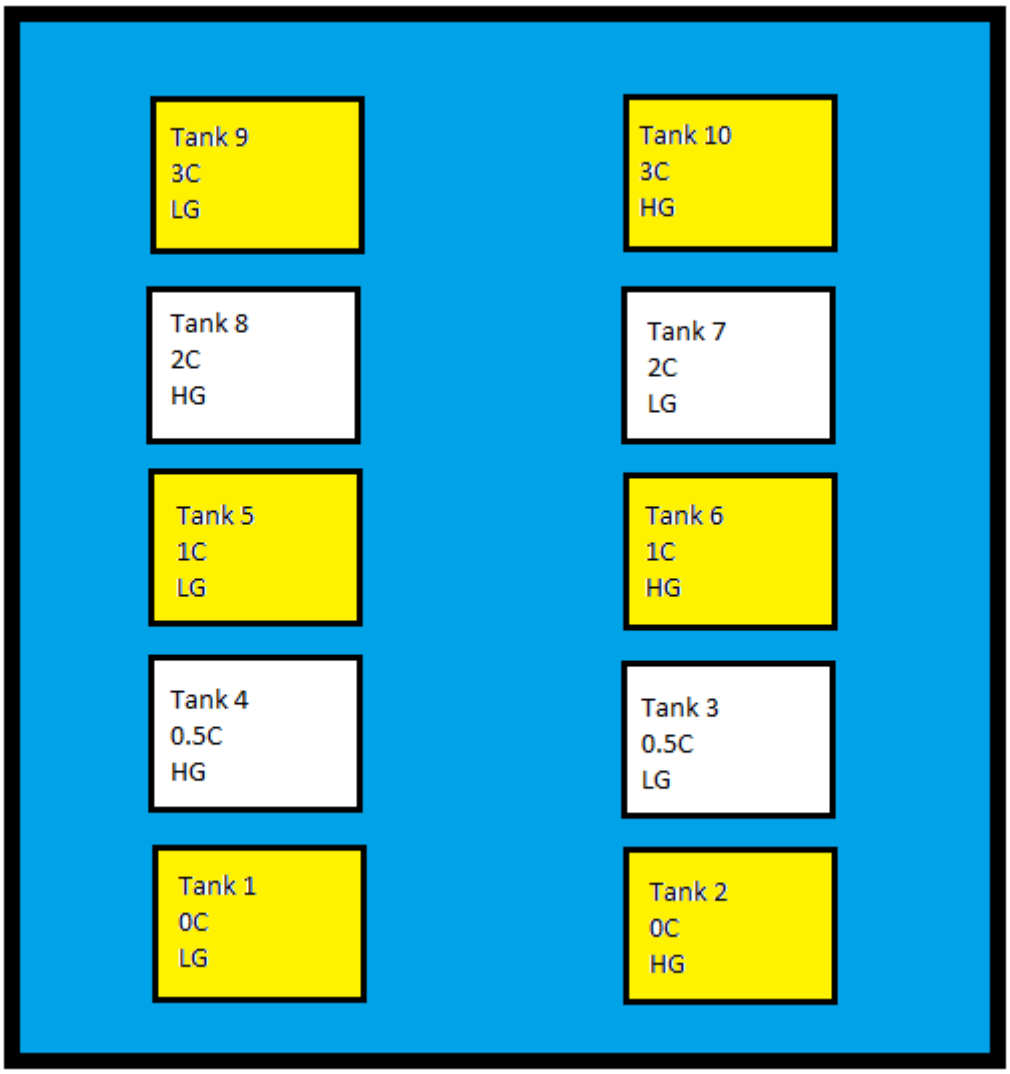

Figure 8: Mesocosm setup in outdoor pool. Tanks are labeled by number, carbon treatment, and whether LG or HG. Yellow tanks indicate tank water used for decomposition experiment.

3.3 Dark Bottle Experiment

After the mesocosm experiment, water from the initial mesocosm experiments were transferred to the dark trace metal clean PE Nalgene™ bottles for incubation. Right before collection, all bottles were rinsed three times with respective tank seawater before filling. Mesocosm tanks 1, 2, 5, 6, 9, and 10 were selected for the decomposition experiment, corresponding to 0C LG, 0C HG, 1C LG, 1C HG, and 3C LG, 3C HG, respectively. However, a summary report of the mesocosm experiment indicated that the zooplankton L^{-1} had swapped. It was decided that the odd numbered tanks would represent high grazing and the even numbered tanks would represent low grazing for the decomposition experiment. For each treatment, there were a total of ten dark 1L bottles, one dark 10L bottle and one trace metal clean 20L transparent collapsible bottle. Each set of bottles contained the same water from their respective tank treatment. All bottles were capped and double-bagged in black plastic and carried to a 21°C ± 0.43 temperature control room in HCMR at approximately 19:45 on May 23rd, 2016. Nutrient samples were to be taken from the 1L dark bottles. All trace metal samples and pH measurements were taken from the 10L dark bottle and the bottle was filled with seawater from the double-bagged, black plastic covered 20L collapsible bottle as necessary to minimize headspace as sample water is removed. The experiment lasted from May 24th, 2016 to May 29th, 2016.

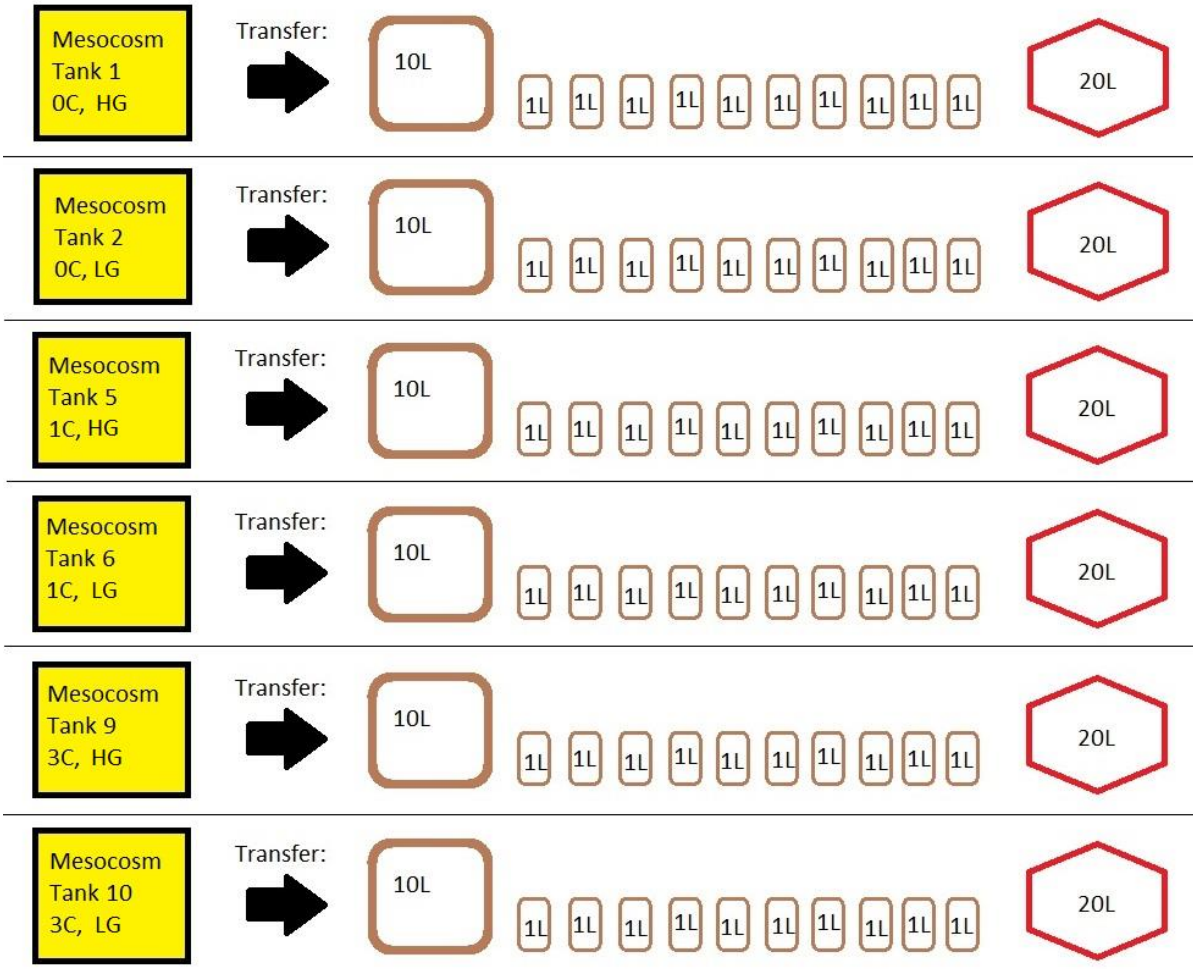

Figure 9: Decomposition Experiment Setup. Tank water from each respective mesocosm treatment was used to fill one 10L amber bottle, ten 1L amber bottles, and one 20L collapsible bottle.

Sampling and Timing

Nutrient samples for ammonium, nitrate, nitrite, phosphate, and silicate were taken on a time-based schedule from the start of the experiment. Samples were taken approximately once each day until the conclusion of the experiment. One 1 L dark bottle from each respective treatment was taken directly from the temperature control room and frozen until it was analyzed by HCMR's nutrient technicians at a later date. Due to the expected low levels of phosphate within Mediterranean water, phosphate was measured by the MAGIC method (Karl et al., 1992; Rimmelin et al., 2005)..

50mL and 125mL PE sampling bottles for trace metals were acid-washed and rinsed with seawater at HCMR prior to the decomposition experiment. Samples were collected for each respective treatment on a time-based schedule from the 10L dark bottle only. Approximately 800mL was collected from each 10L dark bottle via acid washed syringe in the temperature control room into a seawater-rinsed trace metal clean 1L dark bottle. Six bottles, one corresponding to each treatment were then carried to a constructed clean room inside HCMR for subsampling, filtration, and acidification.

Total dissolvable metal samples were collected in the acid-washed 50mL (or 125mL) sampling tubes by pouring directly from the 1 L dark bottle into the 50mL collection tubes after an initial rinse with sample seawater. Dissolved samples were filtered via gravity in the acid-washed and seawater rinsed 50ml (or 125ml) bottles through a cellulose acetate, 0.45µm + 0.2µm filter (Sartorius Sartobran). A total of two filters were used for the entire experiment. Between each tank grouping for dissolved samples, at least 50mL of sample seawater was allowed to drip through the filter to waste to eliminate possible cross contamination between treatments due to any dead volume in the filter. All samples, both total dissolvable and dissolved, were then acidified with 4.0M UltraPure HNO_3 to bring all samples to ~ pH 1.8-2 to release labile metals to solution and for preservation. While HCl is generally recommended for preservation of trace metal samples due to HNO_3 being a strong oxidizing agent (Cutter et al., 2010), HNO_3 was selected because HCl available did not meet ultrapure requirements. Subsamples for each treatment were initially taken in triplicate, however a shortage of sample collection tubes reduced subsequent sampling periods to a total of two total dissolvable, two dissolved for each decomposition treatment. A total of six time periods from the start of the experiment were measured for trace metals. All samples were double bagged and boxed for transport back to NTNU Gløshaugen clean lab. After collection and preservation of trace metal

samples, the remaining water in the 1L collection bottles was measured for pH using a two-point calibrated PHM 203 pH Meter from Meterlab. See Table 1 for sampling scheme.

Table 1: Sampling scheme for decomposition experiment indicating time and sample type

Date	Time, Sample taken
23 May 2016	-1945hr, bottles in dark room
24 May 2016	-1015hr, nutrient -1500hr, trace metals reference, pH -1730hr, nutrient -2200hr, trace metals, pH
25 May 2016	-0030hr, nutrient -1225hr, nutrient, trace metals, pH
26 May 2016	-1220hr, nutrient, trace metals, pH
27 May 2016	-1220hr, nutrient, trace metals, pH
28 May 2016	-1225hr, nutrient, trace metals, pH
29 May 2016	-1225hr, nutrient, trace metals, pH
30 May 2016	-1400hr, TOC, POC

POC and TOC measurement

On the final day of the experiment, POC measurement was carried out using a glass fiber filter (GF/F) technique. 1.5L of treatment seawater was filtered and collected on a precombusted Whatman filter pore size 0.2µm. Filters were removed, folded, and wrapped in aluminum foil and frozen for later analysis. TOC measurement was collected by pouring treatment seawater into a sample rinsed 40mL vial. Samples were then acidified with ~3M HCl to bring pH to ~2 for conversion of inorganic carbon to CO_2 and subsequently frozen. Two TOC samples were collected for each decomposition treatment. TOC analysis was conducted by Total Organic Carbon Analyzer (Shimadzu) by Mathew Avarachen at GEOMAR in Kiel, Germany. This instrument utilizes high temperature combustion to turn all remaining organic carbon into carbon dioxide and is subsequently measured by non-dispersive infrared analysis (ShimadzuCorporation, 2014.). POC and PON analysis was performed at TBS by Kjersti Andresen. The filter is combusted at high heat to convert POC to CO_2 and PON to N_2 and subsequently measured. The concentration of DOC can be estimated by subtracting POC from TOC.

3.4 Trace Metal Analysis by SeaFAST

The SeaFAST autosampler was moved to the NTNU Gløshaugen Class 1000 clean lab and was set up for initial testing and evaluated for the creation of an NTNU User's Protocol. All laboratory work was performed in the Class 1000 clean lab wearing VWR nitrile gloves and under an AirClean work station when necessary to reduce any trace metal contamination.

Instrument Parameters

Used for elution pressure, argon gas pressure recommended by the manufacturer to be at 1.0 bar was evaluated through a series of trial runs by submersing all solution lines into 18.4 MΩ (MilliQ) water and running both the *Prime* and *Sample Run* methods on the instrument. Initial observations revealed that the autosampler probe was at an inadequate height and spraying solution inside the clean enclosure during probe rinsing and sample elution steps. For the *Prime* method, an additional step was added as "Probe Down" while the probe was at the rinse station to avoid spray. For the *Sample Run* method, probe height was edited "-20Z" from initial method starting height. This height was edited specifically for the PTFE collection tubes and corresponds to a probe depth to avoid sample spray out of the tube and to avoid the probe touching the final elution volume. Probe depth was also edited for sample acquisition tubes, to allow full volume pickup without touching the bottom of the tube.

To test elution volume accuracy and precision, a series of trial runs of elution volume at 2mL using MilliQ water was first visually compared against an Eppendorf multipipette volume to evaluate SeaFAST elution volume. Initial inspection prompted each tube to be weighed with a Mettler balance after dispensing of elution solvent for evaluation of precision and accuracy. Additionally, final sample dilution with Eppendorf pipette to 3mL was also evaluated for precision and accuracy. Volume evaluation was done at 1mL elution and 2mL dilution with MilliQ due to ICP-MS volume requirements. A summary of the precision and accuracy of both the SeaFAST and Eppendorf pipette is in Table 2. The instrument is calibrated for the listed volumes only.

Table 2: Summary of SeaFAST precision and accuracy and Eppendorf multipipette precision and accuracy. *For density of 1.5M HNO_3 solution at 20°C. **For density of pure water at 20°C.

	SeaFAST (1mL*) (n=20)	Eppendorf multipipette (2mL**) (n=20)
Precision	0.97g ± 0.03	2.0g ± 0.03
Accuracy	93% ± 2.9	99% ± 1.2

After the final trial run, a NTNU SeaFAST Protocol was written and a Usage Log created to follow and update with each SeaFAST run from this date forward. See Appendix D for an attachment of the SeaFAST protocol. The *Prime* method was to be run at least once each day prior to instrument run.

Blank and Standard Runs

All SeaFAST solution bottles were acid washed for 2 days in 0.1M Ultrapure HNO_3 prior and rinsed five times with MilliQ. Solutions were prepared with trace metal clean reagents. The buffer solution was prepared by mixing Suprapur® 25% ammonium hydroxide (NH_4OH) solution (Merck KaGa) and Suprapur® glacial acetic acid (100%, Merck KaGa) in MilliQ water and adjusted to reach manufacturer recommended pH 6.0 ± 0.2 and confirmed by outside analysis that initial buffer variability does not affect system recovery (Lagerström et al., 2013). A PHM 203 pH meter was calibrated with WTW buffer solutions for two-point calibration curve at pH 4.0 and pH 7.0. All SeaFAST buffer solutions were measured prior to use. The elution solvent was prepared by diluting concentrated Ultrapure HNO_3 with MilliQ to reach final concentration of 1.5M. The rinse solution for the probe was prepared by diluting concentrated Ultrapure HNO_3 with MilliQ to reach concentration of 0.1M.

Sample collection tubes were PTFE Teflon™ tubes that were acid washed for at least one week with 1.0M Ultrapure HNO_3 solution. All tubes were rinsed five times with a MilliQ water gradient to remove any acid remnants. A set of 20mL PE bottles were acid washed in 1.0M Ultrapure HNO_3 solution for use as either blanks or standards. All bottles were rinsed with a MilliQ water gradient five times prior to use. Blank samples were taken directly as both MilliQ water or prepared as matrix-matched ~3.5% ultrapure NaCl solution prepared from an ultra clean 10-11% NaCl solution (ESI). Reference material was taken from NASS-6 standard bottle (National Research Council Canada). Test runs for blanks and reference standards were run as full procedural samples according to the NTNU SeaFAST protocol, going through the full SeaFAST preconcentration method. After preconcentration, both blanks and reference samples were diluted with 2mL MilliQ for ICP-MS analysis. Blanks were evaluated for background concentrations and the NASS-6 reference material was evaluated for accuracy and precision. A summary of test runs for full procedural MilliQ blanks uncorrected for preconcentration is presented in Table 3, selected metals corrected for preconcentration in Table 4 and a summary of NASS-6 SeaFAST values were compared against the certified reference in Table 5.

Table 3: ICP-MS full SeaFAST procedural MilliQ test blank elemental quantification not corrected for preconcentration values. L=Low, M=Mid, H=High, R=Resolution, respectively. If mean<LOD-25%, nd=none detected. For n=12, elements not tested for some blank runs. For 12<n<26, blanks discarded if >3xStdDev.

Element	Mean (µg/L)		Std Dev
Cd114(LR) (n=26)	0,0001	±	0,0005
Mo98(MR) (n=26)	0,740	±	1,26
Sn118(LR) (n=26)	0,0424	±	0,0542
Ce140(LR) (n=26)	0,0002	±	0,0002
Pr141(LR) (n=26)	nd		
Nd146(LR) (n=12)	0,0001	±	0,0002
Sm147(LR) (n=12)	nd		
Tb159(LR) (n=26)	nd		
Dy163(LR) (n=26)	nd		
Ho165(LR) (n=12)	nd		
Er166(LR) (n=26)	nd		
Tm169(LR) (n=26)	nd		
Yb172(LR) (n=26)	nd		
Lu175(LR) (n=26)	nd		
Hf178(LR) (n=26)	0,0002	±	0,0004
Pb208(LR) (n=26)	0,0402	±	0,0362
Th232(LR) (n=26)	nd		
U238(LR) (n=26)	0,0009	±	0,00330
Al27(MR) (n=26)	0,462	±	0,229
Ti47(MR) (n=26)	0,0124	±	0,0096
V51(MR) (n=26)	0,0056	±	0,0088
Mn55(MR) (n=26)	0,0144	±	0,0109
Fe56(MR) (n=26)	0,197	±	0,108
Co59(MR) (n=26)	0,0030	±	0,0027
Ni60(MR) (n=19)	1,87	±	0,868
Cu63(MR) (n=26)	0,0820	±	0,0565
Zn66(MR) (n=22)	1,12	±	0,867
Ga69(MR) (n=26)	nd		
Sr88(MR) (n=26)	0,0771	±	0,0852
La139(MR) (n=26)	0,0010	±	0,0025
Nb93(HR) (n=26)	0,0005	±	0,0006
Eu155(HR) (n=12)	nd		
Gd155(HR) (n=26)	nd		

When corrected for preconcentration according to equation 7 and then converted to nM, the full procedural blank test values for selected metals Cd, Co, Cu, Mn, Fe, Ni and Zn are presented in Table 4.

Table 4: Selected procedural MilliQ blank values for selected metals

Element	Mean (nM)		Std Dev.
Cadmium	0.001	±	0.001
Manganese	0.079	±	0.059
Iron	1.06	±	0.579
Cobalt	0.016	±	0.014
Nickel	9.54	±	4.44
Copper	0.387	±	0.267
Zinc	5.13	±	3.98

NASS-6 values were corrected for preconcentration according to equation 7. In equation 7, C_f represents the final concentration, C_r represents the raw data concentration, V_f represents the final volume (3mL for ICP-MS delivery) and V_s represents the amount of sample preconcentrated. See Appendix A, Figure A.1 for all NASS-6 testing data.

Equation 7

$$C_f = \frac{C_r * V_f}{V_s}$$

Table 5: Undiluted NASS-6 by SeaFAST corrected for preconcentration values compared against certified reference value. Modified from National Research Council Canada. *Informative value only

Element	SeaFAST Value µg/L (n=6)	Certified Value µg/L	Accuracy
Cadmium	0.0305 ± 0.0008	0.0311 ± 0.0019	98%
Cobalt	0.015 ± 0.0009	0.015*	102%
Copper	0.249 ± 0.0108	0.248 ± 0.025	101%
Iron	0.499 ± 0.0341	0.495 ± 0.046	101%
Lead	0.0132 ± 0.0107	0.006 ± 0.002	220%
Manganese	0.489 ± 0.007	0.530 ± 0.050	91%
Molybdenum	4.521 ± 1.076	9.89 ± 0.72	46%
Nickel	0.611 ± 0.189	0.301 ± 0.025	203%
Vanadium	1.248 ± 0.0374	1.46 ± 0.17	86%
Zinc	0.617 ± 0.207	0.257 ± 0.020	240%

High values of some background metals within MilliQ Blanks (Table 4), prompted system cleaning with elution solvent and MilliQ as recommended by manufacturer and described in section 1. 6 before analysis of Crete samples.

Sample Runs

Analysis of Crete samples occurred approximately six months after acidification in November 2016 (Ussher et al., 2013; Worsfold et al., 2014). PTFE Teflon™ tubes were acid-washed in 1.0M Ultrapure HNO_3 for at least one week. One day before SeaFAST preconcentration, each sequence of tubes was rinsed five times with a MilliQ water gradient, capped and placed in the AirClean laminar flow hood before use to reduce contamination from dust particles.

All SeaFAST solutions were prepared according to the NTNU SeaFAST protocol and blanks and reference standards were prepared each day in acid-washed 20mL PE bottles. For each run, a sequence was modified, saved and instrument parameters were recorded. The NTNU SeaFAST protocol was followed for all sample runs. Seawater samples were kept in their original PE bottles and positioned accordingly within the SeaFAST clean enclosure. Seawater sample volume was either 10mL or 20mL, corresponding to 1 sample or 2 sample loops, while elution volume remained the same at 1000µL. Full procedural blanks as MilliQ water and NASS-6 reference were run among Crete samples to track any changes in SeaFAST reproducibility. Samples were diluted to 3mL after elution with MilliQ water to fit ICP-MS requirements and subsequently delivered for ICPMS analysis of 33 elements. If SeaFAST solutions were running low, they were prepared as necessary and noted in the Usage Log. After sequence run samples were kept capped and stored covered in plastic in ventilation hood. Samples were delivered in two main batches for ICP-MS.

3.5 Statistics

Accuracy most typically evaluates the level of closeness of a result to reference value, while trueness also compares the level of closeness and includes the systematic and random error of those measurements (ISO). Precision evaluates the set of measurements in agreement with one another. In this thesis, accuracy (trueness) is expressed as a percentage to a known reference value while precision is expressed as a standard deviation of a set of measurements. Specifically, the accuracy of SeaFAST volume dispensing and SeaFAST NASS-6 test and sample values is reported. The precision of the SeaFAST volume dispensing and of SeaFAST NASS-6 test and sample values is expressed as standard deviations.

A one-sample t-test or one-sample Z-test is used to compare the mean of a population with that of a known population mean or of a known population mean with known standard deviation, respectively. Four assumptions are made, in that the dependent variable is continuous, data is independent, no significant outliers, and data is normally distributed (Laerd, 2013). The one-sample t-test was used to compare Co mean to the NASS-6 reference value while the one-sample Z-test was used to compare other trace metal means to the NASS-6 reference value means. These tests were performed in SPSS. Output at 95% confidence interval with a p-value of <0.05 indicates statistical significance.

An independent two-sample t-test compares the means between populations against the same dependent variable, which is trace metal concentration. It uses the same assumptions as the one-sample t-test in addition that the two populations are independent from one another and there is homogeneity of variances (Laerd, 2013). A two-sample t-test can also be run under the assumption that variances are not equal, with both types of two-sample t-tests reporting significance at a chosen $p<0.05$. In this thesis, an unequal variance two-sample independent t-test was run comparing the value of MilliQ full procedural blanks against the ~3.5% NaCl solution full procedural blanks as well as rate comparisons between high and low grazing groups. Unequal variance assumption was used due to the large difference in *n* and was performed in Excel with the Data Analysis add-on.

A one-way analysis of variance, or ANOVA, is a parametric test used to compare means between two or more groups from one continuous dependent variable. A one-way ANOVA assumes that the data is normally distributed within each group, homogeneity of variances, and independence of observations (Laerd, 2013). At confidence interval 95%, p-value is statistically significant at $p<0.05$. In SPSS, each ANOVA is run with Levene's test for equality of variance to indicate if the data has violated the variance assumption. A statistically significant p-value (<0.05) for Levene's test indicates variance equality was violated. A more robust ANOVA test for variance violations is Welch's ANOVA, which was also tested with the traditional one-way ANOVA. If p-value is significant a post hoc test can be run which can indicate which groups are different. Tukey's HSD post hoc test was run with the ANOVA when variances were statistically equal, and a Games-Howell post hoc test was run with Welch's ANOVA if variances were different. The post-hoc tests can indicate which groups are statistically different ($p<0.05$) from one another. The ANOVA tests and subsequent post hoc tests were performed with SPSS statistics and conducted for differences in tank concentrations, rates at different times, and rates between carbon gradient groups. All statistical tests and tables are presented in Appendix B.

4 Results

4.1 SeaFAST Controls

SeaFAST MilliQ full procedural blank values for selected metals along with full descriptive statistics are presented in Table 6. Blanks suspected of contamination were removed from analysis.

Table 6: MilliQ SeaFAST procedural blanks in nM.

Descriptive Statistics						
	N	Range	Minimum	Maximum	Mean (nM)	Std. Deviation
Fe Blank Conc. MilliQ	31	1.23	.106	1.34	0.415	± 0.255
Mn Blank Conc. MilliQ	38	.186	.0009	.187	0.0213	± 0.0319
Cd Blank Conc. MilliQ	38	.00260	-.0003	.0023	0.000340	± 0.0005
Cu Blank Conc. MilliQ	34	.188	.0272	.215	0.0878	± 0.0541
Ni Blank Conc. MilliQ	28	13.3	.748	14.0	2.85	± 3.28
Zn Blank Conc. MilliQ	34	8.26	.259	8.51	1.55	± 2.24
Co Blank Conc. MilliQ	36	.0993	.0015	.101	0.0191	± .0220

Iron had a mean MilliQ blank value of 0.415nM ± 0.255, representing the background concentration of iron within the SeaFAST system as MilliQ, buffer, elution solvent, and any background material within the SeaFAST itself and sample tubes. A one-way Z-test was performed comparing the Crete sample means to the test sample means. A statistically significant p-value of <0.05 rejects the null hypothesis that the two means are the same. Z-tests were performed for all selected metals and found statistical significance between six of the seven means. Fe, Mn, Cd, Cu, Ni, and Zn from Crete samples all had statistically different and lower means than the initial testing. See Appendix B, Table B.1 for Z-statistics and associated p-values.

The ~3.5% NaCl solution full procedural blanks and associated descriptive statistics for selected metals are presented in Table 7.

Table 7: ~3.5% NaCl (matrix-matched) SeaFAST procedural blanks in nM

Descriptive Statistics						
	N	Range	Minimum	Maximum	Mean (nM)	Std. Deviation
Matrix Fe	6	.390	.459	.849	0.607	0.141
Matrix Mn	6	.0375	.0364	.0739	0.0556	0.0160
Matrix Cd	6	.0012	.0001	.0012	0.000658	0.000455
Matrix Cu	6	.0231	.145	.168	0.155	0.00859
Matrix Ni	6	1.456	5.07	6.52	5.76	0.566
Matrix Zn	6	16.2	16.2	32.3	25.4	6.92
Matrix Co	6	.0113	-.0045	.0068	0.00283	0.00394

Iron had a mean ~3.5% NaCl matrix-matched blank value of 0.607nM ± 0.141, representing the background concentration of iron within the SeaFAST system as NaCl stock solution background iron concentration plus all previously mentioned sources of additional iron for MilliQ blanks. An independent two-sample t-test with Levene's test for equality of variances was performed for iron comparing the MilliQ blank mean to the ~3.5% NaCl solution blank mean. Levene's test was not statistically significant, indicating that the variances are the same. The p-value for the t-test under equal variance was 0.084, with failure to reject the null hypothesis. However, if unequal variances are assumed due to difference in *N*, a statistically significant p-value of 0.022 rejects the null hypothesis. On observation, the MilliQ blank mean versus the NaCl blank mean are similar to each other, with the MilliQ mean slightly lower than the NaCl solution mean.

The NASS-6 control values obtained during Crete sample testing are presented in nM after correcting for preconcentration and subtracting background MilliQ blank values for the seven selected metals in Table 8. Blanks values are included in correction due to the high background concentrations of metals. The accuracy of the metals is compared against the NASS-6 reference values provided by NRCC.

Table 8: Undiluted NASS-6 by SeaFAST for selected metals corrected for preconcentration and MilliQ blank background values compared against certified reference value. Modified from National Research Council Canada. *Informative value only

Element	SeaFAST Value µg/L (n=13)	Certified Value µg/L	Accuracy
Cadmium	0.027 ± 0.002	0.0311 ± 0.0019	94%
Cobalt	0.012 ± 0.0015	0.015*	79%
Copper	0.194 ± 0.016	0.248 ± 0.025	78%
Iron	0.414 ± 0.037	0.495 ± 0.046	84%
Manganese	0.420 ± 0.031	0.530 ± 0.050	79%
Nickel	0.207 ± 0.095	0.301 ± 0.025	69%
Zinc	0.244 ± 0.183	0.257 ± 0.020	95%

Recovery of all metals appeared to decrease as Fe's mean Crete sample value was 0.414µg/L ± 0.037 and an accuracy of 84%. The other selected trace metals also decreased in accuracy. Zinc and nickel appeared much closer to NASS-6 reference value than initial testing yet Zn and Ni also had large standard deviations relative to the mean value. A one-sample Z-test was performed on the Crete samples NASS-6 Fe mean value compared to the reference value. A statistically significant p-value of <0.0001 indicated that the NASS-6 mean obtained during Crete sample testing was lower than the certified value.

4.2 Crete Samples – Dissolved Iron (<0.2µm)

After correction for preconcentration from equation 7, subtraction of MilliQ blank value from Table 6 and conversion to nM, initial trace metal dissolved iron results indicated a large variation within data, particularly from parallel measurements from subsampling. While some parallel samples from the same tank at the same period showed consistency between each other, other parallel samples showed large differences possibly due to intermittent and random levels of contamination.

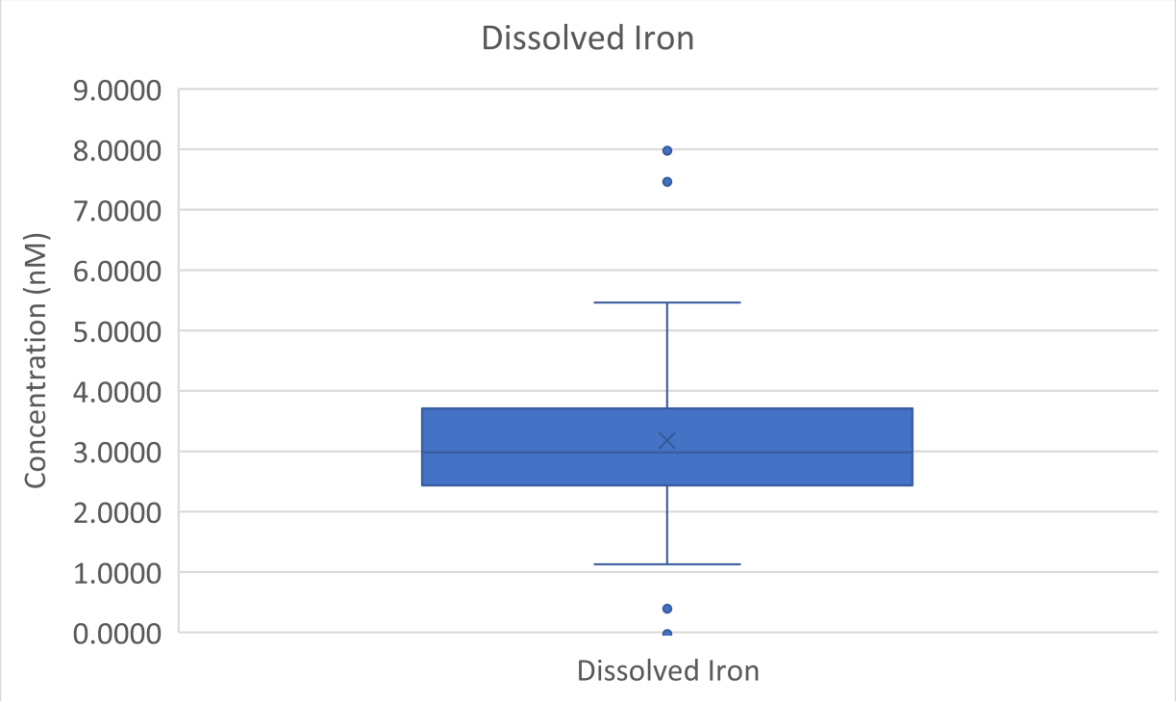

Figure 10: Dissolved Iron (dFe) box and whisker plot for Crete samples in nM not including suspected contaminated samples.

The average concentration of all samples including outliers was 5.97nM ± 10.5. Several samples were much higher than this average and considered suspect for contamination. High values with a large difference between parallels or clear outliers are presented in italics in the raw data in Appendix A, Table A.1; however, they are excluded from the remainder of the analysis entirely. When outlying data points are removed, the average dissolved iron concentration of all tanks was 3.18nM ± 1.36, with n=55, shown in Figure 10.

The 1st sampling period (31hrs) is disconnected from the Time 0 as initial concentrations taken from mesocosm tanks before transfer to decomposition bottles may not accurately reflect true concentrations at the start of the decomposition experiment and can only be speculated. The final sampling period, at 140hrs, is also removed as several tanks suggested levels of contamination.

The following figure represents dissolved iron, <0.2µm filtered, over time for each individual tank. A reference starting concentration from mesocosm tanks was 5.33nM ± 2.11. Odd tank numbers represent high grazing, while even tank numbers represent low grazing. Tanks 1 and 2 represent carbon treatment 0C; tanks 5 and 6 represent carbon treatment 1C, and tanks 9 and 10 represent carbon treatment 3C.

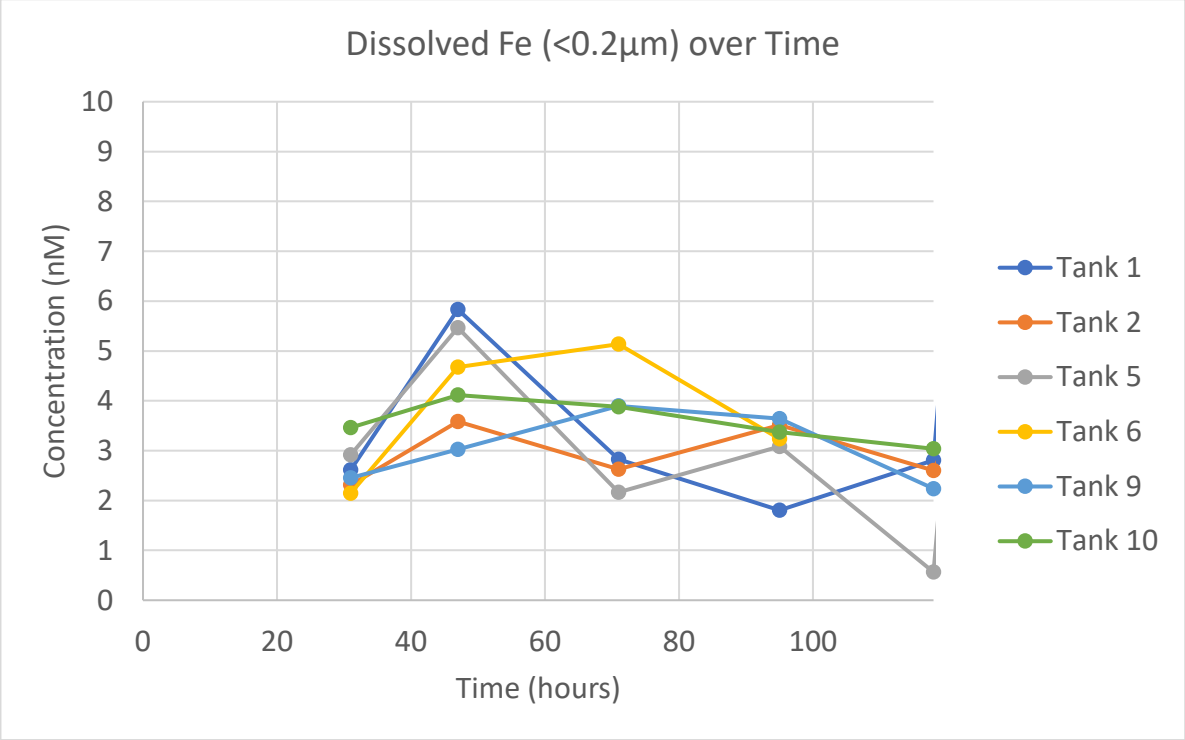

Figure 11: Dissolved iron concentrations (nM) over time for each individual tank. Last time period removed for suspected contamination.

At the first sampling period, most tanks show a first concentration lower than the average mesocosm concentration. From Time 1 (31hrs) to Time 2 (47hrs), all tanks showed an increase in dissolved iron as expected, with Tanks 1, 5, and 6, showing sharper increases with time compared to Tanks 2, 9, and 10. From Time 2 to Time 3, Tanks 1, 2, 5, 10 showed decreases in iron concentration while Tanks 6 and 9 continued to increase. From Time 3, tank concentrations appeared to fluctuate among each tank, with four tanks decreasing in concentration and two tanks increasing. Time 5 was removed for Tank 6 as dissolved iron levels were higher than total dissolvable iron levels (see Figure 15), indicative of

contamination. To assess for differences between concentrations of different tanks, a one-way ANOVA was run to compare dissolved iron concentrations and tanks. A p-value of 0.477 indicated that the concentrations between tanks were not significantly different.

Rates were then calculated from Time 1 to Time 2 for all tanks and are presented in Table 9.

Table 9: Calculated rates of change of iron during between Time 1 and Time 2 (16hrs)

Tank	**Rate**
1 (HG, 0C)	0.201 nM dFe hr^{-1}
2 (LG, 0C)	0.079 nM dFe hr^{-1}
5 (HG, 1C)	0.159 nM dFe hr^{-1}
6 (LG, 1C)	0.158 nM dFe hr^{-1}
9 (HG, 3C)	0.036 nM dFe hr^{-1}
10 (LG, 3C)	0.041 nM dFe hr^{-1}

For the initial rate, the tanks appear to be divided according to their carbon gradient, rather than grazing status, although Tank 2 does not follow a similar rate of increase as compared to Tank 1.

To visually represent the rates of change over time, the slope between each time period was graphed for each decomposition treatment and presented in Figure 12. The X-axis, labeled as 1, 2, 3, 4 represents the difference in time between sampling time 1 and 2, 2 and 3, 3 and 4, and 4 and 5, respectively. A positive value on the y-axis indicates an increase in dFe while a negative value indicates a decrease in dFe.

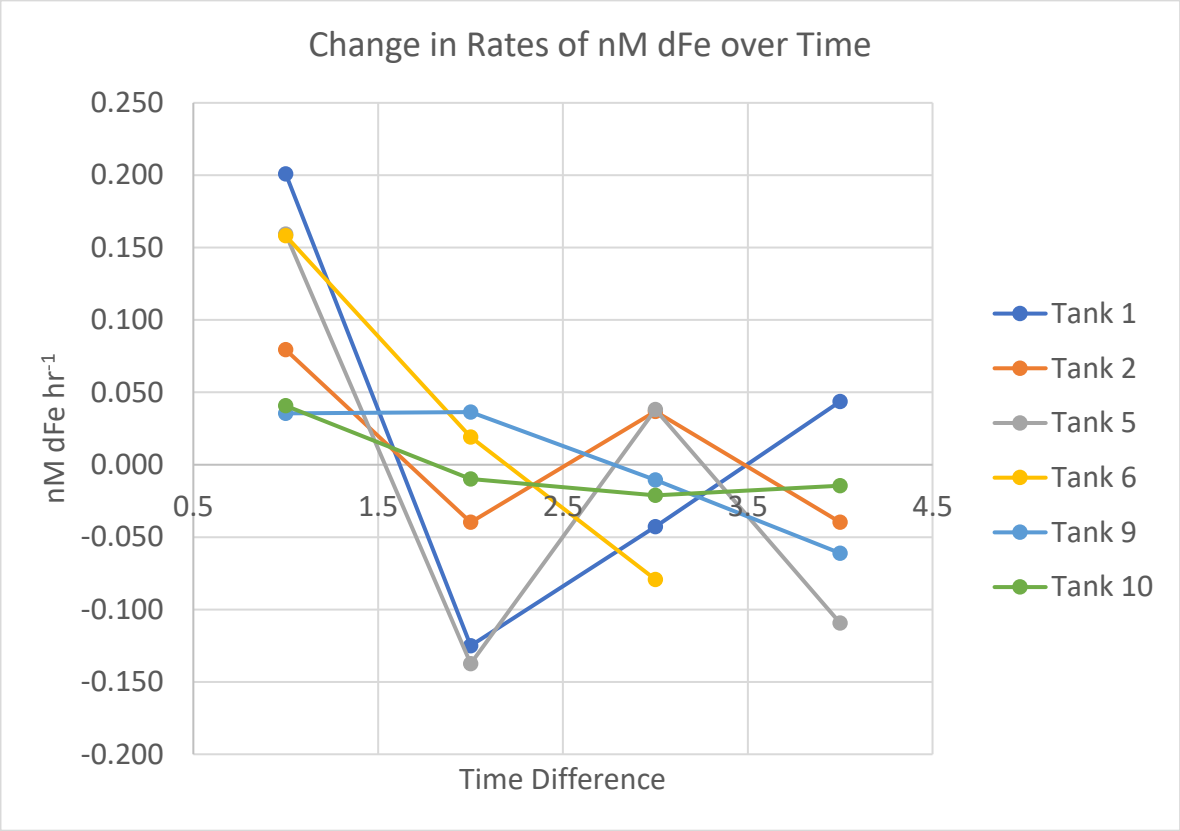

Figure 12: Change in rates of dissolved iron over time differences.

At time difference 1, all tanks have a positive rate of change. Afterwards, tanks appear to diverge on their rate of iron change. At time difference 2, tanks 1, 2, 5, 10 have a net decrease of iron although the rate of change appears to be sharpest for tanks 1 and 5 while tanks 6 and 9 continue to have a positive rate. However, all rates of iron decrease from the initial rate. At time difference 3 and 4, all tanks continue to have a rate of change of iron lower than the initial value at time difference 1. Tanks 1 and 2 both show an increase in rate of change of iron at time difference 3 relative to time difference 2. Tanks 9 and 10 show the smallest fluctuation in rates of change. A statistically significant one-way ANOVA (p-value = 0.001) with Tukey's test indicated that Time difference 1 was significantly higher than Time difference 2, 3 and 4 with p-values of 0.002, 0.015, and 0.005 respectively.

To visually compare for differences in treatments, group rates were combined and averaged as high grazing and low grazing, or according to their respective carbon gradients.

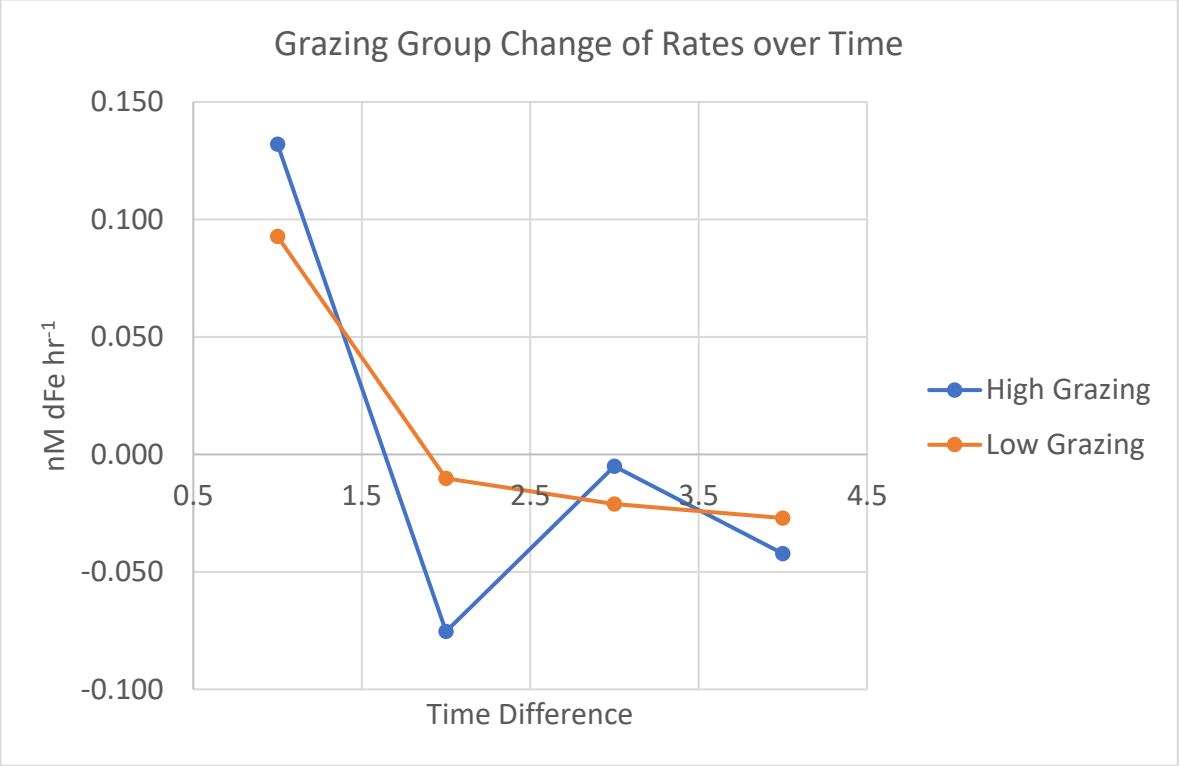

Figure 13: Grazing treatment group dissolved iron rates over time differences.

As groups, the high grazing group had a higher rate than the low grazing group initially. Then, the initial positive rate changed to net negative rate, corresponding to a decrease in iron concentration. The high grazing group also showed a sharper decrease relative to the low grazing group. A two-sample t-test assuming unequal variances was run comparing the rates of high grazing vs. low grazing at time difference 1 and a two-tailed p-value of 0.54 indicated non-significance between the two rates.

Table 10: Calculated rates of change of iron between grazing groups between Time 1 and Time 2

Group	**Rate**
High Grazing (1, 5, 9)	0.132nM dFe hr^{-1}
Low Grazing (2, 6, 10)	0.093nM dFe hr^{-1}

The tanks were also grouped according to carbon gradient.

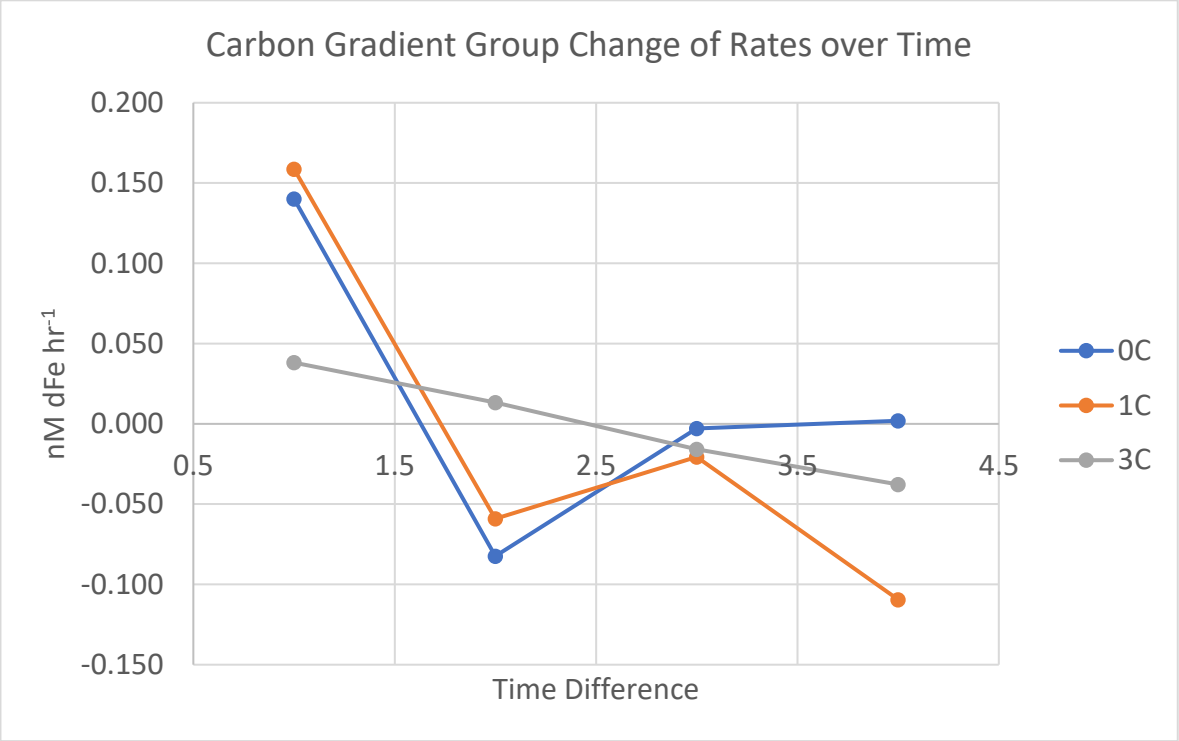

Figure 14: Carbon gradient groups of dissolved iron rates over time differences

At Time difference 1, both 0C and 1C groups exhibited higher rates of increase compared to 3C. From Time difference 1 to Time difference 2, groups 0C and 1C showed a faster rate of change than group 3C. At Time difference 2, both groups 0C and 1C showed a net negative rate, while group 3C showed a net positive rate. However, all groups decreased in release rate relative to Time difference 1. A one-way Welch's ANOVA with Games-Howell was run for comparing rates between groups at Time difference 1. Welch's ANOVA produced a statistically significant p-value of 0.008, indicating one of the groups was statistically different. Games-Howell post hoc test indicated that with a p-value of 0.015, the 1C group rate was statistically different from the 3C group rate.

Table 11: Calculated rates of change of iron between carbon gradient groups from Time 1 to Time 2

Group	Rate
0C	0.140nM dFe hr^{-1}
1C	0.159nM dFe hr^{-1}
3C	0.038nM dFe hr^{-1}

4.3 Crete Samples – Total Dissolvable Iron (>0.2µm)

Total dissolvable samples, or unfiltered acidified seawater samples, can also be subject to contamination and showed similar patterns of inconsistency among parallel samples suggestive of contamination, however no total dissolvable samples were removed from analysis as high levels are possible (Ardelan, personal comm.).

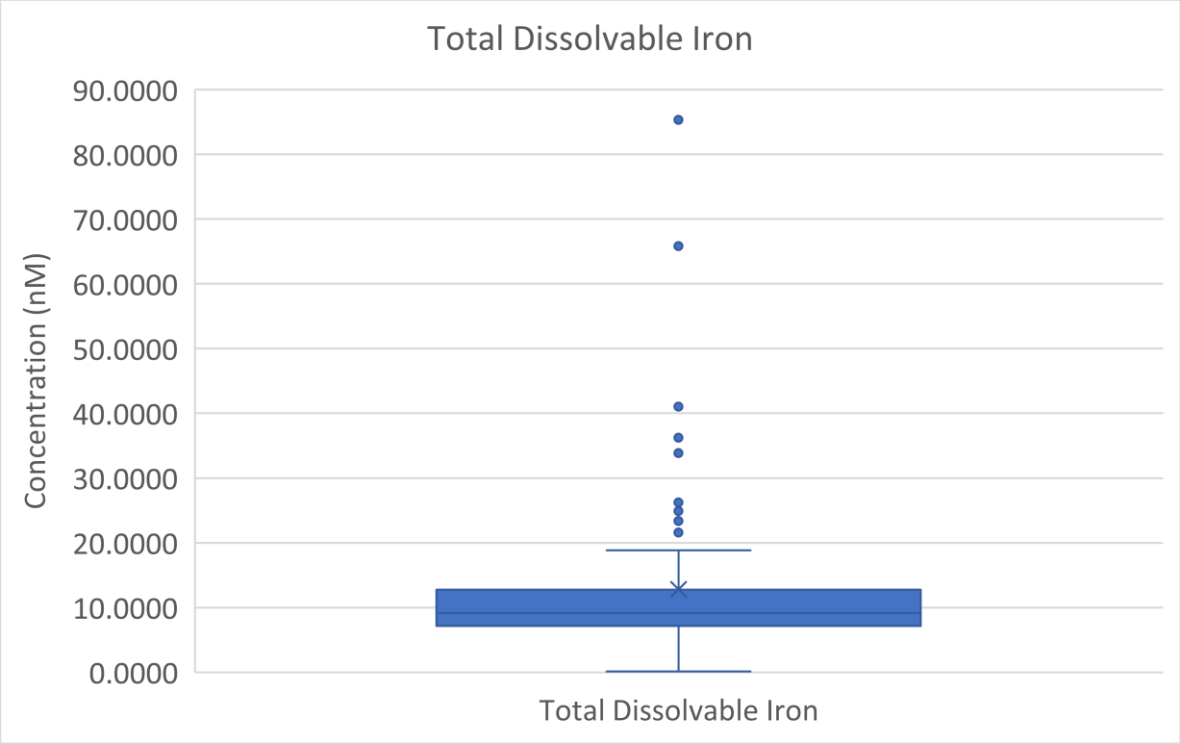

Figure 15: Total dissolvable iron (TFe) in nM

The average of all Crete samples for total dissolvable iron was 12.8nM ± 12.9, indicating a wide range of concentrations. Several samples were above one standard deviation.

Similar to dissolved samples, total dissolvable concentrations are disconnected to Time 0. The concentration of total dissolvable iron from the mesocosm tanks was 12.5nM ± 9.55. To correspond with dissolved sample graph (Figure 11), Time 6 is also removed.

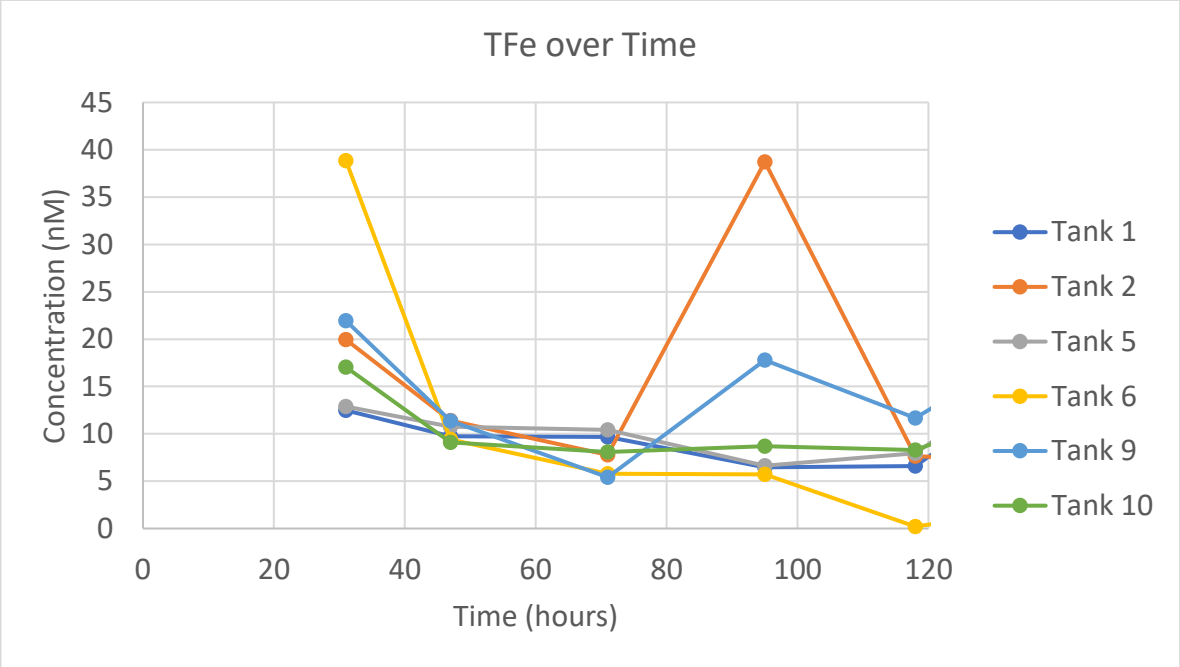

Figure 16: Total dissolvable iron concentrations over time for each individual tank.

TFe values for all tanks showed an initial decrease from Time 1 to Time 3, with Tank 6 exhibiting the largest decrease. From Time 3 to Time 5, tanks 1, 5, 6, and 10 showed relatively stable yet decreasing concentrations of TFe, while Tanks 2 and 9 showed increases at Time 4. By Time 5, Tank 6 had decreased to the lowest value observed. All tanks and fluctuation generally remained within the initial mesocosm reference range. Excluding Time 4 for Tank 2 and 9, all tanks seemed to exhibit relatively steady yet slightly decreasing values over the course of the experiment.

To visually represent the rates of change over time, the slope between each time period was graphed for each decomposition treatment and presented in Figure 17. The X-axis, labeled as 1, 2, 3, 4 represents the difference in time between sampling time 1 and 2, 2 and 3, 3 and 4, and 4 and 5, respectively. A positive value on the y-axis indicates an increase in TFe while a negative value indicates a decrease in TFe.

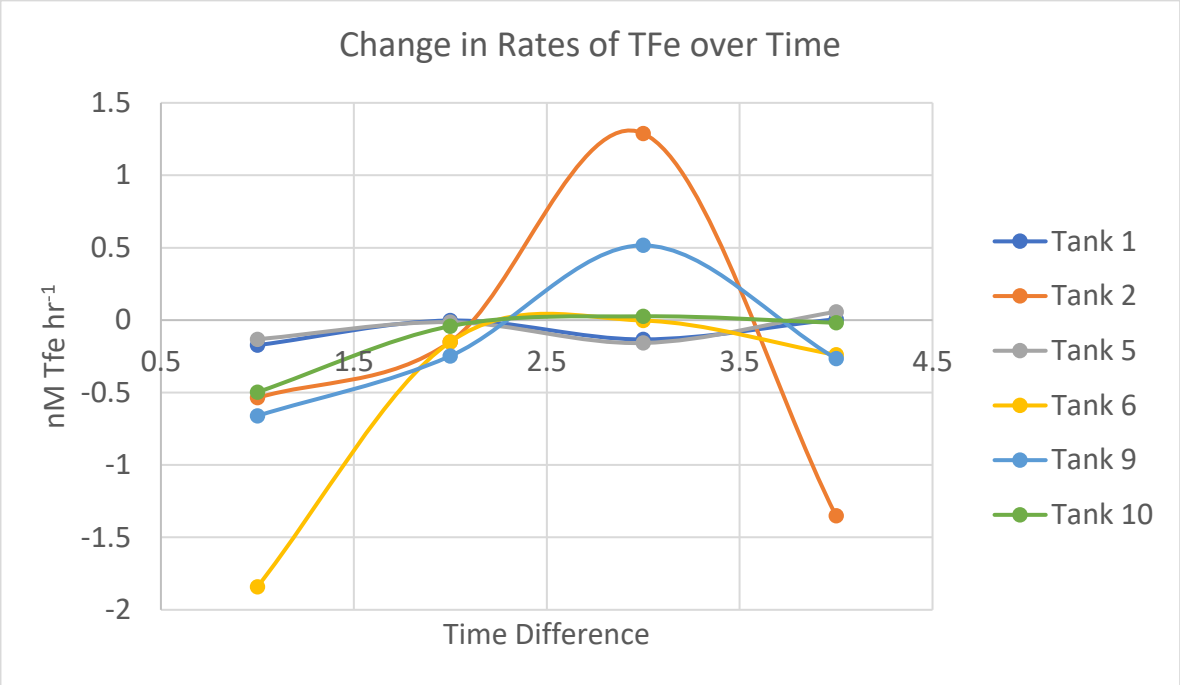

Figure 17: Change in rates of total dissolvable iron over time differences

All tanks show a negative rate of change in iron for time difference 1 and increase closer to zero by time difference 2, with tank 6 undergoing the largest increase. Four tanks hover around zero for the remaining time differences while tanks 2 and 9 show positive rate of change at time 3 until returning to a negative rate of change by time difference 4.

4.4 Crete Samples – pH

All tanks from Time 1 to Time 5 showed an initial rapid decrease followed by relatively stable pH. A small dip occurs at Time 4 and then pH returns to previous levels. Results are presented in Figure 18. Initial pH's for mesocosm end of experiment around ~8.03. Sampling Time 6 is also included. Note the scale on the y-axis.

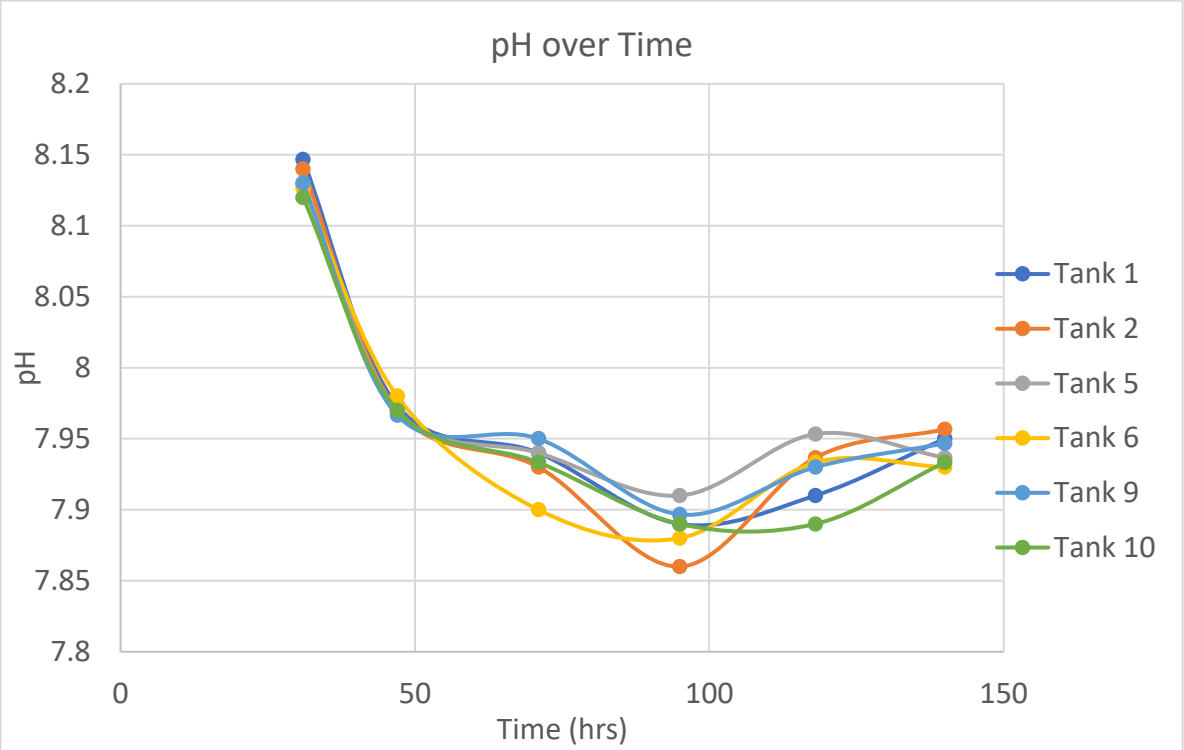

Figure 18: pH of each decomposition treatment over time. Note the y-axis scale.

4.5 Crete Samples – Macronutrients

Macronutrient samples are included from Time 1, where 1st trace metal samples reported, until Time 6 for each tank. N_{Tot} is the sum of the three species of nitrogen (NO_3 + NO_2 + NH_4) as all three were added to the initial mesocosm tanks. PO_4 represents soluble phosphate and SiO_4 represents soluble silicate.

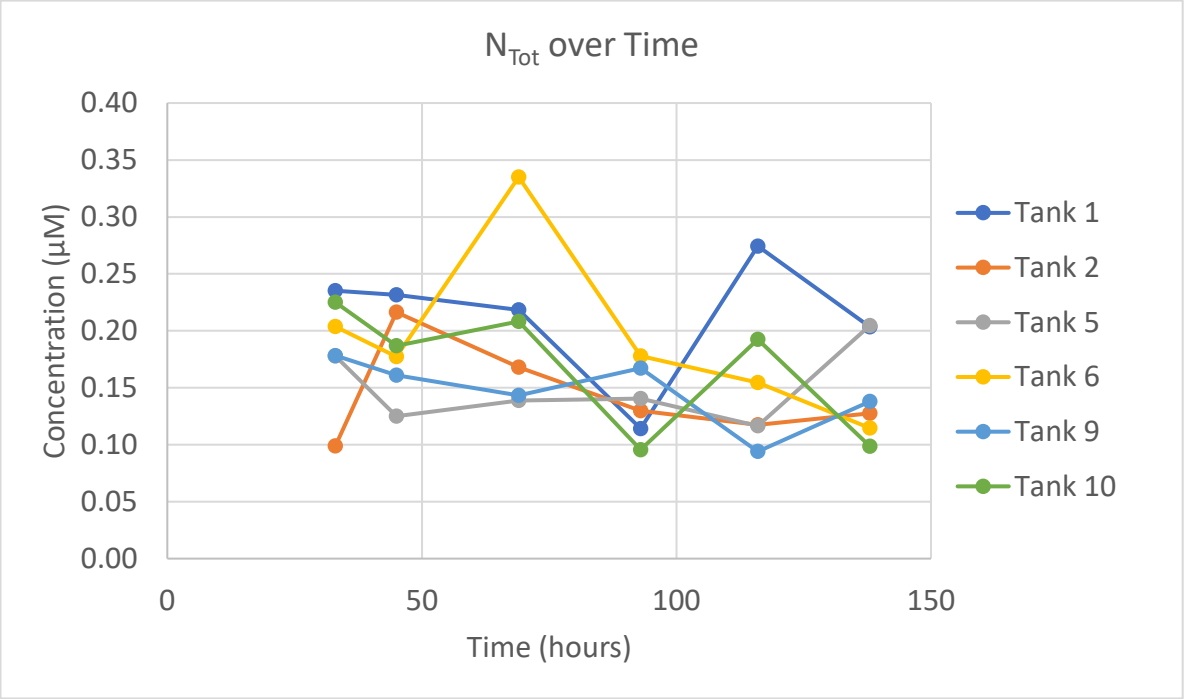

Figure 19: N_{Tot} (NO_3 + NO_2 + NH_4, µM) over time for each decomposition treatment. Starts from 1st trace metal report.

There appears to be no discernible trend among tanks for total nitrogen, except an overall gradual net decrease from the beginning to the end. Most tanks have an initial decrease from Time 1 to Time 2, except for Tank 2. Nitrogen has a decrease at Time 4 for Tank 1 and Tank 10, followed by an increase. Tank 6 shows a jump from Time 2 to Time 3. By Time 6 (140hrs), Tanks 6, 9, 10 are at a lower concentration than Time 1, while Tanks 2 and 5 show slight increase relative to Time 1. Tank 1 appears to be at a similar concentration at Time 6 relative to Time 1.

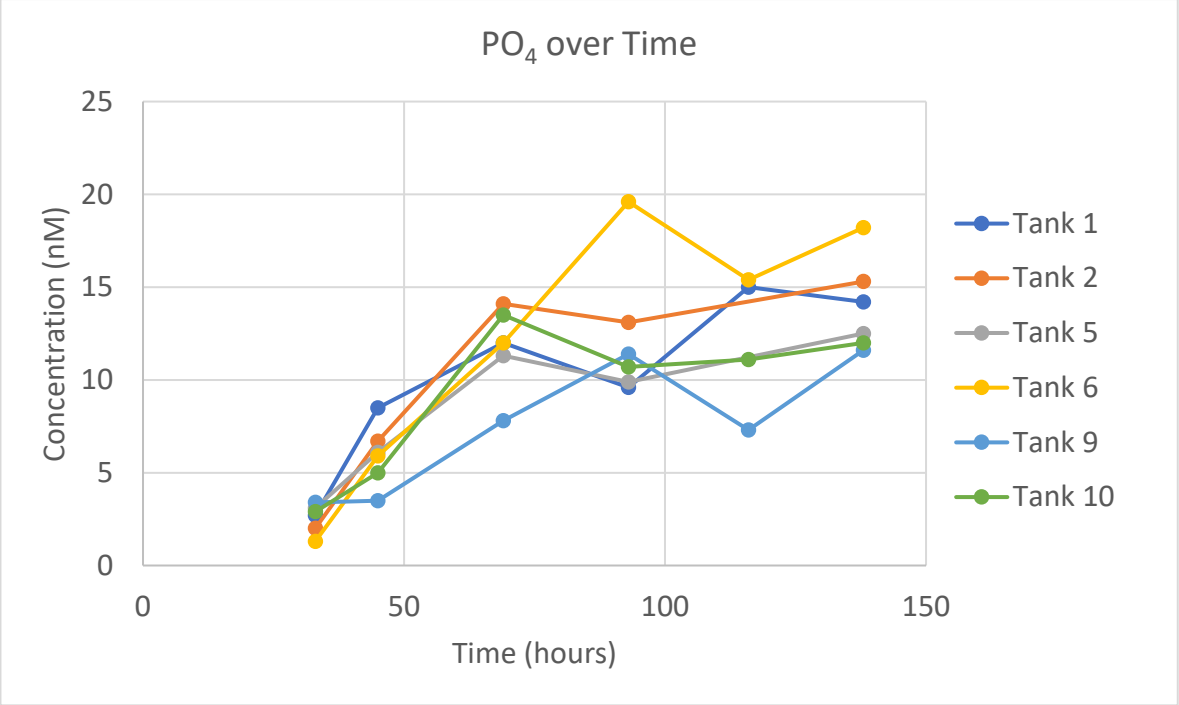

Figure 20: Phosphate concentration (nM) over time for decomposition treatment.

Phosphate concentrations for all tanks at Time 1 are at their lowest point around ~2.5nM. Over time, each tank tends to increase in concentration. The average concentration at the end of the experiment was higher than the average concentration from the beginning of the experiment, indicating a net increase in phosphate concentrations. The net increase in phosphate concentration and associated rate of change for each tank is presented in Table 12.

Table 12: Net increase in PO_4 concentrations from Time 1 to Time 6 for each tank.

Tank	Net PO_4 Increase (nM)	Net Rate of Change (nM/hr)
1 (0C, HG)	11.5	0.110
2 (0C, LG)	13.3	0.127
5 (1C, HG)	9.4	0.0900
6 (1C, LG)	16.9	0.161
9 (3C, HG)	8.2	0.0781
10 (3C, LG)	9.1	0.0867

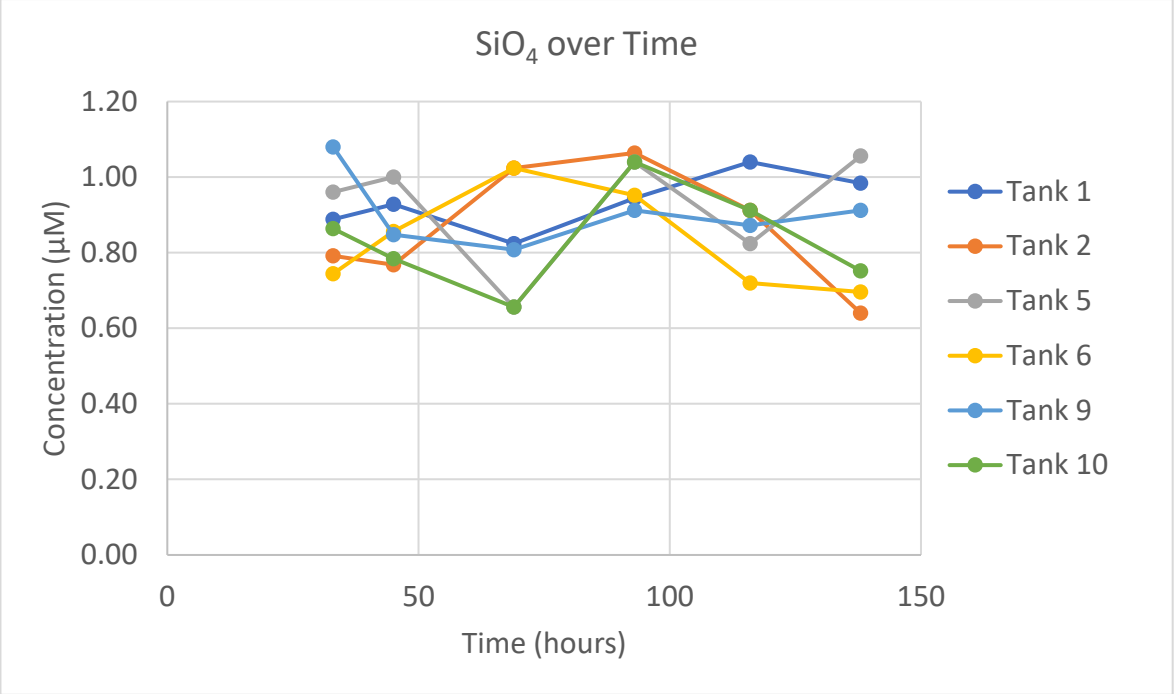

Figure 21: Silicate concentration (µM) over time for each decomposition treatment

Silicate concentrations also did not appear to show any discernible trends for tanks. All tanks were characterized by increases and decreases with silicate over time, with the concentration at the beginning of the experiment and at the end of the experiment visually similar between 0.80 and 1.00µM.

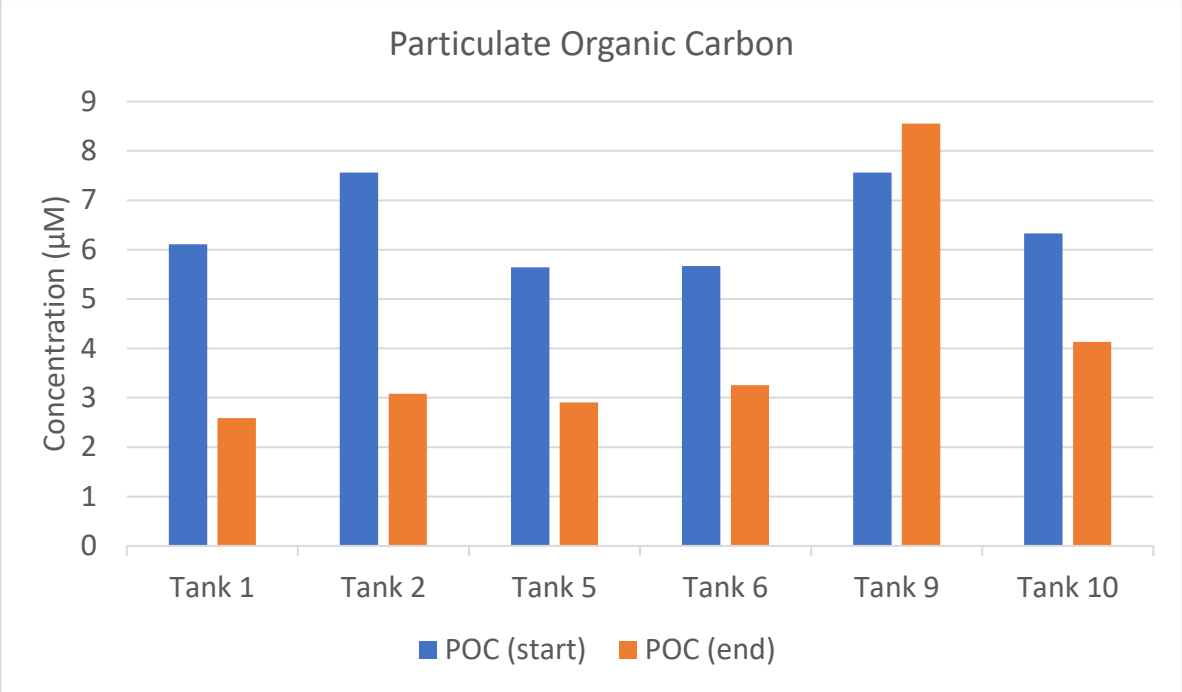

Figure 22: POC of each tank treatment at start and end of decomposition treatment.

POC concentrations at the end of the mesocosm experiment were between 5-8µM. Over the course of the decomposition experiment, all tanks except for Tank 9 decreased in POC concentrations to about 3µM. Tank 9 increased slightly to above 8µM. Tanks did not appear to show any trend with regards to concentrations in terms of grazing group or carbon gradient group. As POC filters were only measured once, it is possible that the increase observed Tank 9 is result of experimental error. The percent difference from beginning to end was calculated for each tank and presented in Table 13. The percent difference appeared to be largest for the lowest carbon gradient group (0C, Tanks 1 and 2) and the smallest for the highest carbon gradient group (3C, Tanks 9 and 10).

Table 13: Percent difference in POC from beginning to end of decomposition experiment.

Tank #	% Difference
Tank 1	57.6
Tank 2	59.2
Tank 5	48.5
Tank 6	42.6
Tank 9	-13.1
Tank 10	34.8

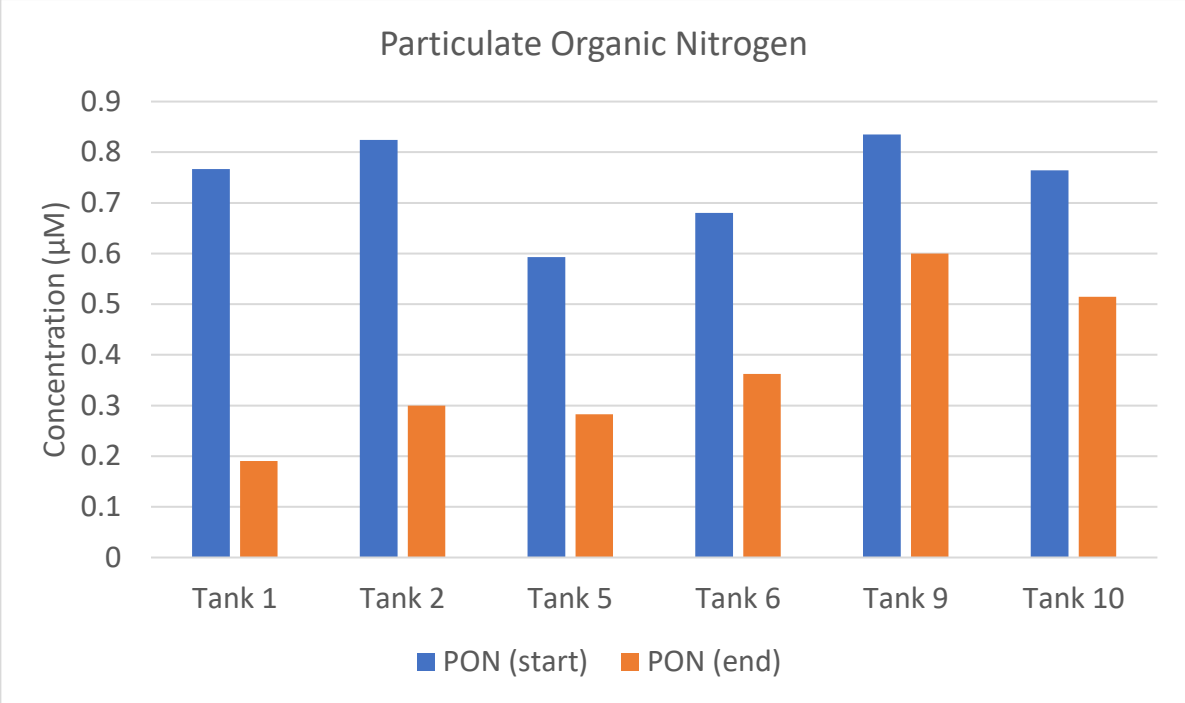

Figure 23: PON of each tank treatment at start and end of decomposition experiment

The levels of PON at the beginning of the decomposition experiment were roughly between 0.6µM-0.9µM. All tanks decreased from the start of the experiment to the end of the experiment, although the percent change appeared to be the largest for the lowest carbon gradient group, Tanks 1 and 2, followed by 5 and 6, and then 9 and 10. The percent difference was calculated for each tank and presented in Table 14. The HG group (1, 5, 9) also appeared to have a higher percent difference than the LG group (2, 6, 10), although this trend is not observed between Tanks 9 and 10.

Table 14: Percent difference in PON from beginning to end of decomposition experiment.

Tank	% Difference
Tank 1	75.2
Tank 2	63.6
Tank 5	52.3
Tank 6	46.7
Tank 9	28.2
Tank 10	32.6

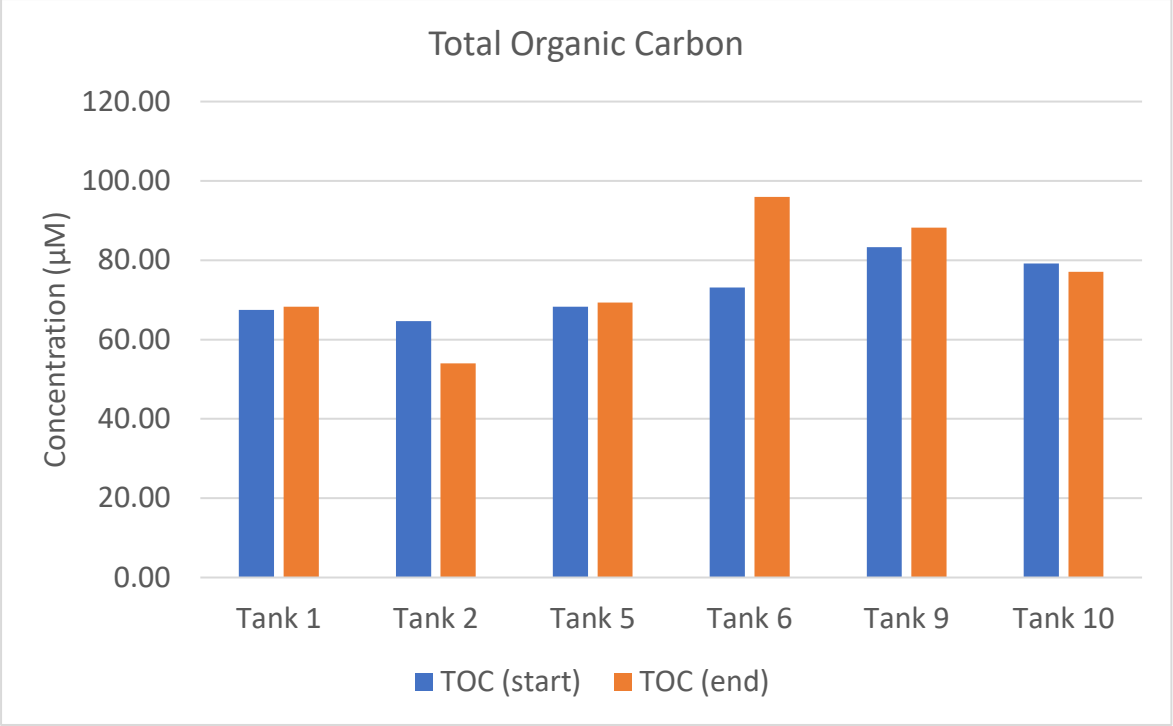

Figure 24: TOC of each tank at start and end of decomposition experiment.

The levels of TOC at the beginning of the decomposition experiment were between 60-85µM. By the end of the experiment, some tanks had experienced in increase in TOC and some tanks had experienced a decrease in TOC, with the final range of TOC concentrations between 50-100µM. The percent difference for each tank was calculated and is presented in Table 15. There appeared to be no trend among grazing groups or carbon gradient groups.

Table 15: Percent difference in TOC from beginning to end of decomposition experiment.

Tank #	% Difference
Tank 1	1.16
Tank 2	-16.5
Tank 5	1.56
Tank 6	31.2
Tank 9	5.94
Tank 10	-2.71

5 Discussion

5.1 Data Variation

As iron is one of the most abundant elements in the Earth's crust, historical research of iron biogeochemistry was heavily influenced by contamination until trace metal clean procedures were developed (Worsfold et al., 2014). As evidenced by the variation between parallel samples in tables A.1 and A.2, the background blank concentrations in the SeaFAST system (Table 6), and some high dissolved iron values (Figure 10), contamination may have influenced the results of this master thesis, with more emphasis placed on the experimental portion than the analytical portion.

Analytically, contamination could come from the SeaFAST system, MilliQ water, reagents, reagent bottles, PTFE Teflon™ vials, QC 20mL bottles, syringes, and background within the laboratory setting. As all SeaFAST work was prepared within a Class 1000 clean lab setting and under an AirClean laminar flow hood Class 100, it was not expected that this atmosphere would contribute to the high variation observed among the samples. Additionally, no exposure to contaminants was expected during preconcentration analysis while sample vials were uncapped within the SeaFAST enclosure as no correlation was found in a previous study (Lagerström et al., 2013). While the final dilution step to 3mL for ICP-MS requirements may increase exposure, background levels within non-preconcentrated MilliQ water were expected to be low and not sufficient to contribute substantially to the varying iron levels observed among samples.

The SeaFAST full procedural background blank of MilliQ for iron at 0.415nM ± 0.255 from Table 6 suggests that this level may come from the reagents or the materials used during preconcentration or from the SeaFAST system itself. As all reagents used were of trace metal quality, it was not suspected that these would contribute substantially to background levels. Furthermore, the trace metal cleanup column, designed to chelate any remaining trace metals within the ammonium acetate buffer, would be expected to reduce iron and other trace metal levels. Therefore, it was possible that the cleaning procedure of reagent bottles and Teflon™ vials may be suspected to increase background levels, as this cleaning was a shortened and modified version from the trace metal clean procedure due to time and resources. A study using an offline SeaFAST preconcentration method reported a similar full procedural background blank value of iron at 0.210nm kg^{-1} (Bown et al., 2016) and offered no suggestion as to the source. This study reported cleaning their elution vials with nitric acid only, suggesting that the similar procedure performed for this thesis may not be sufficient to remove iron within the

Teflon™ vials. However, additional sources of contamination were certainly present, as evidenced by the elevated levels of zinc, nickel, and lead in the background blanks and high reference values for these samples (Table 8). Although initial cleaning of the SeaFAST system with nitric acid and MilliQ water reduced the initial testing full procedural background blank by more than half (Table 6), additional work should be performed with the NTNU SeaFAST system to ascertain the primary source for these background concentrations. This reduction of background blanks for all metals suggests that proper cleaning of SeaFAST is necessary to obtain reliable values for iron and other trace metals at low concentrations, especially after periods of non-use.

Besides SeaFAST, multiple experimental steps introduced the possibility for background contamination. Sources of additional iron could include the initial mesocosm tanks, transferring from mesocosm tanks, decomposition bottles, subsampling materials such as the syringe apparatus, trace metal sampling tubes, filtration devices, acidification, and background levels. The risk from acidification was expected to be low, as this step was performed in the constructed clean lab under the AirClean laminar flow hood using Ultrapure nitric acid in MilliQ water. The filtration of all samples poised a risk as only two filters were used, yet between each set of samples dead volume was eliminated, reducing the risk of cross contamination. As the total dissolvable iron samples also suffered from variability, the filtration and acidification steps were most likely not a significant source of background, suggesting that the sampling bottles used may have been an issue.

As the decomposition bottles were trace metal clean prior to the experiment, it was not expected that they would contribute significantly to the variation observed. The one-way ANOVA (Table B.3) of averaged dissolved iron between tanks with no statistical significance suggests that no significant contamination occurred between the large mesocosm tanks, the transfer to decomposition bottles, and from the decomposition bottles themselves. The variation observed in both the total dissolvable samples and the dissolved samples suggests an alternative primary background source, hypothesized to be the subsampling 50mL and 125mL bottles. As these bottles were cleaned according to a modified procedure with HCl and rinsed with seawater, it was likely that these tubes may have contained residual iron. Additionally, both cleaning and rinsing of these tubes occurred in non-clean environment in HCMR due to space, increasing the background risk from dust particles in the air. Coupled with the Mediterranean's high dust input during the time of the sample cleaning (Figure C.1), and flow of people in and out of the building, this type of environment within HCMR suggested that these subsampling tubes were the biggest contributor to the variation between parallel samples.

The amount of variation appears to be random, occurs within all tanks, is much larger than the SeaFAST blank values, and is not isolated to either total dissolvable or dissolved samples alone, as evidenced in Table A.2.

5.2 SeaFAST Analysis and Recovery

The SeaFAST recovery for iron of 84% for the NASS-6 reference standard obtained during Crete sample testing was statistically significantly lower than the NASS-6 reference standard value according to the one-sample Z-test. The other trace metals when compared to the initial testing values (Table 5) also appeared to visually decrease from the reference standard values for each respective metal. The lower recovery of these elements was not what was found in a similar studies utilizing the SeaFAST with IDA and ED3A preconcentration chelation column (Lagerström et al., 2013) and in offline mode (Bown et al., 2016). The lower recovery of the NASS-6 standard was estimated to be from three main factors: 1) pH, 2) timing, and 3) volume delivery.

1). pH. Too low of initial standard pH or too weak an ammonium acetate buffer would cause trace metals to be eluted to waste. However, the measured pH of the NASS-6 reference standard was approximately 1.9 and the measured pH of all buffer solutions prepared for SeaFAST use were 6.0 ± 0.2, as recommended by manufacturer's recommendations. Furthermore, pH of waste sample after preconcentration was measured to be approximately 5.5, suggesting that both the pH of the samples and the pH of the buffer-MilliQ water solution were within the correct range to chelate trace metals of interest. Commercially, the SeaFAST is capable of recovery of elements in the picomolar concentrations, and a comparison between rare earth element concentrations obtained from these Cretan seawater samples to literature values for the Mediterranean (Table A.3) suggests that efficient chelation and elution was occurring within the SeaFAST instrument.

2). Timing. It was hypothesized that the delivery to ICP-MS of two different batches of Crete samples may have affected the lower recovery, particularly of Batch 1. Batch 1 samples when completed were capped and stored covered with plastic in a chemical ventilation hood. Furthermore, this initial batch took approximately 3 weeks total for SeaFAST preconcentration of all samples followed by additional storage of approximately 1 month before ICP-MS analysis. It was possible that the hood facilitated evaporation of samples if caps were not tight enough. However, this hypothesis is not supported by a two-sample t-test (Table B.7) assuming unequal variance between Batch 1 and Batch 2 NASS-6 reference values. The statistically insignificant p-value of 0.073 suggested that there is not a difference due to sample storage.

3). Volume delivery. Another factor that may have contributed to lower recovery of reference standards of all metals is the volume of SeaFAST elution. A 1mL elution volume specified during the preconcentration method had an accuracy of 93% ± 2.9 for volume delivery (Table 2). The near-perfect accuracy of the Eppendorf multipipette at 99% ± 1.2 (Table 2) would contribute to a slightly higher ratio of MilliQ dilution to sample eluent, underpinning a slightly lower concentration of the final sample delivered for ICP-MS. This small difference coupled with evaporation loss may account for the observed mean departure from reference standard values with Batch 1 Crete samples, while also contributing to a slightly lower accuracy observed for reference standard values with Batch 2 Crete samples.

The overall average concentration value of dissolved iron for non-contaminated Crete samples of 3.18nM ± 1.36 (Figure 10) is about double the dissolved iron values reported for the Cretan Sea (Statham et al., 2005); however, the value is similar to values of dFe in other areas of the Mediterranean, reported between 2-6nM (van den Berg, 1995; Wuttig et al., 2013). The Cretan Sea study reported seasonal changes in dissolved iron concentrations with higher values observed in September compared to March (Statham et al., 2005). As thermal stratification of the water column may increase the accumulation of dissolved iron near the surface due to other limiting nutrients (Bonnet et al., 2005), the temperature of the water at the depth of seawater collection for the mesocosm experiment at 19ºC is similar to the ~22ºC observed in September by Statham and Hart for elevated dissolved iron concentrations, suggesting that seasonal stratification at the seawater collection site may have already begun contributing to the higher value reported here. Furthermore, as dissolved iron concentrations have been shown to increase closer to coastlines (Boye et al., 2003), the mesocosm seawater sampling site at only 10 nautical miles from the Cretan coast may have been influenced by both terrestrial input and resuspended sedimentary iron and further support the observed dissolved iron increase found relative to the literature value. The literature value (Statham et al., 2005) was also reported at further distances from coasts which would suggest slightly lower dFe values than the value reported here. Lastly, as mentioned in the previous discussion section, contamination from background dust particles may have elevated the mean concentration.

5.3 Remineralization and Removal

Iron Remineralization

Between the first and second sampling period for trace metals, all tanks showed an increase in dissolved iron concentrations (Figure 11) corresponding to a positive rate of change of iron represented in Figure 12 at Time Period 1. Assuming no input of external dissolved iron

due to the experimental conditions, a positive rate of change in dissolved iron concentrations would suggest movement from particulate iron to dissolved iron via dissolution and the release of cellular iron. While rapid dissolution of lithogenic particles containing iron can occur in the pelagic ocean in a process called cascade (Fitzsimmons, Hayes, et al., 2015), the closed and experimental nature of the decomposition experiment would not suggest this process. Instead, it was more likely that the increase in dissolved iron concentrations was due to biological processes of bacterial decomposition, grazing, and viral lysis. In addition to decomposition, the concurrent release of weak L4 organic ligands during decomposition from an iron-replete environment has been documented in a previous dark bottle experiment (Bundy et al., 2016), suggesting that a similar process may occur in an iron-replete area like the Mediterranean Sea, which would serve to increase the concentration of organically complexed iron during decomposition as observed in Figure 11.

Furthermore, the processes of grazing by both microzooplankton and mesozooplankton may have facilitated the increase in dissolved iron concentrations and thus the positive rate at Time Period 1. According to the MesoMED post-experimental report of the mesocosm experiment, the amount of heterotrophic protists (microzooplankton) and copepods (mesozooplankton) were higher in the high grazing group (Tanks 1, 5, 9) than the low grazing group (Tanks 2, 6, 10) at the end of the experiment. This difference may account for the higher rate of change for the HG group than the LG group at Time Period 1 (Figure 13) although the rates were not significantly different. This idea is supported by previous experiments which demonstrated an increase in both natural organic ligands and dissolved iron in the presence of copepods (Sarthou et al., 2008) and microzooplankton (Sato et al., 2007), however, for our work, the difference in total zooplankton numbers may not have been large enough to observe a significant difference between the two groups. Different species of heterotrophic protists may also contribute to variable increases in dissolved iron concentrations through grazing (Barbeau et al., 2001), although the specific composition of biological assemblages within the decomposition bottles is unknown.

Another factor that may have separated the HG group and the LG group rates at Time Period 1 may be the difference in heterotrophic bacterial abundances (BA) and bacterial production (BP). Bacterial abundances were higher in the LG group than the HG group at the end of the mesocosm experiment according to the MesoMED report and BP also appeared to be slightly higher for the LG group than the HG group. When feeding on phytoplankton in the absence of micrograzers, bacteria were shown to mobilize iron to different size fractions, with a larger proportion of the iron located within the bacterial fraction than the dissolved fraction

after 72 hours (P. Boyd et al., 2010). As bacteria take up iron for respiratory processes , the difference in BA and BP may support why the LG group release rate of dissolved iron at Time Period 1 is less than the HG group release rate, as more iron is being mobilized to the bacterial fraction. Bacterial production was also shown to be generally higher in the upper carbon gradients from the MesoMED report. A previous study indicated that bacterial production was stimulated with an increasing glucose gradient in Fe-replete waters, suggesting a similar process in our work (David L. Kirchman et al., 2000). This bacterial mobilization is supported by the statistically significant p-value from the one-way Welch's ANOVA comparing rates between carbon gradient groups (Table B.7), where group 3C was lower than group 1C (Figure 14). The percent difference observed among carbon gradient groups for POC and PON (Tables 13 and 14) also suggest less POM lost to the dissolved fraction.

Overall, however, the total rates of change for Time Period 1 between 0.038 nM hr^{-1} and 0.140nM hr^{-1} are much higher than the estimated remineralization rates and observed concentration changes from previous experiments. Other studies observed increases between 0.4nM and 1.0nM of dissolved iron over the course of several days (P. Boyd et al., 2010; Bundy et al., 2016), and another estimated remineralization rates due to bacteria and zooplankton in the pmol day^{-1} range (Bowie et al., 2015). One study may have underestimated the remineralization rate due to the removal of microzooplankton (P. Boyd et al., 2010) while the other acknowledged low levels of mesozooplankton predators (Bowie et al., 2015), leading to lower reported rates. Consequently however, the total rate of increase observed in our work may also be due additional factors. The type of prey for zooplankton, whether picophytoplankton or heterotrophic bacteria or both, may have influenced the large rate of increase observed at Time Period 1. A grazing study illustrated that 90% of iron originally within the heterotrophic bacterial fraction was within the dissolved phase after 24 hours (Strzepek et al., 2005), compared to 25% when the prey was picophytoplankton. As Strzepek's experiment measured the two fractions independently from one another, the natural assemblage of both bacteria and phytoplankton in our decomposition experiment would suggest iron release from both prey sources. Furthermore, the Fe/C quota of these prey sources may be different. Assuming all the iron was released from Time 1 to Time 2 and that the difference in POC from start to end of experiment (Figure 22) represents total decomposition, the average Fe/C ratio released during decomposition from this experiment is 749µmolFe/molC. With iron-replete conditions, using internal Fe/C quotas of 40µmol/mol for phytoplankton (maximum quota) (Aumont et al., 2015), 10µmol/mol for zooplankton (Aumont et al., 2015), and 44µmol/mol for heterotrophic bacteria (Tortell et al., 1996), the sum of all these ratios only

accounts for 12.6% of the Fe/C released. The remaining 87.4% may be adsorbed extracellularly, supported by findings that only 15% of iron released is from within phytoplankton and that a majority may be due to dissolution of iron adsorbed onto phytoplankton cells during grazing (Sato et al., 2007), and that the washing of biogenic particles revealed up to 86% of iron may be adsorbed (Tovar-Sanchez et al., 2003). Furthermore, if phytoplankton participated in luxury uptake during bloom conditions during the mesocosm experiment (W. G. Sunda et al., 1995), more dissolved iron may have been released during decomposition as well, contributing to the higher rate of change observed. However, this ratio of 749μmolFe/molC may be overestimated as the decomposition of DOC and BP is not included in the molC fraction and some of the released dissolved iron may be attributed to lithogenic sources instead of biogenic sources.

Iron Removal

From the 2nd sampling period to the 3rd sampling period (47 hours to 71 hours), all rates of change in iron concentrations for all tanks decreased, with several tanks showing a decrease in dissolved iron concentrations as well. The decline in release rate suggests the iron system moving towards equilibrium in seawater. A negative rate of change may be evidenced by the adsorption of iron onto particle surfaces and the decomposition of organic ligand-iron complexes. Iron was not expected to readsorb onto particles because a previous experiment demonstrated that purely abiotic mechanisms did not result in an iron concentration decrease during sterilized dark bottle incubation (P. Boyd et al., 2010). Additionally, the general decrease of POC concentrations (Figure 22) suggest lower concentration of surface area for iron to adsorb. However, the general decreasing trend of total dissolvable iron (Figure 16) suggests that iron readsorption was indeed taking place. As iron concentrations have been evidenced to decrease in bottle experiments due to adsorption to the walls of the bottle if seawater samples are stored unacidified (Fischer et al., 2007; Schlosser et al., 2011), it was possible that the decrease in both total dissolvable and dissolved iron concentrations in dark decomposition bottles decreased due to the "bottle effect". This phenomenon was not expected to be significant due to pre-equilibration of the bottles with seawater, but may have been accelerated by a high proportion of lithogenic iron material, where in dust-influenced waters, a majority of the dissolved iron may be colloidal lithogenic nanoparticles (Fitzsimmons, Bundy, et al., 2015), suggesting faster adsorption and removal. Although total proportions of lithogenic to biogenic iron for our work were not determined, the influence of the Sahara on dissolved iron concentrations in the Mediterranean (Migon, 2005) suggest a large lithogenic

influence. Interestingly, a similar trend of dissolved iron increase and decrease over time was observed in a previous experiment performed in Ny-Ålesund (Ardelan, personal comm.), suggesting that adsorption of iron after decomposition may have a non-negligible effect on the storage of unacidified seawater.

Macronutrients and Iron

Compared to macronutrients, iron is expected to be remineralized slower than both nitrate and phosphate due to the influence of abiotic and biotic factors (Boyd et al., 2017). As the nitrogen concentrations over the course of the decomposition experiment showed no general trends of increase (Figure 19), timing of the experiment may have been an issue with regards to trend observations. Therefore, it was assumed that nitrogen was rapidly remineralized within the first 31 hours of the experiment due to its faster release rate from particles than both phosphate and iron (Lamborg et al., 2008). The slight visual decrease of N_{Tot} until the end of the experiment may be indicative of bacterial uptake which could also explain the gradual yet variable decrease of dissolved iron in tanks as well due to iron's importance in enzymatic transformations of nitrogen (F. Morel et al., 2003), however a lack of any bacterial data during the decomposition experiment cannot confirm this idea.

Further suggestive of timing issues, silicate typically regenerates rapidly followed by a slow release (Bidle et al., 1999), suggesting that due to the lack of trend within this experiment (Figure 21) regeneration either occurred within the first 31 hours of the experiment or that a majority of the decomposing material was not from silicate-containing diatoms. Size fractionation at the end of the mesocosm experiment illustrated that most of the primary production was within the 0.2-10µm size range, typically indicating small diatoms or flagellates. Although larger phytoplankton species would not be expected in the Cretan sea due to nutrient limitations, the manipulation of nutrient additions in mesocosms may have created a non-natural community; thus, the lack of trend in silicate concentrations cannot be inferred from primary production size fractionation alone without detailed biological speciation.

Change of phosphate concentrations over time (Table 13) are comparable to changes of dissolved iron concentrations for Time Difference 1 only (Table 9), corresponding to the decoupling of phosphate release from iron release (Parekh et al., 2005). Since phosphate may limit bacterial production within the Eastern Mediterranean (Thingstad et al., 2005) in addition to primary production (M. D. Krom et al., 1991), it is possible that the nM levels of phosphate observed would restrict enhanced bacterial production within the dark bottles. If BP is phosphate-limited, this would support the decrease of dissolved iron concentrations due to

adsorption rather than bacterial uptake of iron for enzymatic processes. Although again, no BP data is available during the dark bottle experiment, and cannot confirm.

6 Conclusion

The creation of grazing groups and distribution of a carbon gradient in the mesocosm experiment affected the community structure concerning phytoplankton, bacteria, and zooplankton. The resulting varying communities and biotic mechanisms appeared to have small yet statistically insignificant differences on the remineralization of iron during decomposition of planktonic materials. Consequently, an initial increase of dissolved iron concentrations followed by a general decrease in both total dissolvable and dissolved iron concentrations underpinned the importance of abiotic mechanisms during iron remineralization.

Temporally, the remineralization of iron and other macronutrients most likely occurred within the first 72 hours of the experiment, highlighting the importance of performing future experiments within a rapid time frame. Furthermore, future evaluations of iron remineralization must measure relevant biological parameters over time to better estimate the magnitude of biotic processes on iron release.

The SeaFAST remains a powerful tool in measuring iron concentrations and other elements, but proper cleaning and evaluation of method parameters is important for quantification, demonstrated by background blank levels and elution volume discrepancy. Cleaning procedures in general were demonstrated to be of utmost importance in all experimental steps for trace metals as it may have affected the concentration accuracy for this thesis.

Despite some setbacks, some observations remain important. Much of the initial iron concentration increase may have been due to iron adsorbed extracellularly to biological organisms, while adsorption processes appeared to continue to affect concentrations of iron over time through adsorption to the sides of the bottle, shown through the decrease of both total dissolvable dissolved iron concentrations. Models of iron remineralization should not neglect the impact nor importance of abiotic mechanisms in assessing dissolved iron concentrations within aquatic ecosystems. With more accurate models, researchers will be able to better assess changes to iron cycling and its effect on the biological carbon pump.

7 References

Achterberg, E. P., Holland, T. W., Bowie, A. R., Mantoura, R. F. C., & Worsfold, P. J. (2001). Determination of iron in seawater. *Analytica Chimica Acta, 442*(1), 1-14. doi:10.1016/S0003-2670(01)01091-1

Amin, S. A., Parker, M. S., & Armbrust, E. (2012). Interactions between Diatoms and Bacteria *Microbiol. Mol. Biol. Rev.* (Vol. 76, pp. 667-+).

Aumont, O., Éthé, C., Tagliabue, A., Bopp, L., & Gehlen, M. (2015). PISCES-v2: An ocean biogeochemical model for carbon and ecosystem studies. *Geoscientific Model Development Discussions, 8*(2), 1375-1509.

Azam, F., Fenchel, T., Field, J., Gray, J., Meyer-Reil, L., & Thingstad, F. (1983). The ecological role of water-column microbes in the sea. *Marine ecology progress series. Oldendorf, 10*(3), 257-263.

Barbeau, K., Kujawinski, E., & Moffett, J. (2001). Remineralization and recycling of iron, thorium and organic carbon by heterotrophic marine protists in culture. *Aquatic Microbial Ecology, 24*(1), 69-81.

Bau, M., Möller, P., & Dulski, P. (1997). Yttrium and lanthanides in eastern Mediterranean seawater and their fractionation during redox-cycling. *Marine Chemistry, 56*(1-2), 123-131.

Behrens, M. K., Muratli, J., Pradoux, C., Wu, Y., Böning, P., Brumsack, H.-J., . . . Pahnke, K. (2016). Rapid and precise analysis of rare earth elements in small volumes of seawater - Method and intercomparison. *Marine Chemistry, 186*, 110-120. doi:http://dx.doi.org/10.1016/j.marchem.2016.08.006

Bidle, K. D., & Azam, F. (1999). Accelerated dissolution of diatom silica by marine bacterial assemblages. *Nature, 397*(6719), 508-512.

Biller, D. V., & Bruland, K. W. (2012). Analysis of Mn, Fe, Co, Ni, Cu, Zn, Cd, and Pb in seawater using the Nobias-chelate PA1 resin and magnetic sector inductively coupled plasma mass spectrometry (ICP-MS). *Marine Chemistry, 130–131*, 12-20. doi:http://dx.doi.org/10.1016/j.marchem.2011.12.001

Blondel, J., Aronson, J., & Bodiou, J.-Y. (2010). *The Mediterranean Region : Biological Diversity through Time and Space* (2nd ed. ed.). Oxford: OUP Oxford.

Bonilla-Findji, O., Malits, A., Lefèvre, D., Rochelle-Newall, E., Lemée, R., Weinbauer, M. G., & Gattuso, J.-P. (2008). Viral effects on bacterial respiration, production and growth efficiency: Consistent trends in the Southern Ocean and the Mediterranean Sea. *Deep-Sea Research Part II, 55*(5), 790-800. doi:10.1016/j.dsr2.2007.12.004

Bonnet, S., Guieu, C., Chiaverini, J., Ras, J., & Stock, A. (2005). Effect of atmospheric nutrients on the autotrophic communities in a low nutrient, low chlorophyll system. *Limnology and Oceanography, 50*(6), 1810-1819.

Bowie, A. R., Van Der Merwe, P., Quéroué, F., Trull, T., Fourquez, M., Planchon, F., . . . Blain, S. (2015). Iron budgets for three distinct biogeochemical sites around the Kerguelen Archipelago (Southern Ocean) during the natural fertilisation study, KEOPS-2. *Biogeosciences, 12*(14), 4421-4445. doi:10.5194/bg-12-4421-2015

Bown, J., Laan, P., Ossebaar, S., Bakker, K., Rozema, P., & de Baar, H. J. (2016). Bioactive trace metal time series during Austral summer in Ryder Bay, Western Antarctic Peninsula. *Deep Sea Research Part II: Topical Studies in Oceanography*.

Boyd, P., Ibisanmi, E., Sander, S., Hunter, K., & Jackson, G. (2010). Remineralization of upper ocean particles: Implications for iron biogeochemistry. *Limnology and Oceanography, 55*(3), 1271.

Boyd, P. W., & Ellwood, M. J. (2010). The biogeochemical cycle of iron in the ocean. *Nature Geoscience, 3*(10), 675-682. doi:10.1038/ngeo964

Boyd, P. W., Ellwood, M. J., Tagliabue, A., & Twining, B. S. (2017). Biotic and abiotic retention, recycling and remineralization of metals in the ocean. *Nature Geosci, 10*(3), 167-173. doi:10.1038/ngeo2876

http://www.nature.com/ngeo/journal/v10/n3/abs/ngeo2876.html#supplementary-information
Boyd, P. W., Strzepek, R., Chiswell, S., Chang, H., DeBruyn, J. M., Ellwood, M., . . . Hutchins, D. A. (2012). Microbial control of diatom bloom dynamics in the open ocean. *Geophysical Research Letters, 39*(18), n/a-n/a. doi:10.1029/2012GL053448
Boye, M., Aldrich, A. P., van den Berg, C. M. G., de Jong, J. T. M., Veldhuis, M., & de Baar, H. J. W. (2003). Horizontal gradient of the chemical speciation of iron in surface waters of the northeast Atlantic Ocean. *Marine Chemistry, 80*(2–3), 129-143. doi:http://dx.doi.org/10.1016/S0304-4203(02)00102-0
Bressac, M., & Guieu, C. (2013). Post-depositional processes: What really happens to new atmospheric iron in the ocean's surface? *Global biogeochemical cycles, 27*(3), 859-870.
Buchan, A., LeCleir, G. R., Gulvik, C. A., & Gonzalez, J. M. (2014). Master recyclers: features and functions of bacteria associated with phytoplankton blooms. *Nat Rev Micro, 12*(10), 686-698. doi:10.1038/nrmicro3326
Buck, K. N., Sohst, B., & Sedwick, P. N. (2015). The organic complexation of dissolved iron along the U.S. GEOTRACES (GA03) North Atlantic Section. *Deep Sea Research Part II: Topical Studies in Oceanography, 116*, 152-165. doi:http://doi.org/10.1016/j.dsr2.2014.11.016
Bundy, R. M., Jiang, M., Carter, M., & Barbeau, K. A. (2016). Iron-Binding Ligands in the Southern California Current System: Mechanistic Studies. *Frontiers in Marine Science, 3*(27). doi:10.3389/fmars.2016.00027
Censi, P., Mazzola, S., Sprovieri, M., Bonanno, A., Patti, B., Punturo, R., . . . Alonzo, G. (2004). Rare earth elements distribution in seawater and suspended particulate of the Central Mediterranean Sea. *Chemistry and Ecology, 20*(5), 323-343.
Cutter, G., Andersson, P., Codispoti, L., Croot, P., Francois, R., Lohan, M., . . . Rutgers vd Loeff, M. (2010). Sampling and sample-handling protocols for GEOTRACES cruises: GEOTRACES.
Danovaro, R., Dell'Anno, A., Pusceddu, A., Daniela, M., Della Croce, N., Fabiano, M., & Tselepides, A. (2000). Biochemical composition of pico-, nano- and micro-particulate organic matter and bacterioplankton biomass in the oligotrophic Cretan Sea (NE Mediterranean). *Progress in Oceanography, 46*(2–4), 279-310. doi:http://dx.doi.org/10.1016/S0079-6611(00)00023-9
Fischer, A. C., Kroon, J. J., Verburg, T. G., Teunissen, T., & Wolterbeek, H. T. (2007). On the relevance of iron adsorption to container materials in small-volume experiments on iron marine chemistry: 55Fe-aided assessment of capacity, affinity and kinetics. *Marine Chemistry, 107*(4), 533-546. doi:http://dx.doi.org/10.1016/j.marchem.2007.08.004
Fitzsimmons, J. N., Bundy, R. M., Al-Subiai, S. N., Barbeau, K. A., & Boyle, E. A. (2015). The composition of dissolved iron in the dusty surface ocean: An exploration using size-fractionated iron-binding ligands. *Marine Chemistry, 173*, 125-135. doi:http://doi.org/10.1016/j.marchem.2014.09.002
Fitzsimmons, J. N., Hayes, C. T., Al-Subiai, S. N., Zhang, R., Morton, P. L., Weisend, R. E., . . . Boyle, E. A. (2015). Daily to decadal variability of size-fractionated iron and iron-binding ligands at the Hawaii Ocean Time-series Station ALOHA. *Geochimica et Cosmochimica Acta, 171*, 303-324. doi:http://dx.doi.org/10.1016/j.gca.2015.08.012
Gledhill, M., & Buck, K. (2012). The organic complexation of iron in the marine environment: a review *Front. Microbiol.* (Vol. 3).
Greaves, M., Rudnicki, M., & Elderfield, H. (1991). Rare earth elements in the Mediterranean Sea and mixing in the Mediterranean outflow. *Earth and Planetary Science Letters, 103*(1-4), 169-181.
Hathorne, E. C., Haley, B., Stichel, T., Grasse, P., Zieringer, M., & Frank, M. (2012). Online preconcentration ICP-MS analysis of rare earth elements in seawater. *Geochemistry, Geophysics, Geosystems, 13*(1), n/a-n/a. doi:10.1029/2011GC003907
Hutchins, D., & Bruland, K. (1994). Grazer-mediated regeneration and assimilation of Fe, Zn and Mn from planktonic prey. *Marine Ecology-Progress Series, 110*, 259-259.
ISO, I. 5725-1: 1994. *Accuracy (trueness and precision) of measurement methods and results--part, 1*.

Jickells, T. D., An, Z. S., Andersen, K. K., Baker, A. R., Bergametti, G., Brooks, N., . . . Torres, R. (2005). Global Iron Connections Between Desert Dust, Ocean Biogeochemistry, and Climate. *Science, 308*(5718), 67-71. doi:10.1126/science.1105959

Johnson, K. S., Gordon, R. M., & Coale, K. H. (1997). What controls dissolved iron concentrations in the world ocean? *Marine Chemistry, 57*(3), 137-161.

Karl, D. M., & Tien, G. (1992). MAGIC: A sensitive and precise method for measuring dissolved phosphorus in aquatic environments. *Limnology and Oceanography, 37*(1), 105-116.

Kirchman, D. L. (1996). Oceanography - Microbial ferrous wheel. *Nature, 383*(6598), 303-304.

Kirchman, D. L., Meon, B., Cottrell, M. T., Hutchins, D. A., Weeks, D., & Bruland, K. W. (2000). Carbon versus iron limitation of bacterial growth in the California upwelling regime. *Limnology and Oceanography, 45*(8), 1681-1688. doi:10.4319/lo.2000.45.8.1681

Krom, M., Emeis, K., & Van Cappellen, P. (2010). Why is the Eastern Mediterranean phosphorus limited? *Progress in Oceanography, 85*(3), 236-244.

Krom, M. D., Kress, N., Brenner, S., & Gordon, L. I. (1991). Phosphorus limitation of primary productivity in the eastern Mediterranean Sea. *Limnology and Oceanography, 36*(3), 424-432. doi:10.4319/lo.1991.36.3.0424

Laerd, S. (2013). Laerd Statistics. *Retrieved 2017.*

Lagerström, M. E., Field, M. P., Séguret, M., Fischer, L., Hann, S., & Sherrell, R. M. (2013). Automated on-line flow-injection ICP-MS determination of trace metals (Mn, Fe, Co, Ni, Cu and Zn) in open ocean seawater: Application to the GEOTRACES program. *Marine Chemistry, 155*, 71-80. doi:http://dx.doi.org/10.1016/j.marchem.2013.06.001

Lamborg, C. H., Buesseler, K. O., & Lam, P. J. (2008). Sinking fluxes of minor and trace elements in the North Pacific Ocean measured during the VERTIGO program. *Deep Sea Research Part II: Topical Studies in Oceanography, 55*(14–15), 1564-1577. doi:http://dx.doi.org/10.1016/j.dsr2.2008.04.012

Libes, S. (2009). *Introduction to marine biogeochemistry*: Academic Press.

Liu, X., & Millero, F. J. (2002). The solubility of iron in seawater. *Marine Chemistry, 77*(1), 43-54. doi:http://dx.doi.org/10.1016/S0304-4203(01)00074-3

Luna, G. M. (2015). Diversity of marine microbes in a changing Mediterranean Sea. *Rendiconti Lincei, 26*(1), 49-58. doi:10.1007/s12210-014-0333-x

Martin, J. H. (1990). Glacial-interglacial CO2 change: The iron hypothesis. *Paleoceanography, 5*(1), 1-13.

Melton, E. D., Swanner, E. D., Behrens, S., Schmidt, C., & Kappler, A. (2014). The interplay of microbially mediated and abiotic reactions in the biogeochemical Fe cycle. *Nature Reviews Microbiology*. doi:10.1038/nrmicro3347

Migon, C. (2005). Trace metals in the Mediterranean Sea *The Mediterranean Sea* (pp. 151-176): Springer.

Millero, F. J., Yao, W., & Aicher, J. (1995). The speciation of Fe(II) and Fe(III) in natural waters. *Marine Chemistry, 50*(1), 21-39. doi:http://dx.doi.org/10.1016/0304-4203(95)00024-L

Moore, C. M., Mills, M. M., Arrigo, K., Berman-Frank, I., Bopp, L., Boyd, P., . . . Ulloa, O. (2013). Processes and patterns of oceanic nutrient limitation *Nat. Geosci.* (Vol. 6, pp. 701-710).

Morel, F., & Price, N. (2003). The biogeochemical cycles of trace metals in the oceans. *Science, 300*(5621), 944-947.

Morel, F. M. M. (2008). The co-evolution of phytoplankton and trace element cycles in the oceans. *Geobiology, 6*(3), 318-324. doi:10.1111/j.1472-4669.2008.00144.x

Parekh, P., Follows, M. J., & Boyle, E. A. (2005). Decoupling of iron and phosphate in the global ocean. *Global biogeochemical cycles, 19*(2).

Poehle, S., Schmidt, K., & Koschinsky, A. (2015). Determination of Ti, Zr, Nb, V, W and Mo in seawater by a new online-preconcentration method and subsequent ICP–MS analysis. *Deep Sea Research Part I: Oceanographic Research Papers, 98*, 83-93. doi:http://dx.doi.org/10.1016/j.dsr.2014.11.014

Poorvin, L., Rinta-Kanto, J. M., Hutchins, D. A., & Wilhelm, S. W. (2004). Viral release of iron and its bioavailability to marine plankton. *Limnology and Oceanography, 49*(5), 1734-1741.

Pujo-Pay, M., Conan, P., Oriol, L., Cornet-Barthaux, V., Falco, C., Ghiglione, J. F., . . . Prieur, L. (2011). Integrated survey of elemental stoichiometry (C, N, P) from the western to eastern Mediterranean Sea. *Biogeosciences, 8*(4), 883-899. doi:10.5194/bg-8-883-2011

Rimmelin, P., & Moutin, T. (2005). Re-examination of the MAGIC method to determine low orthophosphate concentration in seawater. *Analytica Chimica Acta, 548*(1–2), 174-182. doi:http://dx.doi.org/10.1016/j.aca.2005.05.071

Rue, E. L., & Bruland, K. W. (1995). Complexation of iron(III) by natural organic ligands in the Central North Pacific as determined by a new competitive ligand equilibration/adsorptive cathodic stripping voltammetric method. *Marine Chemistry, 50*(1), 117-138. doi:http://dx.doi.org/10.1016/0304-4203(95)00031-L

Sarthou, G., Vincent, D., Christaki, U., Obernosterer, I., Timmermans, K. R., & Brussaard, C. P. D. (2008). The fate of biogenic iron during a phytoplankton bloom induced by natural fertilisation: Impact of copepod grazing. *Deep-Sea Research Part II, 55*(5), 734-751. doi:10.1016/j.dsr2.2007.12.033

Sato, M., Takeda, S., & Furuya, K. (2007). Iron regeneration and organic iron (III)-binding ligand production during in situ zooplankton grazing experiment. *Marine Chemistry, 106*(3), 471-488.

Schlosser, C., De La Rocha, C. L., & Croot, P. L. (2011). Effects of iron surface adsorption and sample handling on iron solubility measurements. *Marine Chemistry, 127*(1–4), 48-55. doi:http://dx.doi.org/10.1016/j.marchem.2011.07.008

ShimadzuCorporation. (2014.). Total Organic Carbon Analyzer: User's Manual. .

Sohrin, Y., Urushihara, S., Nakatsuka, S., Kono, T., Higo, E., Minami, T., . . . Umetani, S. (2008). Multielemental Determination of GEOTRACES Key Trace Metals in Seawater by ICPMS after Preconcentration Using an Ethylenediaminetriacetic Acid Chelating Resin. *Analytical Chemistry, 80*(16), 6267-6273. doi:10.1021/ac800500f

Statham, P. J., & Hart, V. (2005). Dissolved iron in the Cretan Sea (eastern Mediterranean. *Limnology and Oceanography, 50*(4), 1142-1148. doi:10.4319/lo.2005.50.4.1142

Strzepek, R., Maldonado, M., Higgins, J., Hall, J., Safi, K., Wilhelm, S., & Boyd, P. (2005). Spinning the "Ferrous Wheel": The importance of the microbial community in an iron budget during the FeCycle experiment. *Global biogeochemical cycles, 19*(4).

Stumm, W., & Morgan, J. J. (1996). *Aquatic Chemistry: Chemical Equilibria and Rates in Natural Waters {Environmental Science and Technology}*: Wiley.

Sunda, W. (2012). Feedback interactions between trace metal nutrients and phytoplankton in the ocean *Front. Microbiol.* (Vol. 3).

Sunda, W. G., & Huntsman, S. A. (1995). Iron uptake and growth limitation in oceanic and coastal phytoplankton. *Marine Chemistry, 50*(1), 189-206. doi:http://dx.doi.org/10.1016/0304-4203(95)00035-P

Tagliabue, A., Bowie, A. R., Boyd, P. W., Buck, K. N., Johnson, K. S., & Saito, M. A. (2017). The integral role of iron in ocean biogeochemistry. *Nature, 543*(7643), 51-59. doi:10.1038/nature21058

Theodosi, C., Markaki, Z., & Mihalopoulos, N. (2010). Iron speciation, solubility and temporal variability in wet and dry deposition in the Eastern Mediterranean. *Marine Chemistry, 120*(1), 100-107.

Thingstad, T., Krom, M., Mantoura, R., Flaten, G. F., Groom, S., Herut, B., . . . Pitta, P. (2005). Nature of phosphorus limitation in the ultraoligotrophic eastern Mediterranean. *Science, 309*(5737), 1068-1071.

Tortell, P. D., Maldonado, M. T., & Price, N. M. (1996). The role of heterotrophic bacteria in iron-limited ocean ecosystems. *Nature, 383*(6598), 330.

Tovar-Sanchez, A., Sañudo-Wilhelmy, S. A., Garcia-Vargas, M., Weaver, R. S., Popels, L. C., & Hutchins, D. A. (2003). A trace metal clean reagent to remove surface-bound iron from

marine phytoplankton. *Marine Chemistry, 82*(1–2), 91-99. doi:http://doi.org/10.1016/S0304-4203(03)00054-9

Tselepides, A., Zervakis, V., Polychronaki, T., Danovaro, R., & Chronis, G. (2000). Distribution of nutrients and particulate organic matter in relation to the prevailing hydrographic features of the Cretan Sea (NE Mediterranean). *Progress in Oceanography, 46*(2–4), 113-142. doi:http://dx.doi.org/10.1016/S0079-6611(00)00015-X

Twining, B. S., Nodder, S. D., King, A. L., Hutchins, D. A., LeCleir, G. R., DeBruyn, J. M., . . . Boyd, P. W. (2014). Differential remineralization of major and trace elements in sinking diatoms. *Limnology and Oceanography, 59*(3), 689-704. doi:10.4319/lo.2014.59.3.0689

Ussher, S. J., Achterberg, E. P., Powell, C., Baker, A. R., Jickells, T. D., Torres, R., & Worsfold, P. J. (2013). Impact of atmospheric deposition on the contrasting iron biogeochemistry of the North and South Atlantic Ocean. *Global biogeochemical cycles, 27*(4), 1096-1107. doi:10.1002/gbc.20056

van den Berg, C. M. (1995). Evidence for organic complexation of iron in seawater. *Marine Chemistry, 50*(1-4), 139-157.

Wagener, T., Guieu, C., & Leblond, N. (2010). Effects of dust deposition on iron cycle in the surface Mediterranean Sea: results from a mesocosm seeding experiment. *Biogeosciences, 7*(11), 3769.

Waite, T. D. (2001). Thermodynamics of the iron system in seawater. *IUPAC series on analytical and physical chemistry of environmental systems, 7*, 291-342.

Whitfield, M. (2001). Interactions between phytoplankton and trace metals in the ocean. *Advances in Marine Biology, 41*, 1-128.

Wolf, R. (2005). What is ICP-MS? and more importantly, what can it do. *US Geological Survey, 7*.

Worsfold, P. J., Lohan, M. C., Ussher, S. J., & Bowie, A. R. (2014). Determination of dissolved iron in seawater: A historical review. *Marine Chemistry, 166*, 25-35. doi:10.1016/j.marchem.2014.08.009

Wu, J., Boyle, E., Sunda, W., Wen, L.-S., & Wu, J. (2001). Soluble and colloidal iron in the oligotrophic North Atlantic and North Pacific. *Science (Washington), 293*(5531), 847-849.

Wuttig, K., Wagener, T., Bressac, M., Dammshäuser, A., Streu, P., Guieu, C., & Croot, P. (2013). Impacts of dust deposition on dissolved trace metal concentrations (Mn, Al and Fe) during a mesocosm experiment. *Biogeosciences, 10*(4), 2583.

Zaballos, M., López-López, A., Ovreas, L., Bartual, S. G., D' Auria, G., Alba, J. C., . . . Rodríguez-Valera, F. (2006). Comparison of prokaryotic diversity at offshore oceanic locations reveals a different microbiota in the Mediterranean Sea. *FEMS Microbiology Ecology, 56*(3), 389-405. doi:10.1111/j.1574-6941.2006.00060.x

Appendix A: ICP-MS Results

	µg/l Cd114(LR)	µg/l Mo98(MR)	µg/l Pb208(LR)	µg/l V51(MR)	µg/l Mn55(MR)	µg/l Fe56(MR)	µg/l Co59(MR)	µg/l Ni60(MR)	µg/l Cu63(MR)	µg/l Zn66(MR)
Seawater NASS-6	0,0303	4,5981	0,0077	1,2647	0,4876	0,4660	0,0143	0,6308	0,2493	0,6915
Seawater NASS-6	0,0297	4,6427	0,0100	1,2588	0,4894	0,4733	0,0153	0,5516	0,2439	0,4277
Seawater NASS-6	0,0301	4,5274	0,0342	1,2785	0,4888	0,5385	0,0148	0,8421	0,2519	0,7544
Seawater NASS-6	0,0312	4,7135	0,0140	1,1739	0,4718	0,5070	0,0147	0,8127	0,2381	0,9278
Seawater NASS-6	0,0318	4,3295	0,0051	1,2551	0,4864	0,4687	0,0161	0,3736	0,2441	0,4615
Seawater NASS-6	0,0302	4,3137	0,0080	1,2597	0,4850	0,5379	0,0165	0,4550	0,2693	0,4378
Average	**0,0305**	**4,5208**	**0,0132**	**1,2484**	**0,4848**	**0,4986**	**0,0153**	**0,6110**	**0,2494**	**0,6168**
Std	0,0008	0,1658	0,0107	0,0374	0,0066	0,0341	0,0009	0,1891	0,0108	0,2065
Rsd % <5, 5-10, >10	2,5	3,7	81,3	3,0	1,4	6,8	5,6	30,9	4,3	33,5
Number	6	6	6	6	6	6	6	6	6	6
NASS Ref (ug/L)	0,0311	9,89	0,006	1,46	0,53	0,495	0,015	0,301	0,248	0,257
Std Dev	0,0019	0,05	0,002	0,17	0,05	0,046		0,025	0,025	0,02
Accuracy	98,17412	45,71103	219,4533	85,50989	91,48008	100,7201	101,8137	202,9767	100,5795	240,0009

Figure A.1: NASS-6 reference values during initial SeaFAST testing corrected for preconcentration

Table A.1: Dissolved iron from ICP-MS corrected for blank and preconcentration

Time	Sample Name	Concentration (µg/L)	Concentration (nM)	Type	Tank
31	1-2 D	0.0936	1.6768	Dissolved	1
31	1-2 D	0.1984	3.5531	Dissolved	1
47	1-3 D	0.4456	7.9793	Dissolved	1
47	1-3 D	0.2056	3.6816	Dissolved	1
71	1-4 D	0.1694	3.0330	Dissolved	1
71	1-4 D	0.1467	2.6272	Dissolved	1
95	1-5 D	0.0218	0.3908	Dissolved	1
95	1-5 D	0.1798	3.2190	Dissolved	1
118	1-6 D	0.1910	3.4195	Dissolved	1
118	1-6 D	0.1229	2.2004	Dissolved	1
140	*1-7 D*	*4.2425*	*75.9689*	*Dissolved*	*1*
140	*1-7 D*	*0.1595*	*2.8562*	*Dissolved*	*1*
31	2-2 D	0.1291	2.3112	Dissolved	2
31	*2-2 D*	*0.5532*	*9.9055*	*Dissolved*	*2*
47	2-3 D	0.2110	3.7787	Dissolved	2
47	2-3 D	0.1890	3.3848	Dissolved	2
71	2-4 D	0.1538	2.7548	Dissolved	2
71	2-4 D	0.1396	2.4998	Dissolved	2
95	2-5 D	0.2109	3.7756	Dissolved	2
95	2-5 D	0.1816	3.2513	Dissolved	2
118	2-6 D	0.1394	2.4970	Dissolved	2
118	2-6 D	0.1509	2.7021	Dissolved	2
140	*2-7 D*	*0.3582*	*6.4140*	*Dissolved*	*2*
140	*2-7 D*	*0.6681*	*11.9626*	*Dissolved*	*2*
31	5-2 D	0.1016	1.8194	Dissolved	5
31	5-2 D	0.2239	4.0094	Dissolved	5
47	5-3 D	0.3051	5.4642	Dissolved	5
47	5-3 D	Sample spoiled		Dissolved	5
71	5-4 D	0.1223	2.1903	Dissolved	5
71	5-4 D	0.1196	2.1416	Dissolved	5
95	5-5 D	0.1627	2.9134	Dissolved	5
95	5-5 D	0.1814	3.2490	Dissolved	5
118	5-6 D	0.0630	1.1277	Dissolved	5
118	5-6 D	-0.0016	-0.0286	Dissolved	5
140	*5-7 D*	*1.5238*	*27.2857*	*Dissolved*	*5*
140	*5-7 D*	*2.3658*	*42.3643*	*Dissolved*	*5*
31	6-2 D	0.0831	1.4878	Dissolved	6
31	6-2 D	0.1566	2.8050	Dissolved	6

47	6-3 D	0.2901	5.1944	Dissolved	6
47	6-3 D	0.2322	4.1586	Dissolved	6
71	6-4 D	0.1571	2.8125	Dissolved	6
71	6-4 D	0.4167	7.4613	Dissolved	6
95	6-5 D	0.2012	3.6024	Dissolved	6
95	6-5 D	0.1602	2.8695	Dissolved	6
118	*6-6 D*	*1.0228*	*18.3142*	*Dissolved*	*6*
118	*6-6 D*	*0.6428*	*11.5104*	*Dissolved*	*6*
140	*6-7 D*	*0.4614*	*8.2627*	*Dissolved*	*6*
140	*6-7 D*	*0.9752*	*17.4630*	*Dissolved*	*6*
31	9-2 D	0.1327	2.3754	Dissolved	9
31	9-2 D	0.1415	2.5339	Dissolved	9
47	9-3 D	0.1552	2.7787	Dissolved	9
47	9-3 D	0.1825	3.2688	Dissolved	9
71	9-4 D	0.2711	4.8543	Dissolved	9
71	9-4 D	0.1641	2.9392	Dissolved	9
95	9-5 D	0.2404	4.3051	Dissolved	9
95	9-5 D	0.1665	2.9815	Dissolved	9
118	9-6 D	0.1322	2.3666	Dissolved	9
118	9-6 D	0.1179	2.1110	Dissolved	9
140	*9-7 D*	*0.1535*	*2.7481*	*Dissolved*	*9*
140	*9-7 D*	*0.1795*	*3.2142*	*Dissolved*	*9*
31	10-2 D	0.2640	4.7274	Dissolved	10
31	10-2 D	0.1228	2.1987	Dissolved	10
47	10-3 D	0.1970	3.5283	Dissolved	10
47	10-3 D	0.2625	4.7012	Dissolved	10
71	10-4 D	0.2395	4.2890	Dissolved	10
71	10-4 D	0.1935	3.4657	Dissolved	10
95	10-5 D	0.1678	3.0051	Dissolved	10
95	10-5 D	0.2085	3.7344	Dissolved	10
118	10-6 D	0.1573	2.8170	Dissolved	10
118	10-6 D	0.1820	3.2588	Dissolved	10
140	*10-7 D*	*-0.0219*	*-0.3929*	*Dissolved*	*10*
140	*10-7 D*	*0.4336*	*7.7648*	*Dissolved*	*10*

Mean	0.333415073	5.970365701
Standard Deviation	0.584210293	10.46128199
Sample Variance	0.341301666	109.4384209
Range	4.264424041	76.36178782
Minimum	-0.021941835	-0.392905986

	Maximum	4.242482206	75.96888183	
	Count	71	71	

Table A.2: Total dissolvable iron from ICP-MS corrected for blank and preconcentration

Time	Sample Name	Concentration (µg/L)	Concentration (nM)	Type	Tank
31	1-2 T	0.2994	5.3611	Total	1
31	1-2 T	1.0130	18.1395	Total	1
31	1-2 T	0.7802	13.9703	Total	1
47	1-3 T	0.6706	12.0084	Total	1
47	1-3 T	0.4153	7.4358	Total	1
71	1-4 T	0.6091	10.9072	Total	1
71	1-4 T	0.4696	8.4084	Total	1
95	1-5 T	0.3167	5.6718	Total	1
95	1-5 T	0.4049	7.2498	Total	1
118	1-6 T	0.2085	3.7344	Total	1
118	1-6 T	0.5295	9.4816	Total	1
140	1-7 T	0.4670	8.3632	Total	1
140	1-7 T	1.4652	26.2372	Total	1
31	2-2 T	0.5163	9.2459	Total	2
31	2-2 T	2.2906	41.0170	Total	2
31	2-2 T	0.5380	9.6345	Total	2
47	2-3 T	0.5505	9.8577	Total	2
47	2-3 T	0.7212	12.9136	Total	2
71	2-4 T	0.4798	8.5909	Total	2
71	2-4 T	0.3900	6.9839	Total	2
95	2-5 T	3.6775	65.8511	Total	2
95	2-5 T	0.6472	11.5898	Total	2
118	2-6 T	0.4416	7.9076	Total	2
118	2-6 T	0.4111	7.3621	Total	2
140	2-7 T	0.3999	7.1607	Total	2
140	2-7 T	0.3790	6.7861	Total	2
31	5-2 T	0.2958	5.2964	Total	5
31	5-2 T	0.5426	9.7167	Total	5
31	5-2 T	1.3185	23.6092	Total	5
47	5-3 T	0.6264	11.2174	Total	5
47	5-3 T	0.5753	10.3022	Total	5
71	5-4 T	0.4054	7.2596	Total	5
71	5-4 T	0.7585	13.5822	Total	5
95	5-5 T	0.4073	7.2929	Total	5
95	5-5 T	0.3334	5.9692	Total	5
118	5-6 T	0.4522	8.0971	Total	5
118	5-6 T	0.4359	7.8052	Total	5
140	5-7 T	0.1599	2.8634	Total	5

140	5-7 T	1.8897	33.8391	Total	5
31	6-2 T	4.7639	85.3059	Total	6
31	6-2 T	1.0512	18.8228	Total	6
31	6-2 T	0.6957	12.4583	Total	6
47	6-3 T	0.5441	9.7425	Total	6
47	6-3 T	0.5060	9.0600	Total	6
71	6-4 T	0.3067	5.4917	Total	6
71	6-4 T	0.3400	6.0875	Total	6
95	6-5 T	0.3229	5.7826	Total	6
95	6-5 T	0.3162	5.6625	Total	6
118	6-6 T	0.0145	0.2593	Total	6
118	6-6 T	0.0088	0.1572	Total	6
140	6-7 T	0.1253	2.2433	Total	6
140	6-7 T	0.1439	2.5764	Total	6
31	9-2 T	0.4455	7.9783	Total	9
31	9-2 T	1.2062	21.5982	Total	9
31	9-2 T	2.0242	36.2461	Total	9
47	9-3 T	0.6267	11.2227	Total	9
47	9-3 T	0.6430	11.5131	Total	9
71	9-4 T	0.3067	5.4924	Total	9
71	9-4 T	0.2981	5.3379	Total	9
95	9-5 T	1.3041	23.3515	Total	9
95	9-5 T	0.6831	12.2320	Total	9
118	9-6 T	0.7094	12.7033	Total	9
118	9-6 T	0.5947	10.6485	Total	9
140	9-7 T	0.9406	16.8437	Total	9
140	9-7 T	1.3911	24.9103	Total	9
31	10-2 T	1.4738	26.3909	Total	10
31	10-2 T	0.3979	7.1248	Total	10
31	10-2 T	0.9838	17.6171	Total	10
47	10-3 T	0.4757	8.5187	Total	10
47	10-3 T	0.5388	9.6484	Total	10
71	10-4 T	0.4188	7.5001	Total	10
71	10-4 T	0.4835	8.6581	Total	10
95	10-5 T	0.5512	9.8705	Total	10
95	10-5 T	0.4212	7.5415	Total	10
118	10-6 T	0.4571	8.1856	Total	10
118	10-6 T	0.4673	8.3686	Total	10
140	10-7 T	0.5746	10.2889	Total	10
140	10-7 T	0.9700	17.3688	Total	10

Mean	0.715625237	12.81449076
Standard Deviation	0.717950024	12.85612004
Sample Variance	0.515452236	165.2798225
Range	4.755130791	85.14872936
Minimum	0.008779715	0.157215778
Maximum	4.763910506	85.30594514
Count	78	78

Table A.3: REE Values from Batch 1 of Crete samples compared to literature values. Concentrations in pmol/kg

pmol kg^{-1}	**This study Cretan Sea, 10m depth, n=98**	**(Bau et al., 1997) Eastern Med., 100m depth**	**(Censi et al., 2004) Sicily, 15-20m depth**	**(Greaves et al., 1991) NW Med, 25m depth**
Lanthanum	24.7 ± 4.87	25.6	26.9	26.1
Cerium	25.7 ± 8.05	n/a	19.1	20.9
Praseodymium	5.32 ± 1.13	5.73	5.02	n/a
Neodymium	26.4 ± 5.78	25.7	25.8	24.4
Samarium	6.04 ± 1.25	6.25	5.54	5.53
Dysprosium	9.24 ± 1.39	10.7	9.80	8.76
Holmium	2.21 ± 0.31	2.80	2.84	2.66
Erbium	7.42 ± 1.01	8.84	8.55	6.78
Ytterbium	6.84 ± 0.93	8.31	8.07	6.11

Tables A.4, A.5, A.6: Macronutrient data for phosphate, silicate, and total nitrogen for each tank at each time period.

PO_4 (nM)	TANK					
Time period	**1**	**2**	**5**	**6**	**9**	**10**
33	2.7	2	3.1	1.3	3.4	2.9
45	8.5	6.7	6.1	5.9	3.5	5
69	12	14.1	11.3	12	7.8	13.5
93	9.6	13.1	9.9	19.6	11.4	10.7
116	15	***408***	***36.3***	15.4	7.3	11.1
131	14.2	15.3	12.5	18.2	11.6	12

SiO_4 (µM)						
Time period	**1**	**2**	**5**	**6**	**9**	**10**
33	0.89	0.79	0.96	0.74	1.08	0.86
45	0.93	0.77	1.00	0.86	0.85	0.78
69	0.82	1.02	0.66	1.02	0.81	0.66
93	0.94	1.06	1.04	0.95	0.91	1.04
116	1.04	0.91	0.82	0.72	0.87	0.91
138	0.98	0.64	1.06	0.70	0.91	0.75

N_{Tot}(µM)	TANK					
Time period	**1**	**2**	**5**	**6**	**9**	**10**
33	0.24	0.10	0.18	0.20	0.18	0.23
45	0.23	0.22	0.13	0.18	0.16	0.19
69	0.22	0.17	0.14	0.34	0.14	0.21
93	0.11	0.13	0.14	0.18	0.17	0.10
116	0.27	0.12	0.12	0.15	0.09	0.19
138	0.20	0.13	0.20	0.11	0.14	0.10

Table A.7: NASS-6 values corrected for blank and preconcentration run during Crete samples

ICPMS	Fe	Mn	Cu	Ni	Cd (114)	Co	Zn
Batch 1	0.423	0.422	0.207	0.329	0.031	0.013	0.237
Batch 1	0.481	0.426	0.210	0.322	0.030	0.012	0.670
Batch 1	0.365	0.380	0.177	0.345	0.027	0.011	0.217
Batch 1	0.342	0.360	0.170	0.306	0.025	0.011	0.200
Batch 1	0.414	0.432	0.202	0.304	0.029	0.014	0.240
Batch 1	0.410	0.427	0.198	0.337	0.028	0.013	0.247
Batch 1	0.370	0.405	0.185	0.286	0.027	0.011	0.230
Batch 1	0.427	0.427	0.200	0.309	0.029	0.013	0.239
Batch 1	0.413	0.386	0.184	0.306	0.028	0.013	0.231
Batch 2	0.425	0.447	0.220	0.482	0.032	0.015	0.740
Batch 2	0.439	0.455	0.220	0.554	0.031	0.013	0.338
Batch 2	0.427	0.445	0.212	0.462	0.031	0.014	0.392
Batch 2	0.448	0.467	0.217	0.525	0.031	0.016	0.523
molar mass	55.845	54.938	63.546	58.6934	112.411	58.93	65.8
BLANK VALUE in nM	0.415	0.0213	0.0878	2.85	0.00034	0.0191	1.55
Blank Value in µg/L	0.023	0.00117	0.00558	0.167	0.00004	0.00113	0.102
NUMBER	13	13	13	13	13	13	13
AVERAGE (µg/L) corrected	**0.414**	**0.420**	**0.194**	**0.207**	**0.029**	**0.012**	**0.244**
MINIMUM (µg/L)	0.342	0.360	0.170	0.286	0.025	0.011	0.200
MAXIMUM (µg/L)	0.481	0.467	0.220	0.554	0.032	0.016	0.740
STD DEV	**0.0369**	**0.0310**	**0.0164**	**0.0946**	**0.00211**	**0.00153**	**0.183**
CONF INTERVAL (95%)	0.0213	0.0179	0.00946	0.0546	0.00122	0.0009	0.106
RSD	**5.15**	**4.26**	**4.86**	**26.4**	**4.17**	**7.48**	**43.3**
CERTIFIED NASS VALUE (µg/L)	0.495	0.53	0.248	0.301	0.0311	0.015	0.257
CERTIFIED NASS RANGE + -(µg/L)	0.046	0.05	0.025	0.025	0.0019		0.02
ACCEPTED RANGE %	9.29	9.43	10.1	8.31	6.11		7.78
ACCURACY	**83.6**	**79.3**	**78.4**	**68.8**	**93.8**	**79.0**	**95.1**

Table A.8: Blank values for MilliQ run among Crete samples. Includes concentration in nM and ug/L corrected for preconcentration. "u###" indicates blank value excluded in mean value.

Project-number	nM*	Conc.	nM*	Conc.	nM*	Conc.	nM*	Conc.	nM*	Conc.	nM*	Conc.	nM*	Conc.
	Cd 114	µg/L	Mn 55	µg/L	Fe 56	µg/L	Ni 60	µg/L	Cu 63	µg/L	Zn 66	µg/L	Co 59	µg/L
1		u0.0041	**0.067**	0.024		u2.01	**0.86**	0.33		u0.086		u1.33		u0.026
2	**0.0005**	0.0004	**0.062**	0.023		u1.35		u0.68	**0.086**	0.036	**0.75**	0.33	**0.014**	0.006
3	**0.0005**	0.0004	**0.009**	0.003	**0.470**	0.175		u1.38	**0.102**	0.043	**1.26**	0.55	**0.013**	0.005
16	**0.0010**	0.0008	**0.187**	0.069		u1.00	**1.39**	0.54		u0.233		u1.91	**0.035**	0.014
17	**0.0007**	0.0005	**0.008**	0.003	**0.430**	0.160		u1.38	**0.073**	0.031	**0.48**	0.21	**0.042**	0.016
18	**0.0002**	0.0002	**0.025**	0.009		u0.495		u6.34		u0.098		u0.78	**0.011**	0.004
31	**0.0000**	0.0000	**0.013**	0.005		u0.261	**1.53**	0.60	**0.078**	0.033	**0.49**	0.21	**0.011**	0.004
32	**-0.0003**	-0.0003	**0.017**	0.006		u0.272		u0.73	**0.137**	0.058	**1.16**	0.51	**0.015**	0.006
33	**0.0001**	0.0001	**0.017**	0.006	**0.375**	0.140		u0.9	**0.140**	0.059	**0.72**	0.31	**0.018**	0.007
46	**0.0001**	0.0001	**0.015**	0.006	**0.235**	0.087	**1.36**	0.53	**0.059**	0.025	**0.44**	0.19	**0.014**	0.005
47	**0.0002**	0.0002	**0.015**	0.005	**0.571**	0.213	**1.40**	0.55	**0.047**	0.020	**1.08**	0.47	**0.008**	0.003
48	**0.0000**	0.0000	**0.011**	0.004	**0.549**	0.204		u0.91	**0.089**	0.038	**0.50**	0.22	**0.009**	0.004
61	**-0.0001**	-0.0001	**0.006**	0.002	**0.263**	0.098	**1.19**	0.46	**0.045**	0.019	**0.35**	0.15	**0.009**	0.003
62	**0.0023**	0.0017		u0.117	**0.549**	0.204		u0.92		u0.439		u3.58	**0.029**	0.012
63	**0.0006**	0.0004	**0.057**	0.021	**0.416**	0.155		u1.07		u0.088		u26.44	**0.027**	0.010
76	**0.0002**	0.0001	**0.016**	0.006	**0.408**	0.152	**1.28**	0.50	**0.095**	0.040	**0.46**	0.20	**0.011**	0.004
77	**-0.0002**	-0.0001	**0.009**	0.003	**0.151**	0.056	**1.30**	0.51	**0.035**	0.015	**0.29**	0.13	**0.008**	0.003

78	**-0.0002**	-0.0002	**0.008**	0.003	**0.217**	0.081	**0.75**	0.29	**0.027**	0.012	**0.26**	0.11		u0.021
91	**0.0008**	0.0006	**0.003**	0.001	**0.330**	0.123	**1.03**	0.40	**0.029**	0.012	**0.26**	0.11	**0.030**	0.012
92	**0.0003**	0.0002	**0.011**	0.004	**0.236**	0.088	**1.28**	0.50	**0.048**	0.020	**0.64**	0.28	**0.009**	0.004
93	**0.0001**	0.0001	**0.003**	0.001	**0.316**	0.118	**1.07**	0.42	**0.033**	0.014	**0.49**	0.22		u0.016
106	**0.0005**	0.0004	**0.015**	0.006		u0.377		u1.11	**0.062**	0.026	**0.39**	0.17	**0.011**	0.004
107	**0.0003**	0.0002	**0.008**	0.003	**0.433**	0.161	**0.78**	0.30	**0.046**	0.020	**0.38**	0.17	**0.004**	0.002
108	**0.0000**	0.0000	**0.001**	0.000	**0.111**	0.041	**0.81**	0.32	**0.030**	0.013	**0.29**	0.13	**0.004**	0.002
121	**0.0007**	0.0005	**0.004**	0.001	**0.310**	0.115	**1.01**	0.40	**0.027**	0.012	**0.40**	0.17	**0.002**	0.001
122	**0.0004**	0.0003	**0.004**	0.001	**0.337**	0.125	**0.84**	0.33	**0.028**	0.012	**0.35**	0.15	**0.003**	0.001
123	**0.0001**	0.0001	**0.008**	0.003	**0.310**	0.116	**0.84**	0.33	**0.029**	0.012	**0.37**	0.16	**0.002**	0.001
136	**0.0007**	0.0005	**0.019**	0.007	**0.724**	0.270	**0.82**	0.32	**0.091**	0.038	**0.63**	0.27	**0.003**	0.001
137	**0.0008**	0.0006	**0.008**	0.003	**0.600**	0.223		u0.63	**0.044**	0.018	**0.45**	0.20	**0.004**	0.002
138	**0.0008**	0.0006	**0.025**	0.009		u0.46	**0.92**	0.36	**0.095**	0.040	**0.56**	0.25	**0.005**	0.002
151	**-0.0002**	-0.0001	**0.023**	0.004	**0.395**	0.074	**3.75**	0.73	**0.187**	0.040	**8.51**	1.86	**0.050**	0.010
152	**0.0000**	0.0000	**0.036**	0.007	**0.498**	0.093	**3.04**	0.59	**0.140**	0.030	**8.35**	1.82	**0.078**	0.015
153	**0.0000**	0.0000	**0.039**	0.007	**1.010**	0.188	**3.28**	0.64	**0.135**	0.029	**7.75**	1.69	**0.056**	0.011
181	**0.0006**	0.0002	**0.015**	0.003	**1.340**	0.249	**8.65**	1.69	**0.215**	0.046	**2.46**	0.54	**0.005**	0.001
182	**0.0003**	0.0001	**0.001**	0.000	**0.250**	0.047	**5.28**	1.03	**0.180**	0.038	**1.95**	0.42	**0.101**	0.020
183	**0.0003**	0.0001	**0.002**	0.000	**0.277**	0.051	**7.89**	1.54	**0.190**	0.040	**1.82**	0.40	**0.020**	0.004
211	**0.0025**	0.0009	**0.019**	0.004	**0.484**	0.090	**14.01**	2.74	**0.137**	0.029	**2.99**	0.65	**0.010**	0.002
212	**0.0009**	0.0003	**0.007**	0.001	**0.173**	0.032	**4.70**	0.92	**0.108**	0.023	**2.36**	0.52	**0.008**	0.002
213	**0.0009**	0.0003	**0.015**	0.003	**0.106**	0.020	**8.76**	1.71	**0.119**	0.025	**2.90**	0.63	**0.012**	0.002
Avg	0.0004	0.0003	0.021	0.007	0.415	0.127	2.850	0.70	0.088	0.028	1.545	0.42	0.019	0.006
Avg			**0.021**	**0.007**	**0.415**	**0.127**	**2.850**	**0.70**	**0.088**	**0.03**	**1.545**	**0.42**	**0.019**	**0.006**
Min	-0.0003	-0.0003	0.001	0.000	0.106	0.020	0.748	0.29	0.027	0.012	0.259	0.11	0.002	0.001

Max	**0.0025**	**0.0017**	**0.187**	**0.069**	**1.340**	**0.270**	**14.012**	**2.74**	**0.215**	**0.059**	**8.514**	**1.86**	**0.101**	**0.020**
Std Dev	0.0006	0.0004	0.032	0.012	0.255	0.066	3.276	0.57	0.054	0.013	2.244	0.46	0.022	0.005
RSD %	135.9	132.6	150.0	166.3	61.4	51.8	114.9	81.1	61.6	46.4	145.2	108.5	114.8	88.0
Conf Interval	0.0002	0.0001	0.010	0.004	0.093	0.024	1.261	0.22	0.019	0.005	0.781	0.16	0.007	0.002
Conf Interval %	44.7	43.6	49.3	54.7	22.4	18.9	44.2	31.2	21.5	16.1	50.6	37.8	38.8	29.7
Count	38	38	38	38	31	31	28	28	34	34	34	34	36	36

Table A.9: TOC, POC, PON from start (end of mesocosm) and end of decomposition.

	(µM)	Tank 1	Tank 2	Tank 5	Tank 6	Tank 9	Tank 10
Start	**TOC**	67.5	64.7	68.3	73.1	83.3	79.2
	POC	6.11	7.56	5.64	5.67	7.56	6.33
	PON	0.767	0.824	0.593	0.680	0.835	0.764
End	**TOC**	68.3	54.0	69.3	96.0	88.2	77.1
	POC	2.59	3.08	2.91	3.25	8.55	4.13
	PON	0.190	0.300	0.283	0.362	0.600	0.515

Appendix B: Statistical Tables

Table B.1: One-sample Z-test results calculated using Syntax in SPSS.

Element	Z-statistic	p-value (0.05)
Fe	-6.1735	<0.0001
Mn	-6.02859	<0.0001
Cd	-4.06851	<0.0001
Cu	-6.53416	<0.0001
Ni	-7.97660	<0.0001
Zn	-5.23554	<0.0001
Co	1.32857	0.18399

Table B.2: Levene's Test for Equality of Variance and Two-Sample t-test for Equality of Means for Crete blanks of MilliQ and 3.5% NaCl

Independent Samples Test

		Levene's Test for Equality of Variances		t-test for Equality of Means	
		F	Sig.	t	df
Fe Blank Conc.	Equal variances assumed	.720	.402	-1.780	35
	Equal variances not assumed			-2.617	12.548

Independent Samples Test

		t-test for Equality of Means		
		Sig. (2-tailed)	Mean Difference	Std.Error Difference
Fe Blank Conc.	Equal variances assumed	.084	-.1921248	.1079310
	Equal variances not assumed	.022	-.1921248	.0734277

Independent Samples Test

		t-test for Equality of Means 95% Confidence Interval of the Difference	
		Lower	Upper
Fe Blank Conc.	Equal variances assumed	-.4112364	.0269869
	Equal variances not assumed	-.3513392	-.0329104

Table B.3: One-way ANOVA of dissolved iron concentration and tanks.

Descriptives

Dissolved Fe

	N	Mean	Std. Deviation	Std. Error
1	10	3.178070	1.9666382	.6219056
2	9	2.995033	.5640758	.1880253
5	9	2.546111	1.6046153	.5348718
6	8	3.798938	1.8398129	.6504721
9	10	3.051450	.8843956	.2796704
10	10	3.572560	.8191566	.2590401
Total	56	3.183618	1.3712649	.1832430

Test of Homogeneity of Variances

Dissolved Fe

Levene Statistic	df1	df2	Sig.
1.470	5	50	.216

ANOVA

Dissolved Fe

	Sum of Squares	df	Mean Square	F	Sig.
Between Groups	8.695	5	1.739	.918	.477
Within Groups	94.726	50	1.895		
Total	103.420	55			

Table B.4: Independent two-sample t-test for rates of high grazing vs. low grazing from Time 1 to Time 2.

t-Test: Two-Sample Assuming Unequal Variances		
	Variable 1	*Variable 2*
Mean	0.132	0.092667
Variance	0.007353	0.003562
Observations	3	3
Hypothesized Mean Difference	0	
df	4	
t Stat	0.652083	
P(T<=t) one-tail	0.27496	
t Critical one-tail	2.131847	
P(T<=t) two-tail	0.549921	
t Critical two-tail	2.776445	

Table B.5: One-way ANOVA of carbon gradient group rates from at time difference 1. Includes Levene's test for equality of variance, Welch's ANOVA, and Games-Howell post hoc test.

Test of Homogeneity of Variances

Rate (T1-T2)

Levene Statistic	df1	df2	Sig.
.	2	.	.

ANOVA

Rate (T1-T2)

	Sum of Squares	df	Mean Square	F	Sig.
Between Groups	.017	2	.008	3.359	.171
Within Groups	.007	3	.002		
Total	.024	5			

Robust Tests of Equality of Means

Rate (T1-T2)

	Statistic[a]	df1	df2	Sig.
Welch	747.711	2	1.385	.008

a. Asymptotically F distributed.

Multiple Comparisons

Dependent Variable: Rate (T1-T2)

Games-Howell

(I) Carbon Gradient	(J) Carbon Gradient	Mean Difference (I-J)	Std. Error	Sig.	95% CI Lower Bound
0C	1C	-.0185000	.0610020	.953	-1.181699
	3C	.1015000	.0610512	.497	-1.053315
1C	0C	.0185000	.0610020	.953	-1.144699
	3C	.1200000*	.0025495	.015	.079534
3C	0C	-.1015000	.0610512	.497	-1.256315
	1C	-.1200000*	.0025495	.015	-.160466

Table B.6: One-way ANOVA of rates and time differences:

Descriptives

Rate of Change

	N	Mean	Std. Deviation	Std. Error	95% Confidence Interval for Mean		Minimum
					Lower Bound	Upper Bound	
1	6	.112333	.0695001	.0283733	.039397	.185269	.0360
2	6	-.042833	.0731339	.0298568	-.119583	.033916	-.1370
3	6	-.013167	.0456614	.0186412	-.061085	.034752	-.0790
4	5	-.036000	.0566877	.0253515	-.106387	.034387	-.1090
Total	23	.006870	.0872115	.0181849	-.030844	.044583	-.1370

Test of Homogeneity of Variances

Rate of Change

Levene Statistic	df1	df2	Sig.
1.155	3	19	.353

ANOVA

Rate of Change

	Sum of Squares	df	Mean Square	F	Sig.
Between Groups	.093	3	.031	7.954	.001
Within Groups	.074	19	.004		
Total	.167	22			

Multiple Comparisons

Dependent Variable: Rate of Change

Tukey HSD

(I)Time Difference	(J)Time Difference	Mean Difference (I-J)	Std. Error	Sig.	95% Confidence Interval Lower Bound
1	2	.1551667*	.0360733	.002	.053734

	3	.1255000*	.0360733	.012	.024068
	4	.1483333*	.0378340	.005	.041950
2	1	-.1551667*	.0360733	.002	-.256599
	3	-.0296667	.0360733	.843	-.131099
	4	-.0068333	.0378340	.998	-.113217
3	1	-.1255000*	.0360733	.012	-.226932
	2	.0296667	.0360733	.843	-.071766
	4	.0228333	.0378340	.930	-.083550
4	1	-.1483333*	.0378340	.005	-.254717
	2	.0068333	.0378340	.998	-.099550
	3	-.0228333	.0378340	.930	-.129217

*. The mean difference is significant at the 0.05 level.

Table B.7: Two-sample independent t-test for Batch 1 NASS-6 reference against Batch 2 NASS-6 reference.

t-Test: Two-Sample Assuming Unequal Variances

	Variable 1	*Variable 2*
Mean	0.404983	0.434507
Variance	0.001702	0.000115
Observations	9	4
Hypothesized Mean Difference	0	
df	10	
t Stat	-2.00049	
P(T<=t) one-tail	0.036664	
t Critical one-tail	1.812461	
P(T<=t) two-tail	0.073328	
t Critical two-tail	2.228139	

Appendix C: Dust Report

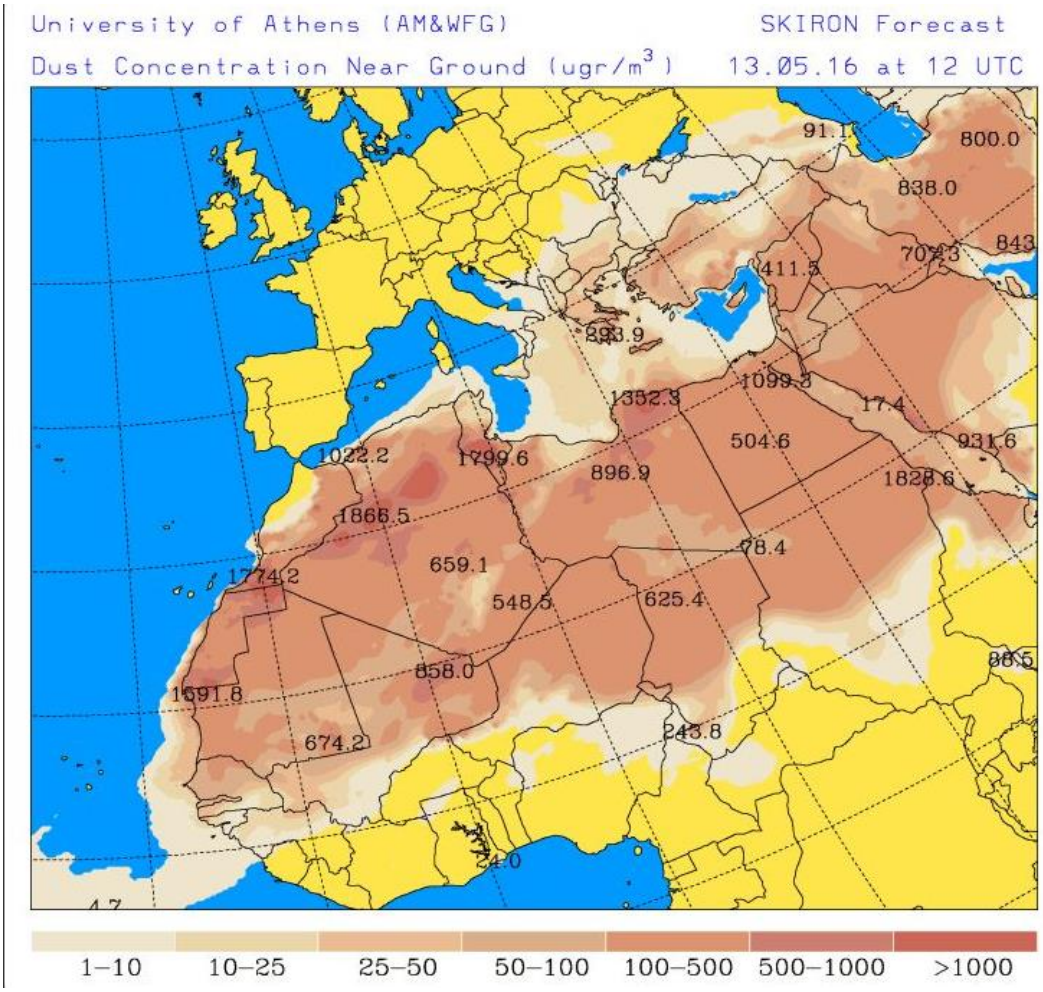

Figure C.1: Dust concentration over Mediterranean region on May 13th, 2016 during mesocosm experiment and bottle cleaning.

Appendix D

SeaFAST Usage Protocol

Modified: 5Oct2016

START UP

1) Turn on the syringes and autosampler and the computer.
2) Open the main argon canister valve all the way.
3) Turn on the ventilator to LOW.
4) Log on under Administrator, password is 12345678
5) Start the ESI / SC Fast software located on the desktop.
6) Press "Initialize" under the FAST submethod to connect the software with the instrument
7) Under the "FAST submethod" choose *Prime SeaFAST*
8) Check the SeaFAST log to see what has been done the days before.
9) Press the "Play" button to prime the instrument.
    a. Prime the instrument twice if you or someone else has changed anything from the previous day
10) Observe the probe and the instrument as it is priming to watch for leakages. Check the inside of the autosampler, the syringes, the rotors, and behind the autosampler.
11) Check the gas pressure on the blue valve above the outlet. It should read at or around 1 bar. (+ or – 0.1)
12) Check the volume levels MilliQ, Eluent, Buffer, Rinse, and Waste. Remake / empty as appropriate.

METHOD RUNS

1) Choose your rack setup and rack types for the desired racks you will use. (ex: Select Tray, 2x2). Choose rack type (ex: 3x7, LG or MG –will most likely be LG).
2) Place an empty destination tube/vial with the cap off in the destination rack
3) At the Main Menu, click on Manual.
4) Enter your empty destination tube's position (ex Rack 4, Position 21) and click "Go Here". Recommended to do this for every destination tube to ensure probe will go into each vial.
5) The probe will move to the location and move vertically downward as if dispensing a sample. Adjust the height by pressing the "-10Z" so the probe

does not touch the bottom of the vial and will not be touching the final sample volume.

6) Place your samples and destination vials in the appropriate locations on the SeaFast.
7) Go to "Configure" and select *Prep Fast Offline*.
8) Click the button *Enable SeaFastpico*.
9) Edit and add rows to your sequence. DOUBLE CHECK THAT YOUR SEQUENCE IS CORRECT. Otherwise you will have wasted sample and possible contamination of other samples.
10) Right click under the method tab. Select *Edit submethod parameters*. Check and/or change your final sample volume. Check and/or change the # of 10mL loops. (ex: 2 10mL loops will aspirate 20mL of initial sample). Do not change the final elution flow rate.
11) When finished editing the method parameters, click *Save* and then *Close* for each section. Right click on the method tab for the first sample and click *Copy cell contents to all rows below*.
12) Change the name of your sequence / method to your initials and date. Click *Save*. When ready to begin, press *Start prepFAST offline*.
13) It is important to check that your sample caps are OFF and that the racks are aligned PERFECTLY. Otherwise you will have errors and spills in your sequence. You must also CHECK EACH DESTINATION VIAL INDIVIDUALLY to ensure that the probe will not hit the side of the tube and deliver the volume where you intend it to.

SHUT DOWN

1) Remove your original samples and destination samples from the autosampler
2) Keep the racks in the autosampler
3) Check the levels of the MilliQ water, the Eluent, and the buffer, and the rinse
4) Make sure the instrument has stopped running and completed the full method --- IF YOU HAVE INTERRUPTED THE METHOD YOU MUST CONDITION THE COLUMNS AGAIN BEFORE NEXT USE
5) Close the ESI software by clicking File, Close, OK.
6) Log off and then shut down the computer.
7) Turn off the syringes, autosampler, and ventilator.
8) Check the waste level. If high, empty waste into the hood while running the water to dilute the waste.

9) Re-insert the waste lines into the waste bottle. Keep the smaller diameter waste lines separate from the large waste lines.
10) Close the main valve on the argon canister.

WASH AND SOLUTION PREPARATION

For acid washing prior to use, an acid concentration of approx. 0.1M was used for the buffer, rinse, and eluent bottles. Rinse bottle at 4L so approx. 28mL of 14.4M ultrapure HNO3 was added. Eluent and buffer bottles at 2L so approx. 14mL of 14.4M ultrapure HNO3 was added.

Buffer. Ammonium concentration at 25%. Calculations indicate that 170mL of 25% ammonium hydroxide be added for buffer solution along with 140mL of glacial acetic acid to 150mL ultrapure deionized water. Then diluted to 500mL. If greater quantities of buffer are needed, double all volumes. Prepare under the hood, exothermic reaction. Add acetic acid slowly to the water and ammonium hydroxide mixture. Let react and cool before measuring pH. Add dropwise glacial acetic or ammonium hydroxide until pH between 5.8 and 6. (preferably 6.0). Record pH by first calibrating pH meter and then pouring a small amount of buffer out and measuring. Do NOT put the probe into the full solution.

Calculations derived from ESI Solution Preparation guide. 140mL of 29%, 148mL of 28%, 192mL of 22%.

Eluent. To 250mL ultrapure deionized water, add 53mL of ultrapure 14.4M nitric acid and dilute to 500mL. If greater quantities of eluent are needed, double all volumes. Final molarity is around 1.5M

Rinse. Make 0.1M HNO3 solution using the rinse solution bottle. Ex: 13.9mL of ultrapure HNO3 diluted to 2L.